Stony Brook University

INDUSTRIAL SHIPS' WAKE PROPAGATION AND ASSOCIATED SEDIMENT RESUSPENSION IN THE VENICE LAGOON

A Thesis Presented by

Morgan Elise Gelinas

to

The Graduate School
in Partial Fulfillment of the
Requirements
for the Degree of

Master of Science

in

Marine and Atmospheric Science

Stony Brook University
May 2011

Stony Brook University
The Graduate School

Morgan E. Gelinas

We, the thesis committee for the above candidate for the
Master of Science degree, **hereby** recommend
acceptance of this thesis.

Henry Bokuniewicz – Co-Advisor
Professor of Oceanography
School of Marine and Atmospheric Sciences
Stony Brook University

John Rapaglia – Co-Advisor
PhD Marine and Atmospheric Science
'Future Ocean' Excellence Cluster
Christian Albrechts Universität-zu-Kiel
Kiel, Germany

Kamazima Lwiza
Professor of Oceanography
School of Marine and Atmospheric Sciences
Stony Brook University

This thesis is accepted by the Graduate School

Lawrence Martin
Dean of the Graduate School

Abstract of the Thesis

Industrial Ships' Wake Propagation and Associated Sediment Resuspension in the Venice Lagoon

by

Morgan E. Gelinas

Master of Science

in

Marine and Atmospheric Science

Stony Brook University

2011

Shallow water, breaking waves have been observed along the shoals east of the Malamocco-Marghera canal in the Venice Lagoon after the passage of large (>100 m length) industrial ships. These waves are characterized by a solitary, asymmetrical trough that increases in asymmetry as it propagates over the neighboring shoals. The waves create massive sediment resuspension events due to high water particle velocities. This resuspension is of ecological and economic concern in the Venice Lagoon due to the high level of sediment contamination from the nearby Porto Marghera industrial zone and the necessity for increased dredging, respectively. Water level, water velocity, and suspended particulate matter (SPM) were measured continuously for 9 days in July 2009 with 10 pressure sensors, 1 S4 electromagnetic current meter and an automatic water sampler. The pressure sensors were aligned in three offset transects perpendicular to the channel to obtain wave direction and extent of lateral energy. Ship dimensions and velocity were recorded using an Automatic Identification System (AIS). Wave characteristics were analyzed and correlated to ship parameters by using the ship depth-based Froude number, Fr_D, and blocking coefficient, S. Of the 22 recorded waves, the largest wake produced in this study was a trough displacement of 0.73 m, and the largest SPM concentrations were >400 mg/L, lasting for minutes after a ship passed. These recorded resuspension events were compared to predicted values using a relationship between sediment flux and boundary shear stress. These waves could be playing a role in the extreme erosion alongside the canal that has occurred over the past 30 years. The shape of these waves is particularly intriguing and empirically a double N-wave is used to model them as they propagate onto the shoals. This equation has been used to model tsunami propagation prior to this study.

Table of Contents

List of Figures

List of Tables

Acknowledgements

To my family, who support me in all that I do. Who raised me to love the ocean and honor the environment, and who I know will always be behind me as I move forward.

This thesis has allowed me to travel the world as a participant, not just a touristic observer. I got hopelessly lost on German trains, but couldn't help but smile when I told people I was trying to get back to my apartment, not a hostel, in Kiel. I (bravely) dove for lost instruments in the Venice Lagoon, and then was told to "shower for at least 20 minutes, with lots of soap". I was not just collecting data and observing people; I was experiencing places and building friendships.

This thesis holds more than the science behind my degree. It has taught me the power of collaboration, to recognize and value the unique personal connections that are created in this field. I have learned so much about wave physics, but also about communicating with people to ensure my results were understandable and will be built upon in the future.

So thank you to everyone who has listened to me talk about this project; you have all made me think about it from a different angle and exercised my creativity.

Thank you especially to Henry Bokuniewicz, for all of your patience and support through the jungles of wave theory, and graduate school in general. You are an amazing teacher and mentor; I would have drowned in this thesis without you telling me to take it one step at a time.

Kamazima Lwiza, although I complain a lot about Matlab and would never attempt to call myself competent at it, your unwavering faith that I could do this project has helped me through so many frustrated rages at technology. I always remember your laugh and try to channel your curious approach towards scripts that refuse to work rather than my furious one.

Luca Zaggia: *Ciao, Bello*! You can cook for me anytime. We'll meet on the dance floor again soon.

And John Rapaglia: I owe you so many beers. I can never repay you for this experience.

Thank you.

He who commands the sea commands the trade routes of the world. He who commands the trade routes, commands the trade. He who commands the trade, commands the riches of the world, and hence the world itself."
--Sir Walter Raleigh

1. INTRODUCTION

According to a first-order estimate, 40%-78% of the world's population lives within 50 km of the sea coast (Small and Nicholls 2003), and this number is expected to rise. These environments are the transition between maritime and terrestrial commerce, concentrating nations' industrial trade into physically fragile and biologically productive ecosystems. It is imperative that the world sees these environments are necessary for the natural maintenance of the coast. Maintaining them ultimately affects quality of life and lucrative economies for coastal populations. Impacts might be expected to be most intense in ports where shipping is focused in confined marine environments among dense populations.

In 2007, the global shipping industry shipped more than eight million tons of product over a distance of about four million miles, close to 33,000 billion ton-miles of total trade (Smith 2009). This form of trade has more than quintupled since 1960. On an even more recent timescale, revenue increased from $75.9 billion in 2001 to $148.30 billion at the end of 2008, an average of 10.1% growth per year. This rapid growth was largely due to the industrialization of the Chinese economy and the high demand for cheap manufactured goods in developed countries (Smith 2009). At present, about 80% of all international trade is carried by sea, ultimately funneled through ports.
It is therefore crucial to better understand the environmental impact of shipping on the shallow-water environments of industrial harbors in order to ensure sustainable development as the industry continues its rapid expansion. Ports located near shallow, low-energy coasts are particularly vulnerable to increased wave activity causing sediment resuspension and erosion (Soomere 2007). Of particular concern are ports where deep, narrow channels are dredged through shallow shoals. The channels are dredged to accommodate the large displacement of water created by ships; however the adjacent shoals are left unchanged and are adversely affected by the resulting increase in wave energy from the resulting wakes.

Large ships, greater than fifty meters in length, create wakes which are characterized by a significant draw down and surge of water (Houser 2010). It is known variously as the Bernoulli wake (PIANC 2003), depression-area wake (Soomere 2007, Gourlay 2006, 2008), drawdown-and-surge wave (Houser 2010; Nanson et al. 1994) or

the ship-induced bore (Ravens and Thomas 2008). For simplicity the term "Bernoulli wake" will be used in this document.

As a ship moves, it creates a water-velocity field around the hull due to dynamic displacement of water (PIANC 2003). The hull displaces water; velocity around the side of the ship increases to replace it, and a depression is created around the ship (Oebius 2000). This velocity field creates a pressure gradient, which is the main way Bernoulli wakes are created by moving ships. When recorded on an instrument within the deep channel near the ship, the Bernoulli wake produced by this pressure difference has been described as a symmetrical, solitary wave (Oebius 2000). Once over the shoals, Bernoulli wakes can produce high current velocities (Bauer et al. 2002), hence high, bottom shear stress, leading to substantial sediment resuspension (Erm et al. 2009; Hofmann et al. 2008; Schoellhamer 1996; Wiberg and Sherwood 2008). In shallow environments, high current velocities might disturb benthic communities and reshape shorelines (Soomere et al 2009). In addition, although coastal waters are naturally turbid due to shallow depths, terrestrial runoff and human development (Neil et al. 2002), an increase in suspended sediment concentrations can be detrimental to ecological health by blocking sunlight and, possibly, by releasing excess nutrients. Some of the resuspended material may also settle in the channel, increasing dredging demand (Rapaglia et al. 2011). Dredging creates further stress on the environment due to elaborate machinery and increased ship traffic (Umgiesser et al. 2004).

Sediment resuspension also remobilizes industrial, sediment-bound contaminants. Of particular concern are heavy metals and persistent organic pollutants, (POPs), which are released as byproducts related to various aspects of the production of chlorine-based products and the majority of combustion processes (Racanelli and Bonamin 2000), processes commonly used in or near industrialized ports. POPs are a part of several families of chemically inert, organic compounds characterized by toxicity and a long residence time in the environment (Racanelli and Bonamin 2000). POPs have very low solubility in water and thus adhere readily to particulate matter, specifically sediments. In most low-energy environments, gradual sedimentation *via* natural processes should eventually cap these toxins and immobilize them from the environment. However, when resuspended, these toxins continue to become bio-available. Their chemical stability and lipophilicity cause them to biomagnify (Racanelli and Bonamin 2000), posing a greater threat as they work up the marine food web. The wakes of large ship wakes can play an important role both in sediment resuspension and, ultimately, in POP dispersion and bioavailability.

In large bays of open water, it may be difficult to distinguish ships' wakes from wind waves using conventional instruments, thereby making it impossible to isolate the effect of vessel-generated waves (Nanson et al. 1994, PIANC 2003). Thus there is little published information on ship wakes in restricted waterways and even less understanding of wave propagation into shallow water after the wake leaves a channel or of its effects on sediment resuspension. However, in fairways, enclosed lagoons and protected harbors, ships' wakes can be distinguished easily from wind waves (PIANC 2003). Venice Lagoon (Figure 1) is, therefore, an ideal location to better understand of impact of large vessel wakes in a restricted environment.

It is important to evaluate the physical characteristics of industrial ship wakes as they propagate outside of shipping channels in coastal ports to determine sediment

dynamics. Bernoulli wakes observed in the Venice Lagoon, Italy will be described. Initial results are described in Rapaglia et al. (2011); however, wave characteristics, water velocities and associated suspended sediment concentrations produced as these wakes propagate over adjacent shoals will be further documented. In addition, a new model will be suggested for these wakes because it can produce the varied features. Ultimately, the impact of ships' wakes needs to be forecast and perhaps, controlled. Expedients will be suggested based on the observations for anticipatory impacts.

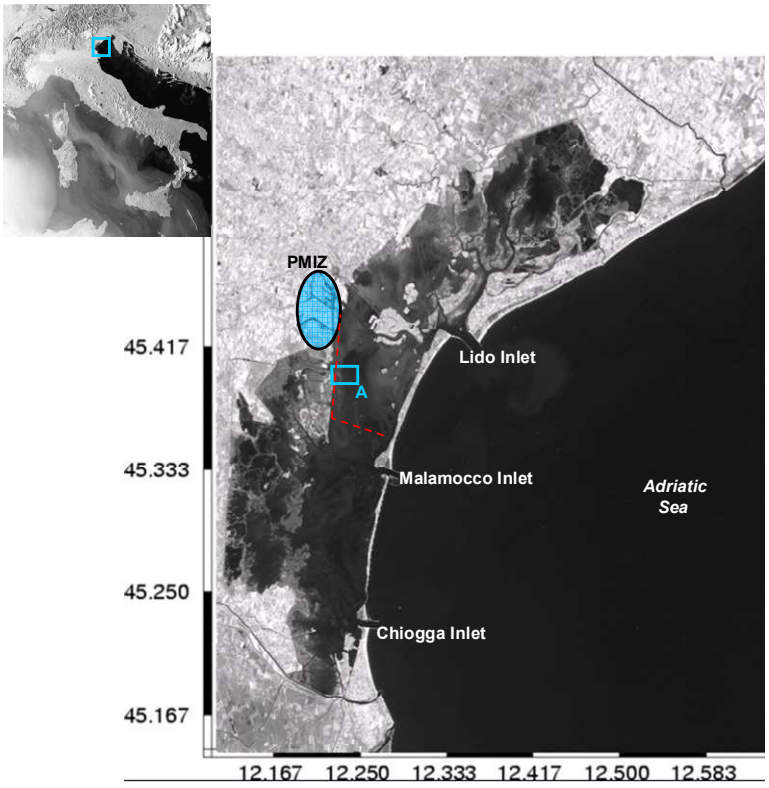

Figure 1: Map of study area. The Porto Marghera Industrial Zone, PMIZ, is circled and labeled. The Malamocco-Marghera shipping canal is denoted by the red dotted line, box "A" next to it outlines the location of instruments and is enhanced in Figure 7.

2. PREVIOUS WORK

Previous studies of the development and propagation of waves from passing vessels (e.g. Velegrakis et al. 2007), include investigations concerned with the properties of the wake once it leaves the channel (e.g. Didenkulova et al. 2009; Houser 2010; Parnell and Kofoed-Hansen 2001; Schoellhamer 1996) and consequent resuspension (Erm et al.

2009; Hofmann et al. 2008; Nanson et al. 1994; Osborne and Boak 1999; Schoellhamer 1996; Soomere and Kask 2003; Soomere et al. 2007). Most, however, have been concerned with the investigation of a far-field wake from fast ferries and its effect on sediment erosion and resuspension on the shoreline (e.g. Parnell et al. 2008). The situation in the Venice Lagoon is different and perhaps more representative of compact, industrial ports. The shoals are immediately adjacent to the shipping channel and are thus affected by the near-field Bernoulli wake long before the wake reaches a shoreline (Soomere 2007). The propagation of this Bernoulli wake, both its wave shape as well as its propagation direction, is poorly understood, in part because there are few environments where it can be studied.

Different types of wakes dominate in different situations. They are often distinguished by their plan-view, or the angle they make with the ship's track. In deep, open water, a ship creates bow and stern divergent wave trains, drawdown of water levels, and propeller wash, along with transverse waves behind it (Houser 2010). This wedge-shaped wake, or Kelvin wedge, is a result of the fluid mechanical flow around the ship hull (Reed and Milgram 2002). A wave is considered a Kelvin wave when gravity and the Coriolis force are the restoring forces (Stewart 2004). The apex angle of this Kelvin wedge typically has an apex angle of 19.5˚ (Hennings et al. 1999). It is possible to distinguish between diverging waves and transverse waves by the angle at which they are oriented to the vessel track; the diverging wave crests propagate at an angle between 90° and 35° while the transverse waves appear at angles less than 35°. In steady conditions, these transverse waves propagate in the same direction as the ship (PIANC 2003). In deep water, this wave pattern is best characterized by the dimensionless length Froude number, Fr_L:

$$Fr_L = \frac{U_b}{\sqrt{gL}} \tag{1}$$

where U_b is ship speed, g is acceleration due to gravity and L is ship length (PIANC 2003). In deep water, wavelength is a function of ship speed, therefore the faster a ship travels, the longer the created wake. The non-Kelvin aspects of ship wakes include local features at the ship such as breaking bow and stern waves, and the viscous wake containing the rotational flow from the ship's boundary layers (Reed and Milgram 2002).

The characteristic pattern becomes altered when ships travel in restricted, shallow waterways, such as in the Venice Lagoon. The waves are better described by the depth-based Froude number, Fr_D:

$$Fr_D = \frac{U_b}{\sqrt{gh}} \tag{2}$$

where h is the water depth. The ship is creating the same physical features; however these features are not fully understood in a shallow near-field setting. Specifically, while there is a relatively well-understood relationship between waves and shoaling bathymetry, there is little research on how a leading-trough wave, such as the Bernoulli wake, propagates in these conditions.

Although propagation of the Bernoulli wake is poorly characterized, Houser (2010) and Schoellhamer (1996) analyzed the extent of the depression ships make. They concluded that the main factor is the ratio of vessel cross-sectional area to that of the navigational

channel cross-sectional area, or blockage ratio, S:

$$S = \frac{BD}{bd} \tag{3}$$

Where B and D are the width and draft of the ship, respectively, and b and d are the width and depth of the channel, respectively. In shallow water, Schoellhamer (1996) concluded that wake height is determined by a combination of the depth-based Froude number, Fr_D, and S of the ship. The relationship $Fr^{2.4}S^{1.6}$ produced a linear correlation with non-dimensional wave height (γ= H/h where H is the wake wave height). Recent work done by Rapaglia et al. (2011) analyzed this relationship in regards to suspended sediment concentrations caused by industrial ship wakes at this study site and concluded that a better description for this location is $Fr^{3.5}S^{1.6}$. This suggests a higher sensitivity to ship speed, and the authors suggested speed regulations to reduce the occurrence of large, destructive wake heights.

Waves are categorized as shallow water waves once they propagate into water where the depth is less than 1/20 their wavelength. At this depth, wave crests become higher and more peaked, separated by wider, flatter troughs (Komar 1998). Solitary waves are described by the non-linear equation

$$\eta(x,t) = H \sec h^2((K_s - ct)), \qquad K_s = \frac{1}{h}\sqrt{\frac{3H}{4h}} \tag{4}$$

where η is the vertical coordinate above the still-water line at a horizontal distance x from the crest; the height H and water depth h are also in reference to the still-water level. The wavenumber, K_s, is defined by the ratio of the wave height to the water depth (Madsen and Schaeffer 2010).

The shallow-water transformation continues to evolve into:

$$c = \sqrt{gh} * \left[1 + \frac{1H}{2h} - \frac{3}{20}\left(\frac{H}{h}\right)^2 + \ldots\right] \tag{5}$$

This is greater than the shallow-water phase velocity of Airy waves due to the inclusion of terms that depend on H/h. This relationship is nearly equal to:

$$c = \sqrt{gh\left(1 + \frac{H}{h}\right)} = \sqrt{g(h+H)} \tag{6}$$

This is a first-order approximation to the solution of the equations of wave motion (Komar 1998).

As will be discussed later, wakes observed along the shoals of the Venice Lagoon were solitary waves, that is, not part of a multiple wave packet. However, a better description of their overall shape is as an N-wave. This solution satisfies the Korteweg de Vries wave equation. N-waves are now widely used to model tsunamis as they approach the shore (Tadepalli and Synolakis 1994, Tadepalli and Synolakis1996, Lin and Hwang 2008, Madsen and Schaeffer 2010). A principal characteristic of such a tsunami is the observation that water at the coast recedes before a tsunami arrives, suggesting tsunamis can be described as leading-depression waves. Earlier work attempted to maintain solitary wave theory in models, describing the wave as a combination of a solitary and N-wave (Tadepalli 1996); however, this did not accurately describe all wave shapes as tsunami approached the shore along non-uniform bathymetry. Madsen and Schaeffer (2010) explored other forms, presenting a formula for a double N-wave as:

$$\eta_i\,(x_0,\,t) = A_1\mathrm{sech}^2\Omega_1(t - t_1) - A_2\mathrm{sech}^2\Omega_2(t - t_2) \qquad (7)$$

where the six subscripted parameters can be chosen freely to represent the shape at different times of propagation. This equation allowed them to better describe the observations of the tsunamis they modeled. The authors note that during shoaling from the deep ocean to the nearshore, nonlinearity increases, while the effect of dispersion decreases. This causes the asymmetry of the wave profiles to increase and, close to the beach face, the tsunami may become steep enough to disintegrate into an undular bore with short and steep transient waves (Madsen and Schaeffer 2010). As will be discussed later, the wakes in the Venice Lagoon showed similar behavior to the tsunami characteristics described by Madsen and Schaeffer (2010). Their asymmetry increased as they propagated, and steep, transient waves developed as they moved farther away from the channel. Although the wakes are not created by a natural disaster; they were the result of a large, sudden displacement of water propagated as a shallow water wave, similar in principle to a tsunami.

In shallow water, the orbital water velocity under surface waves intercepts the bottom, causing distortion and increased elliptical or bi-directional water motion. Water velocity creates shear stress as it flows over the bottom sediments (Sternberg 1972). Assuming steady, two-dimensional, turbulent flow in an open channel, the quadratic stress law relates bottom stress, τ_0, to velocity the following way:

$$\tau_0 = C_D \rho \overline{U}^2 \qquad (8)$$

Where ρ is the density of the fluid, $\overline{U}$ is the average water velocity and C_D an empirical drag coefficient, which relates the mean velocity near the seabed to the force exerted by the fluid per unit area of the bed (Sternberg 1972). Sediment resuspension is initiated by waves when a critical shear stress/orbital velocity is reached (le Roux 2001). This threshold varies depending on water and sediment parameters, but the generally accepted relationship originally determined by Hjülstrom (1935) (Figure 2).

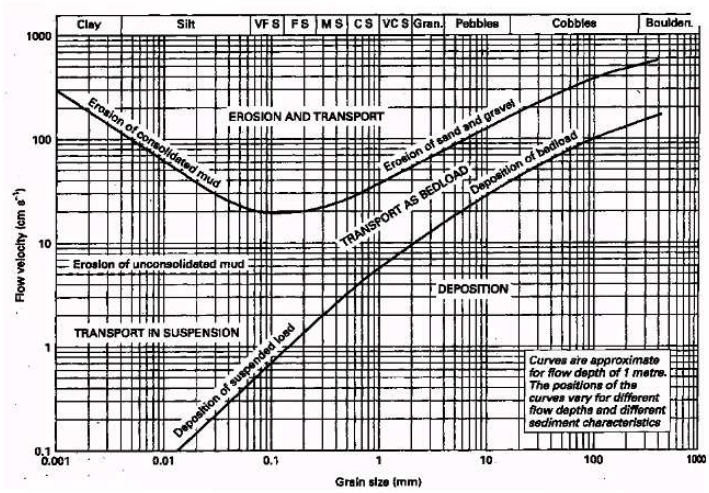

Figure 2: Hjülstrom diagram depicting critical flow velocities required for transport of different grain sizes.

The sediment budget in the Venice Lagoon indicates the extensive anthropogenic manipulation throughout the area. There have been substantial bathymetric changes in the past 100 years resulting from a combination of natural processes, human activities, and sedimentological responses to such activities (Sarretta et al. 2010). Riverine sediment input to the lagoon is almost completely cut off due to upstream damming and breakwaters constructed at the inlets have greatly reduced coarse marine sediment input. This has created a sediment-starved environment, reducing tidal flat stability and ultimately changing the overall morphology of the lagoon from a complex, well-developed micro lagoon during the 1930s to a subsidence-dominated lagoon in the 1970s and finally to the high-energy-dominated, flat-bottomed and more bay-like environment seen today (Sarretta et al. 2010).

3. STUDY LOCATION

The Venice lagoon, located in northeastern Italy, covers about 550 km^2, making it the largest Italian lagoon (Brambati et al. 2003). It is connected to the Adriatic Sea by three inlets: Lido, Malamocco and Chiogga, north to south (Figure 1). The lagoon has a microtidal range of 0.3 m during neap tides and 1.1 m during spring tides (Molinaroli et al. 2009). The Venice Lagoon has an average depth of 0.8 m, but is bisected by a network of both natural and man-made canals that are actively dredged to 10 m or deeper to accommodate large commercial ship traffic, tankers, cargo vessels and cruise liners (Gačić et al. 2002).

The Porto Marghera Industrial Zone (PMIZ) is a major port in the Venice Lagoon and serves as a main transfer location between marine and terrestrial shipping methods.

Development along the northwest shore began in the 1920's, reaching an area of about 24 km^2 and then was expanded in the 1950's to double its size, making it the third largest industrial district in Italy (Bellucci et al. 2002). Though recently the PMIZ has been marked by a decline in manpower and total production, several important factories such as oil refineries, chemical industries and power plants still remain. The byproducts of these industries have a long history of contaminating the sediments of the adjacent areas (Bellucci et al. 2002). Of particular concern are the high concentrations of POPs (persistent organic pollutants) found throughout the lagoon. Raccanelli and Bonamin (2000), found POP sediment concentrations ranging from 10 ng/kg in the central lagoon to a maximum of 2857 ng/kg next to the industrial zone. For comparison, the concentration in the Adriatic Sea was 0.17 ng/kg. The quality of the sediment was considered to be so poor that the area has been designated a "contaminated area of national interest" (Bernadello et al. 2006, Secco et al. 2005, Zonta et al. 2007). Concurrent with the development of the PMIZ, the Malamocco-Marghera Canal, locally known as the Canale di Petroli, was dredged to a depth of 12 m from the Malamocco Inlet to the PMIZ. It has a total length of 20 km, and a mean width of 200 m to accommodate medium-sized container ships and tankers. From Malamocco Inlet, the canal heads directly west towards the mainland, bisecting the smaller Fisolo and Spignon channels. It then makes a sharp turn north towards the PMIZ, where it travels alongside the mainland for 14 km (Figure 1). The sides of the channel are exceptionally steep, rising towards the shoal with a slope of about 0.25 on the east side and 0.30 on the west side (Rapaglia et al. 2011). Grain size at the channel bottom was coarse, 56.3% sand, attributed to the strong currents in the canal (Bellucci et al. 2002). Bellucci et al. (2002) analyzed grain size east of the canal and found that the closest sites had the coarsest composition, 56.3% sand, 27.53% silt, 16.17% clay. In contrast, a site located 2.5 km from the canal had a finer composition of 9.61% sand, 66.89% silt and 23.5% clay. The modal grain size in the sediments along the Malamocco-Marghera canal was between 11 and 31 μm, or 4 to 8φ (Figure 3) (Bellucci et al. 2002). East of the canal the seafloor quickly shoals to 1 to 2 m depth (Figure 4). The adjacent shoal extends five to eight kilometers lagoonward of the channel for its entire length. In many locations along the channel a ship's wake can travel unimpeded along the shoal for several hundred meters, up to kilometers (Rapaglia et al. 2011).

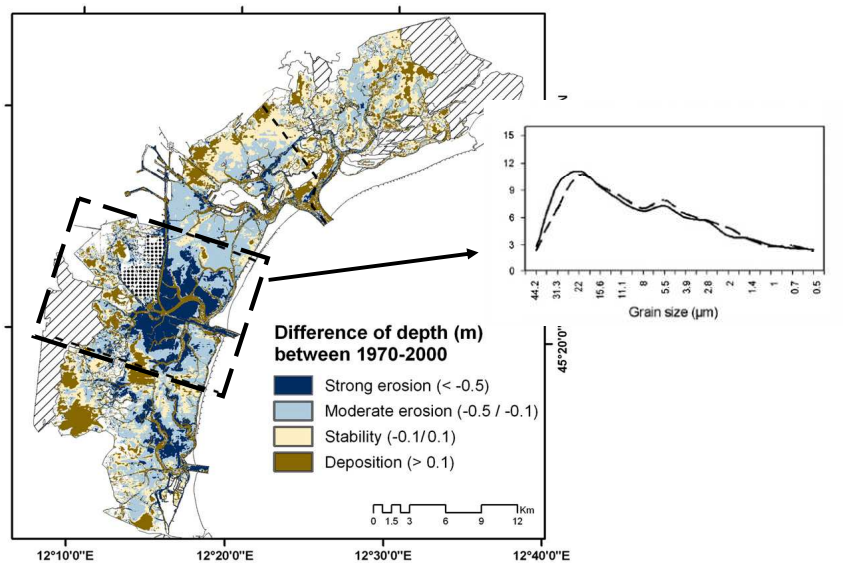

Figure 3: Figure from Molinaroli et al. (2009) of the Venice Lagoon, showing the strong erosion in the vicinity of the Malamocco-Marghera canal. Highlighted area in box shows the average frequency distribution of bottom grain sizes, from Bellucci et al. 2002. Dotted line is from 1970, solid line is from 2000.

Molinaroli et al. (2009) quantified bathymetric changes in the Venice Lagoon from 1970-2000 and concluded that there was a shift in sedimentary facies from lower to higher energy patterns during this thirty year period, coincident with the construction of the Malamocco-Marghera Canal. Erosion rates greater than 0.5 m over 30 years were found along the Malamocco-Marghera canal where the study site is located (Figure 3) (Molinaroli et al. 2009). Sarretta et al. (2010) estimated that approximately 80% of all losses from the lagoon between 1927 and 2002 came from the area surrounding the shipping canal alone (Figure 5), about 900,000 tons per year. Assuming a conversion factor of 1.66, 900,000 tons per year corresponds to 1.5 million cubic meters per year. Both studies attributed this erosional hotspot to transgressive effects caused by human-induced subsidence superimposed on natural sea-level rise. However, they both admit that this cannot be the sole factor in such rapid erosion and suggest some sort of hydrodynamic forcing. Wave action and industrial shipping were not considered. The losses are comparable to maintenance dredging ni the lagoon which is estimated to be one million cubic meters per year (MAV-CVN, 2004 as cited in Saretta et al., 2010).

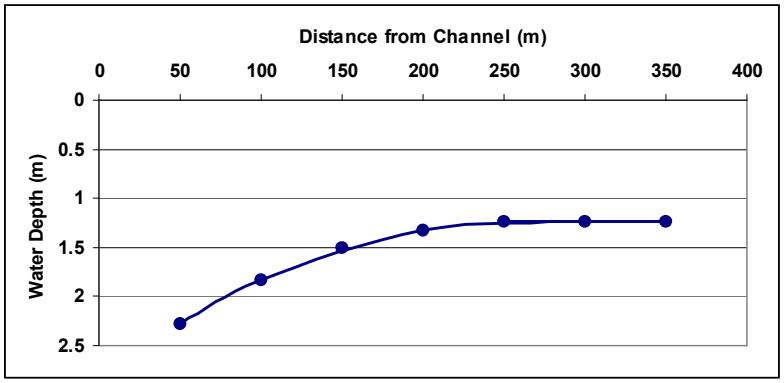

Figure 4: Tidal-averaged depths to show bathymetry of study area along shoals next to Malamocco-Marghera Canal.

The study site (Figure 1) was located in these eastern shoals, 2 km south of the PMIZ and directly seaward of Fusina. Tidal currents in this part of the lagoon were low, less than 0.05 m s^{-1}, however winds can increase currents to over 0.15 m s^{-1} (Coraci et al. 2007). The lagoon is naturally sheltered from high wind waves, due to limited fetch length. Southeasterly winds caused significant wave heights in the study period of up to 0.2 m due to the relatively large fetch of about 8 km in this direction. An analysis of annual hourly wind data from 2009 provided by the Comune di Venezia shows that the study period was representative of the annual wind climate with an average wind speed of 3.23 m s^{-1} during the study period, which was slightly higher than the annual mean of 3.11 m s^{-1} (Rapaglia et al 2011).

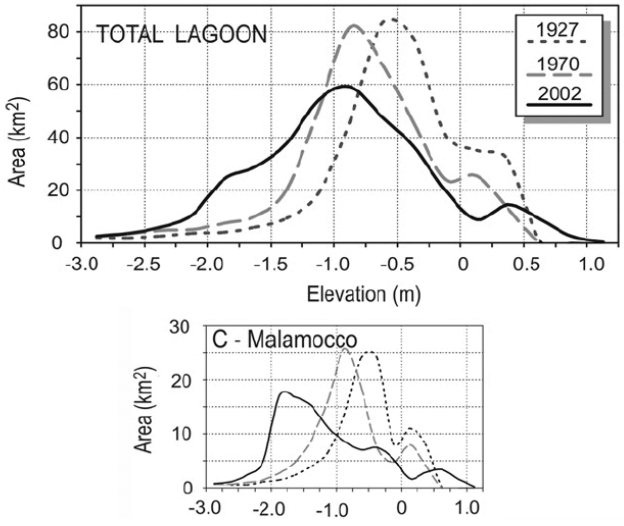

Figure 5: Figure from Sarretto et al. (2010) of the Venice Lagoon, showing the substantial elevation changes seen near the Malamocco-Marghera canal between 1970 and 2002.

Amos et al. (2004) addressed the stability of tidal flats in the Venice Lagoon. They found that during the summer mean bed density was highest near the study location, where the sediment density was 1907 $\pm$ 60 kg/m^3 and that bed strength was four times higher in the summer than in the winter. This mean bed density was much higher than that of newly-deposited materials or of typical estuarine muds, which typically range between 1250 and 1350 kg/ m^3 (Amos et al. 2004). This indicates the mud has experienced compaction due to loading. The average summer critical erosion threshold nearest my site, τ_c, was calculated to be 0.68 $\pm$ 0.20 Pa (Amos et al. 2004), however, the values throughout the lagoon were highly variable during this season, with an average of 1.10 $\pm$ 0.69 Pa. They do not present the analyzed data, but do provide a graph of the resuspended sediment flux as a function of bed shear stress. (Figure 6, Curve 9) (Amos et al. 2004) In this thesis their graphed relationships will be represented as:

$$\log_{10}(F) = 0.4711\ln(\tau) - 2.5846 \qquad (9)$$

where F is flux in kg/m^2/sec and τ is boundary stress in Pa. They determined the average settling speed, W_s, to be 0.00041 $\pm$ .00032 m/s. These relationships will be used later to compare recorded sediment concentrations to predicted concentrations after using water velocity to determine the boundary stress.

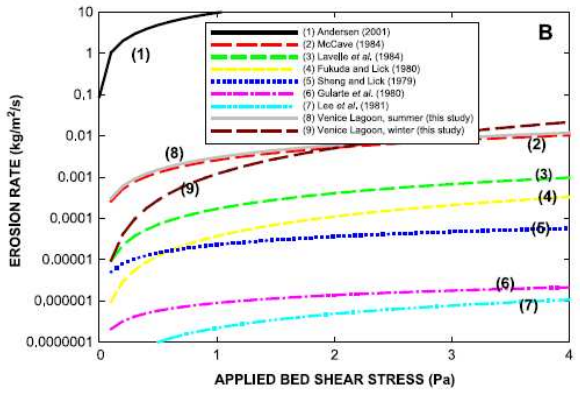

Figure 6: Results of Amos et al. (2004), bed erosion rate as a function of applied shear stress. The curve that should fit out data is curve 8 (gray), Venice Lagoon in the summer, and I represented this relationship as: $\log_{10}(F) = 0.4711\ln(\tau) - 2.5846$ (Equation 9).

During a preliminary sampling in March 2009 by Rapaglia et al. (2011), an acoustic Doppler current profiler (600kHz Teledyne-RDI Workhorse Rio Grande ADCP) was used to collect current data before and after the passage of ships show resuspension directly in the path of ships with drafts greater than 8 m (Figure 7). The ADCP data show that resuspension producing suspended sediment concentrations greater than 100 mg L^{-1} occurred throughout the water column directly below the ship; these sediments remained in suspension within the channel between 5 and 20 minutes after the passage of the ship.

Between 2000 and 3000 large ships greater than 100 m long pass through this shipping channel every year (http://www.port.venice.it/pdv/Home.do?metodo=carica_home).

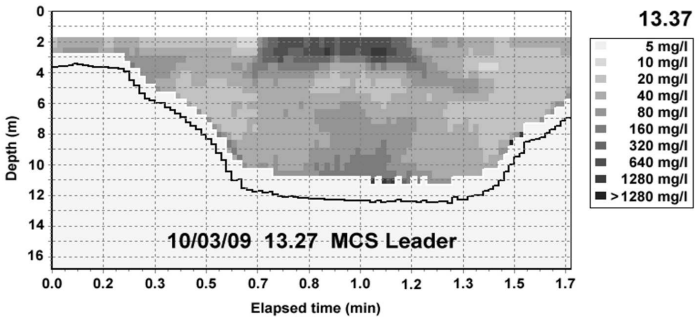

Figure 7: From Rapaglia et al. (2011). Preliminary ADCP data done in March 2009 showing water column after passage of ship MCS Leader. The data show that significant resuspension (greater than 100 mg L-1) occurs throughout the water column directly below the ship; these sediments remain in suspension within the channel for 5 to 20 minutes after the passage of the ship. There is a distinct dark cloud near the surface of the water column but this cloud quickly disappears suggesting it is most likely bubbles created by the propeller motion.

Ships travel near maximum allowed speed of 5.56 m s^{-1}. When passing the study location the speed of inbound (northward) ships was 4.4 m/s, slightly less than the average speed of 4.7 m/s for outbound (southerly) ships (Table 1). The ships were assigned ID numbers based on the date of passage with the decimal hour to indicate what time they passed during that day. There also has been a recent proposal to deepen the Malamocco-Marghera Canal to allow cruise ships to enter from this inlet (Associated Press 2009). Cruise ships are larger than the current industrial traffic and could therefore create even larger waves and resuspension events.

Table 1: Ships with assigned ID number, speed and size, blocking coefficient, S, and Froude Number, Fr_D. Ships in italics indicate those that were not recorded by the S4 and therefore not included in water velocity calculations and suspended sediment/flux analysis.

Ship ID	Name	Speed (m/s)	Length (m)	Width (m)	Draft (m)	Displace. (m^3)	S	Fr_D
Inbound								
8.304	Grande Sicilia	4.32	177	31	8.3	45542.1	0.106	0.396
8.510	Lia Ievoli	4.63	131	20	7.6	19912	0.059	0.412
8.562	East Coast	4.94	64	9	4.5	2592	0.016	0.439
13.707	Clipper Karina	4.63	116	20	6.1	14152	0.047	0.411
16.278	*Hellenic Voyager*	*4.84*	*193*	*27*	*6.5*	*33871.5*	*0.070*	*0.436*
16.292	*Wehr Elbe*	*3.91*	*208*	*30*	*9.3*	*58032*	*0.111*	*0.353*
16.494	*Mar Elena*	*4.17*	*144*	*23*	*5.7*	*18878.4*	*.053*	*.3797*
16.508	*MSC Leader*	*3.96*	*201*	*33*	*6.7*	*44441.1*	*.090*	*0.361*
Outbound								
8.365	Tucana	5.66	88	12	3.9	4118.4	0.019	0.512
8.440	Coral Leaf	5.04	108	17	6	11016	0.040	0.451
8.443	MV Nurettin Amca	4.58	118	18	4.6	9770.4	0.032	0.410
8.647	Jia Xing	3.65	169	27	7.4	33766.2	0.080	0.330
8.659	Ain Zeft	5.14	109	15	5	8175	0.030	0.462
13.743	St. Constantine	4.89	104	16	4.5	7488	0.028	0.436
13.785	MSC Mirella	3.45	177	32	9.1	51542.4	0.115	0.309
13.813	Novorossiysk Star	4.37	180	26	7.7	36036	0.079	0.394
15.697	TK Istanbul	5.40	114	18	4.6	9439.2	0.032	0.481
15.726	Uni Assent	4.22	165	27	7.3	32521.5	0.077	0.376
15.984	Salerno Express	4.84	144	19	5.5	15048	0.042	0.439
16.042	M/T Tigullio	5.61	123	18	4.8	10627.2	.0346	0.507
16.394	*Calajunco M*	*4.22*	*162*	*23*	*7.1*	*26454.6*	*0.066*	*0.38*
16.410	*Hokuetsu Ace II*	*3.65*	*210*	*32*	*8*	*53760*	*0.103*	*0.331*

4. METHODS

4.1 Data Collection

Data were collected from 6-18 July 2009, 0.5 km south of the PMIZ, where shallow water waves had been previously observed (Rapaglia et al. 2011). Vessel data were collected using an Automatic Identification System (AIS), with software (Ship Plotter) provided by www.vesseltracker.com. This system received ship signals for a range of 30 km and plotted them on a nautical chart georeferenced into the AIS software. It obtained ship dimensions, speed, direction and heading (Cairns 2005). Ten pressure sensors (PS1-PS10, Cera-Diver data logger, Schlumberger Water Services) were placed in three alternating linear transects perpendicular to the shipping channel from 6 July to 16 July (Figure 3). PS6 did not function property and no data were available. The middle transect contained PS1-PS4, with PS1 and PS2 located 50m apart and PS2 – PS4 each placed 100 m apart. There were two Optical Backscatter (OBS) arrays, each with sensors fixed at 0.1, 0.5, and 1.0 m above the seafloor, designated as "OBS1" and "OBS2". OBS1 and OBS2 were deployed at PS 2 and PS4, respectively. PS9, PS7 and PS5 were located 100 m south of this transect, and PS10, PS8 and PS6 located 100 m north of it (Figure 8). An interocean S4 electric current meter was moored next to OBS1 and PS2. It collected data at 2 Hz from 6 July – 10 July 2009. After 10:44:00 on 10 July 2009 it collected data at 1 Hz. The fourth instrument moored in this cluster was an autosampler set to collect 200 mL of water at 1 m below the surface. It was activated via command message from a mobile phone, allowing both background and instantaneous suspended sediment samples to be taken. Hand samples were taken using a peristaltic pump to aid in calibrating this suite of instruments (Figure 9). Water samples were filtered to verify suspended sediment concentrations recorded by the S4.

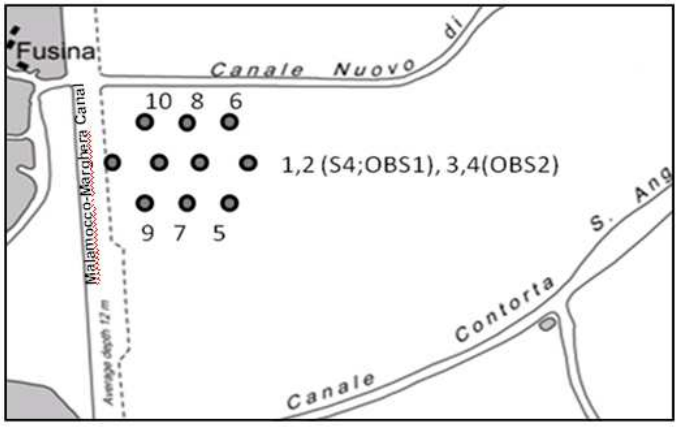

Figure 8: Instrument layout, enlarged from box "A" in Figure 1

Due to occasional instrument malfunctions complete data sets are only available on July 8 and 13-16. The wakes of twenty-two ships were documented, eight of which are inbound, heading north in the channel, and fourteen outbound, heading south in the channel (Table 1). The observed wakes were produced by ships with a maximum draft

of 9 m and a maximum beam of 31 m. Such large ships would occupy about 75% of the channel's water depth and take up about 12% of the cross-sectional area of the channel.

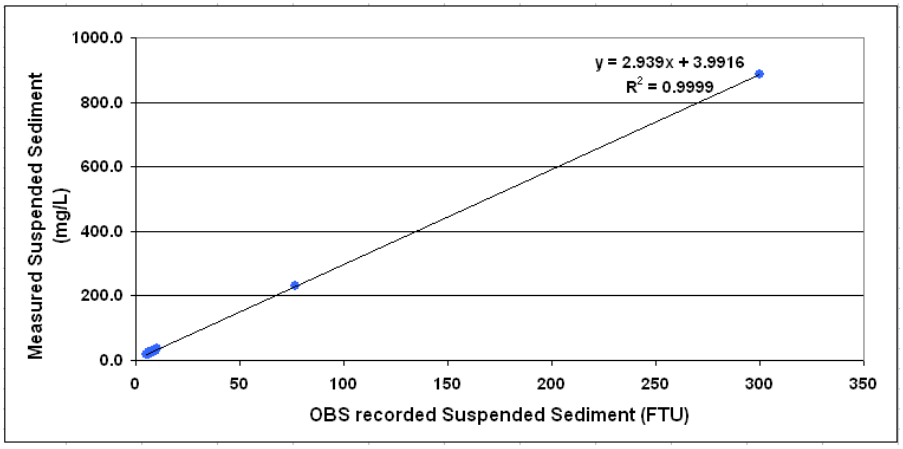

Figure 9: Calibration plot of OBS on S4 with measured suspended sediment from filtered water samples.

4.2 Data Analysis

The S4 current meter provided both water level and water velocity at a distance of 100 m from the channel. It was taken out of the water a day earlier than the pressure sensors and only provides records of the first 16 of the 22 listed waves. The pressure sensors were used to obtain high-resolution wake heights data while the S4 data were used predominantly for velocity changes. Wake heights shown from the S4 were not normalized, but should be proportional to PS2. A Matlab script was used to remove the M_2 and S_2 tidal signals from the velocity data, leaving the non-tidal current. The non-tidal current is assumed to contain the residual and wake-induced current components expressed as north (v) and east (u) velocity vectors. Progressive vector plots for the wakes of interest were plotted for each event (Appendix III). (The data points were numbered sequentially and every fifth point is labeled to more easily describe the changes in velocity as the wave passed; these numbers therefore do not represent time in seconds but rather the order of data points from the defined start time of the wave). As previously mentioned, the S4 collected data at 2 Hz, until 10 July, at which point it collected it at 1 Hz. These progressive vector plots were converted to distance plots using the timestep of each wave event.

The water speed recorded by the S4 was used to approximate bottom shear stress as the wakes passed. Average current velocity is conventionally defined at 0.38 m in a one-meter profile to account for the logarithmic decrease in speed with depth due to bottom friction and energy loss. The S4 sat about 0.5 m off of the bottom; therefore the

speed records may have yielded a slight overestimate. The shear stress, τ, was calculated using Equation 8, where C_D is the drag coefficient of the sediment, ρ is the density of the water and $\bar{U}$ is the water speed (Sternberg 1972). C_D was set at 0.002 (Sternberg 1972) and ρ was 1025 kg/m^3, the average density of water in the Venice Lagoon (Ferrarin et al 2010).

This shear stress was then used to calculate theoretical sediment flux from the bed using the previously-mentioned relationship experimentally determined by Amos et al (2004), which was parameterized here as Equation 9. This flux was used to determine the theoretical mass of sediment into the water column, using the following equation:

$$m_n = \left(m_{n-1} + F_n \Delta t\right)\left(1 - \frac{W_s \Delta t}{D_n}\right) \tag{10}$$

where m is the mass inventory of sediment, in mg/m^2, and D is depth. To compare this to recorded suspended sediment concentrations, this value was divided by the recorded water depth at each timestep.

The water level data from the pressure sensors were used to document wake shape as well as angle of propagation as the wakes traveled onto the shoals, providing more spatial resolution than the S4. The tidal signal was removed from the water-level records so that heights could be directly compared to each other. Tidal data were obtained in 15-minute intervals from Diga del Lido and interpolated using a cubic spline to match the pressure sensor frequency (1Hz). The mean water level difference between the two locations was subtracted from the water levels measured at each pressure sensor to remove the tide from the recorded values. This did not fully remove the tidal signal because the pressure sensor time series was relatively short, causing the wake troughs to offset the average. The data was then low-passed using a ten minute filter. A low-pass filter eliminates frequencies above the set filter limit but allows frequencies below the filter to remain. As a result, a low-pass filter can remove tidal waves but keep the ship wakes of interest. Because the still-water height, h, differed at each pressure sensor, the water elevation was normalized by h. The still water height at all the pressure sensor locations was set to 0. The largest trough depth, H_{max}, was defined as the largest displacement from the still water height, h, out of all the recorded waves. The rest of the waves were plotted as a ratio to H_{max}. This allowed the wave shapes to be compared and overlaid to trace similarities. Selected ship wakes were then isolated and described as a double N-wave (Madsen and Schaeffer 2010) by iterations on the six adjustable parameters. The result produced a modeled wake shape with the lowest sum squared error (SSE) as compared to the observed wake.

5. RESULTS:

5.1 Wake characteristics

The dominant feature of all 22 wakes was basically a leading-trough, asymmetrical, inverted solitary wave, observed in pressure sensor data up to 800 m eastward of the shipping channel (Rapaglia et al. 2011).

At PS1 and PS2, 50 and 100 m from the channel, respectively, the arrival of a wake generally was marked by a slight crest (Figure 10), during which the water level increases a few centimeters for a period of 20 to 60 seconds. This is followed by the dominant feature, which is a sharp decrease in water depth to its lowest point within the next 20 to 30 seconds, characteristic of a leading-trough wave. The water level then returns in between 4 and 10 seconds, less time than its draw-out, and oscillates around the still-water level for minutes after the ship passage. The characteristics of all the trough sizes at the S4, 100 m from the channel, are shown in Table 2. The largest trough recorded by the S4 had a displacement of 0.64 m over 30 seconds from the ship Grande Sicilia (Appendix I). The smallest trough observed had a displacement of 0.04 m over 22 seconds at PS1 created by the ship East Coast (Appendix I). A typical example of the wave shape near the channel is shown in Figure 10.

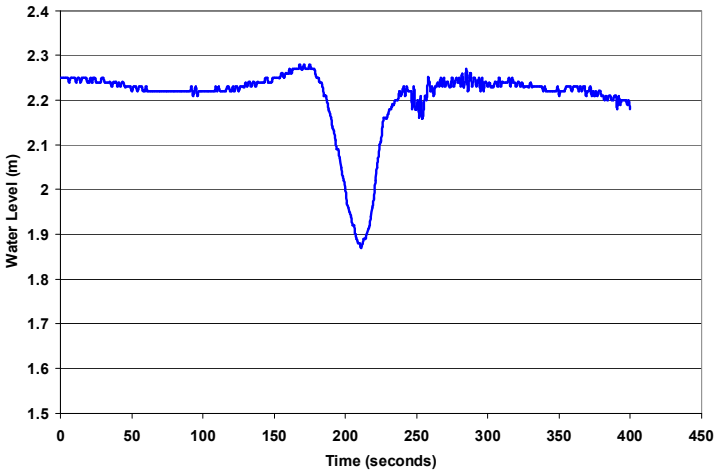

Figure 10: Typical wake shape seen close to the channel (50-100 m). Wake of Calajunco M (16.394) at PS1, with a trough displacement of 0.40 m.

As the wakes propagate away from the channel, the trough depth decreased (Figure 11**)** while the asymmetry increased. Trough depths tended to be reduced by 50% within 350 m of the channel. At the same time, the trailing edge became steeper.

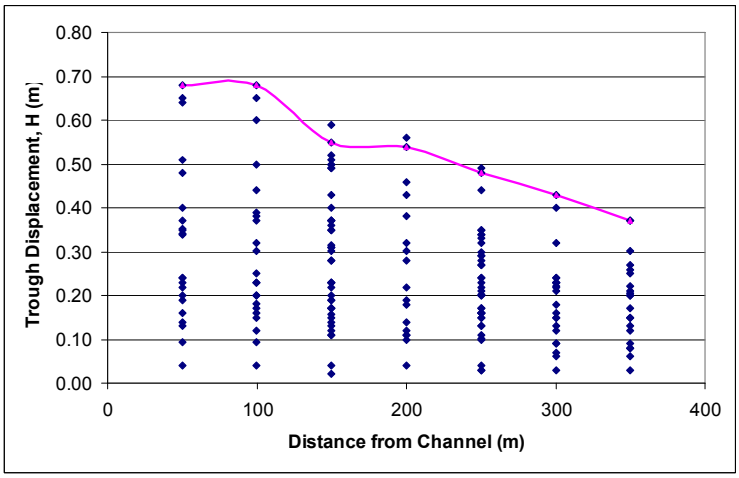

Figure 11: Trough displacements at each pressure sensor for all 22 recorded ships. The ship wake from Hellenic Voyager (16.278) has been connected to illustrate the change in displacement as it propagates away from the channel.

At a distance of 300 to 400m from the channel, the trailing edge was notably steeper, sometimes returning to the still water level within 3 to 5 seconds (Figure 12).

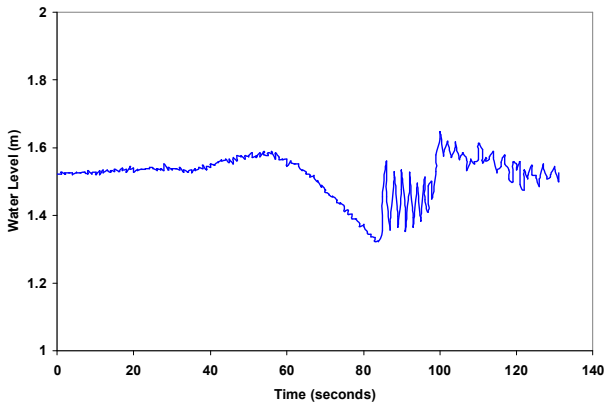

Figure 12: Wake of Coral Leaf (8.440) at PS5 (350 m outside of channel); trailing edge has become very steep.

As previously discussed, Rapaglia et al. (2011) correlated suspended sediment concentrations to F_D and S. This same relationship was used for the trough height at pressure sensor 1 (Figure 13) and produced an R-squared value of 0.81. This suggests that while both ship speed and size influence the size of trough displacement, speed plays a larger role.

The initial trough depth, in meters, might be forecast by:

$$H = 6.9(F_D{}^{3.5} S^{1.6}) + 0.018 \qquad (11)$$

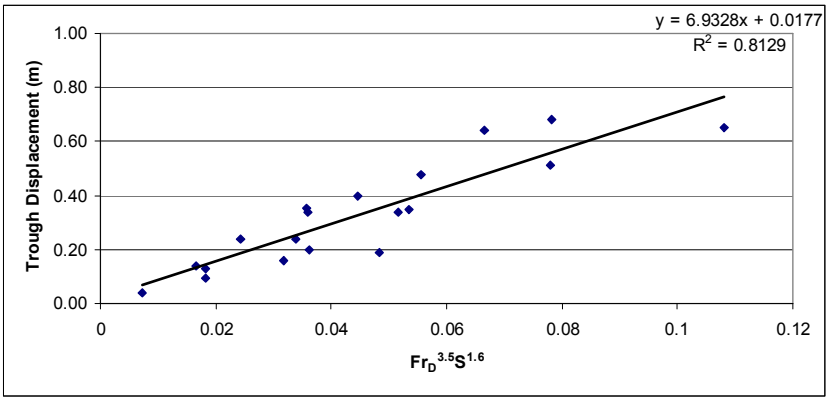

Figure 13: Comparing trough displacements at pressure sensor 1, 50m from the channel, to the relationship of Froude number, $Fr_D^{3.5}$, and blocking coefficient, $S^{1.6}$, determined by Rapaglia et al. 2011 for this location.

5.2 Wake Plane Geometry

The plane-views of wakes were reconstructed from the arrival times of the trough at each pressure sensor and the calculated position of the ships at each arrival time. The distances traveled between PS9 and PS10 as well as between PS7 and PS8 were averaged. This was done because these pressure sensors were equidistant to the middle transect and the angle had to be calculated from one perpendicular transect. The angle of wake propagation, α, is relative to the channel orientation, or in other words, ship's heading. This angle can be calculated three ways. First, the average angle can be calculated by plotting the arrival times of the trough at each pressure sensor and approximating the wakes as a linear feature, (Figure 14). The arctangent of the slope gave the angle of the wakes' propagation relative to the channel orientation and averaged over the distance the wake has traveled. This is referred to as the linear spatially-averaged angle, α_1. The average value of α_1 for all twenty-two cases recorded was 43.6˚. α_1 was slightly larger for outbound ships, 45.7˚, and slightly smaller for inbound ships, 39.96˚. This difference cannot be explained with these data, but it may be due to the ships' speed, because the average speed of outbound ships was 4.7 m/s, while the average speed of inbound ships was 4.4 m/s. The values of α_1 for all wakes are in Appendix II. The plane geometry of the wakes was better described, however, by a second-order polynominal (Figure 15). This angle, α_2, is a function of the distance from the channel.

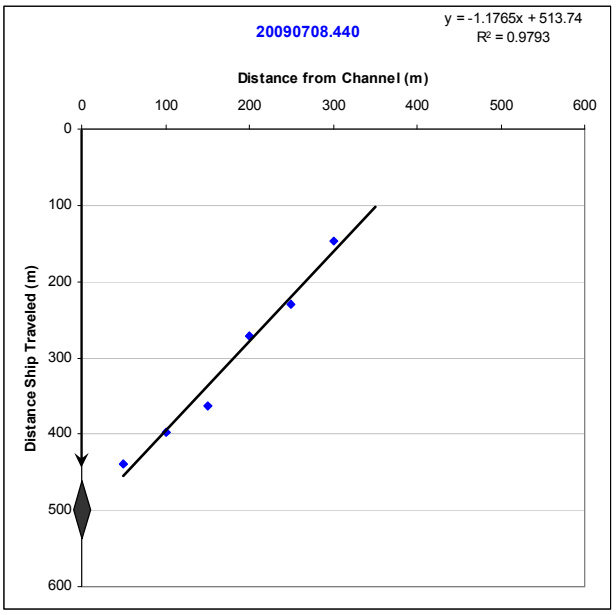

Figure 14: Plane view of the wake from the southbound Coral Leaf (8.440) with a linear fit. The best fit equation is in the top right corner. (All wakes with linear fit in Appendix II). The ship has been traveling downward along the y-axis and would be at a distance along the channel of about 430 m at the instant this wake is plotted.

The derivative of the polynomial evaluated at x =0 defines the angle of the wake as it leaves the channel. When the arctangent for this resulting slope is calculated, it yields a polynomial spatially-averaged angle, α_2, representing the wake's angle at the channel's edge. The average value of α_2 for all twenty-two cases recorded was 24˚. It was slightly smaller for outbound ships, 20˚ and slightly larger for inbound ships, 33˚. The wake angle relative to the channel decreased with distance from the channel, creating a concave shape as the wake propagates from the channel. There were three cases where the opposite happened, the angle seemed to increase with distance from the channel, creating a convex shape as it propagated. For the ships Lia Ievoli (8.510), Mar Elena (16.292) and Wehr Elbe (16.494) the wake angle appeared to increase slightly with distance from the channel rather than to decrease (Appendix III), creating a concave polynomial fit that was not seen in any other data. The wakes from these ships had a better linear fit than the others; the convex shape seemed to be an artifact of the scatter in the data rather than a physical anomaly in the wake propagation. The polynomial fits for all wakes are in Appendix III.

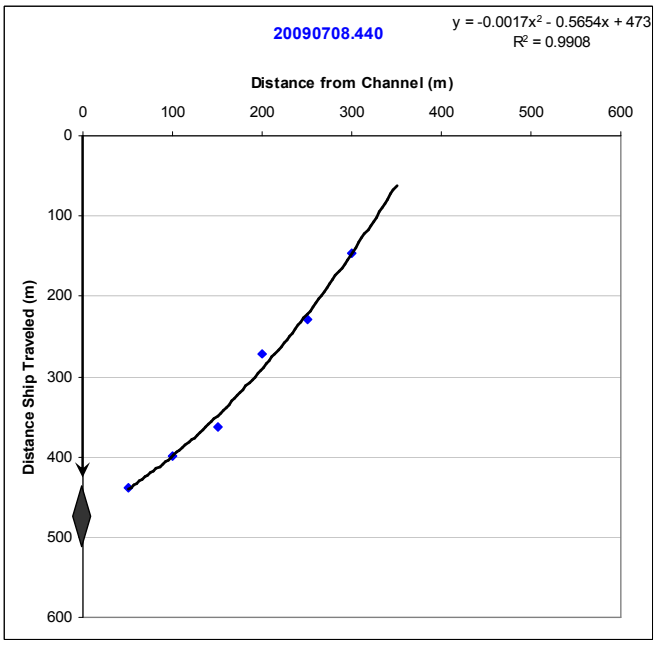

Figure 15: Plane view of southbound Coral Leaf's wake described as a second-order polynomial equation. (All wakes with polynomial fit can be found in Appendix III).

The third calculation of the propagation angle was based on the theoretical celerity of the wake which was taken to be a vector perpendicular to the wake's trough. The angle calculated this way was called α_3; it is the angle that the wake makes with respect to the channel orientation at any distance from the channel. The wake's celerity was assumed to be perpendicular to the wake's trough, with a theoretical celerity, c, of a shallow water wave, $c = \sqrt{g(h+H)}$ where g is the acceleration due to gravity, h is the still water depth and H is the height of the wave, in this case, the depth of the trough below still water. H is therefore less than zero. The velocity of propagation along the lines of sensors, v, was calculated using the known distance between pressure sensors, ΔD, and the difference in arrival times, ΔT, between two pressure sensors, so

$$v = \frac{\Delta D}{\Delta T} \qquad (12)$$

The celerity and speed of propagation were used to approximate the angle of propagation along perpendicular transects using similar triangles (Figure 16). The angle, α_3, was then calculated:

$$\alpha_3 = \cos^{-1}\left(\frac{c}{v}\right) \qquad (13)$$

The angle was calculated along the middle transect (PS1-PS4) because it contained the most pressure sensors and therefore provided the best spatial resolution. Values ranged between 22˚ and 84˚ at 100 m from the channel, then decreased with distance. Values ranged from 13˚ to 73˚ at a distance of 300 m from the channel. α_3 should be the same as α_2 but it was not (Figure 17a and 17b). The analysis was redone using equation 5 for c instead of its approximation (equation 6) without substantially changing the results. There was a strong correlation between these two calculated angles for outbound ships with an R^2 of 0.65 (Figure 17a).

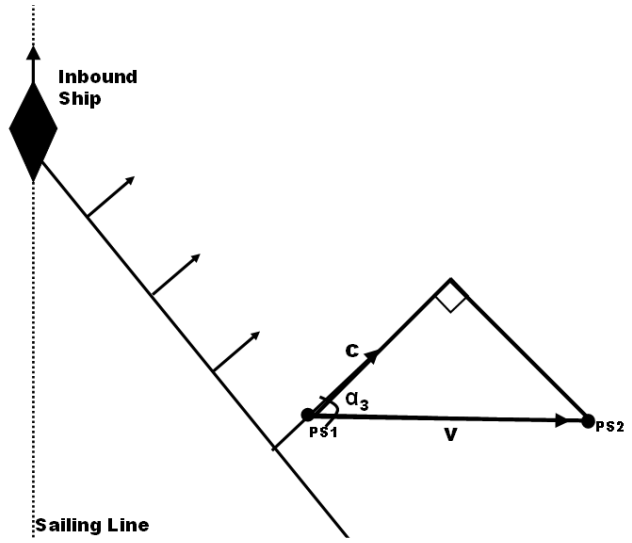

Figure 16: A schematic depicting wave angle derivation. Where $c = \sqrt{g(h+H)}$, $v = \frac{\Delta D}{\Delta T}$, and $\alpha_3 = \cos^{-1}\left(\frac{c}{v}\right)$ This uses an inbound (north-heading) ship as an example, however, the same method was used for outbound ships.

While α_2 values were similar in magnitude close to the channel for the outbound ships, α_3, calculated from the celerity, was smaller than that defined by the polynomial fit to the plane wake. That is, the angle calculated from the celerity, α_3, was more acutely oriented with respect to the channel. Far from the channel the situation was reversed. The values of α_3 from the inbound ships were poorly correlated to α_2, having an R^2 of 0.2 (Figure 17b). The two outliers, labeled in Figure 17a, are Wehr Elbe and Mar Elena, both measured at PS4. When removed, the R^2 value increases to 0.55.

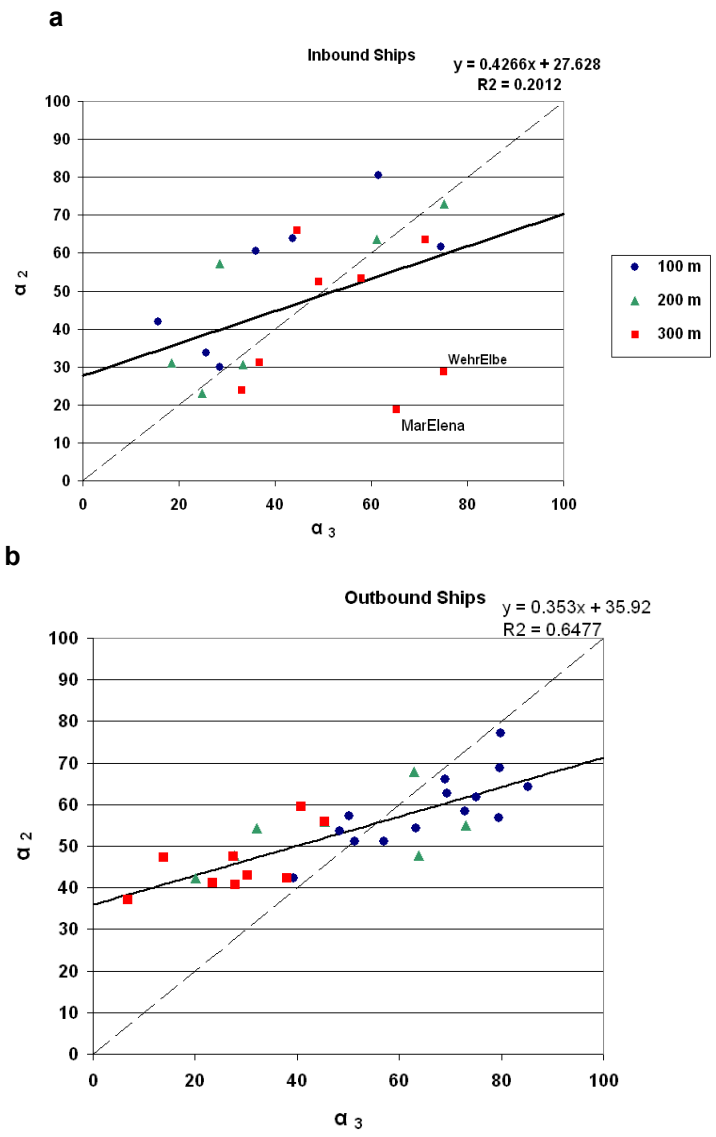

Figure 17a and 17b: Comparing $\alpha_1$to α_2 for inbound ships (top, a) and outbound ships (bottom, b). The solid line is the best fit for each, with the equation at the top right. The dotted line is a 1:1 line for reference.

5.3 Water velocity

Water particle velocity was detected only after the passing of wakes with trough depths greater than 0.2 m. For example, East Coast (8.562, Appendix IV) shows no water velocities generated by wake. Under the small crest at the beginning of each wake, water travels away from the channel perpendicular to the wake of the trough, southeast for outbound ships and northeast for inbound ships. The particle velocity direction then reverses to be directed towards the channel and increases speed as the leading edge of the trough draws the water surface down. Figure 18a for inbound ship Grande Sicilia (8.304) shows the water level while Figure 18b shows the displacement plot for the recorded particle velocities at that site. As the leading crest of the wake arrived (points 16 to 46 in Figure 18b), the velocity was directed away from the channel in a northeast direction at speeds of about 0.25 m/s. As the water level dropped, forming the leading edge of the trough (points 46 to 74 in Figure 18b), the water flowed towards the channel in a southwest orientation, and the speed increased to 1 m/s. The maximum particle speed of this wave, 2.1 m/s, occurred under the trailing edge (points 74-76 in Figure 18b) of the trough, in the direction of wake propagation.

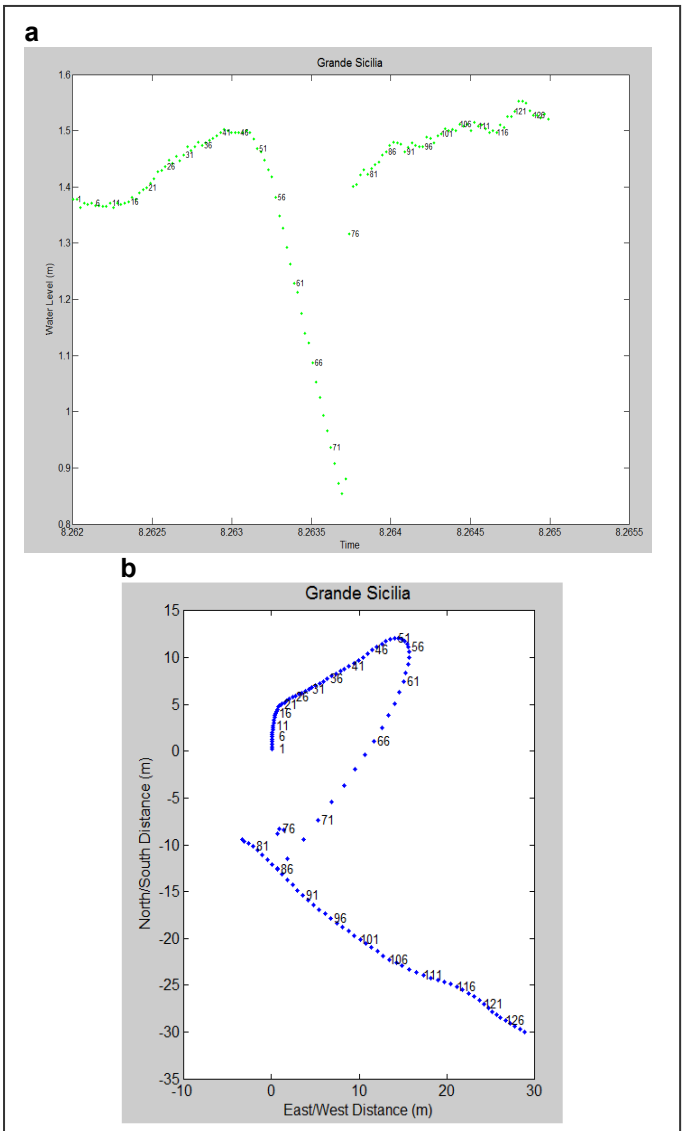

Figure 18a, 18b: S4 water level record on top (a), distance plot on bottom (b) for inbound ship, Grande Sicilia (8.304). Plots have the same start and stop times for the event, therefore each data point is a function of time on both plots. The data points have been labeled with successive numbers so that the wave progress can be tracked in the progressive vector plot. All water level and distance plots for ships recorded by the S4 are located in Appendix IV.

The outbound ship Novorossiysk Star (13.813), showed a similar pattern (Figures 19a, 19b). The small leading trough (points 1 to 71) corresponded to particle flow roughly in the direction of wave propagation, away from the channel at speeds of about 0.27 m/s. The water particle speed increased to 1.2 m/s under the leading edge of the trough as the water level rapidly dropped (points 71 to 121). The flow was back towards the channel, opposite to the direction of wake propagation. The particle velocity, 1.3 m/s, occurred under the trailing edge of the trough as the water returned towards its still-water height. As the trailing crest passed (after point 431) the velocity almost returned to

previous levels, flowing between 0.25 m/s and 0.32 m/s, in the direction of the wake propagation (Figures 19a, 19b). Water level and distance plots for all wakes are in Appendix IV.

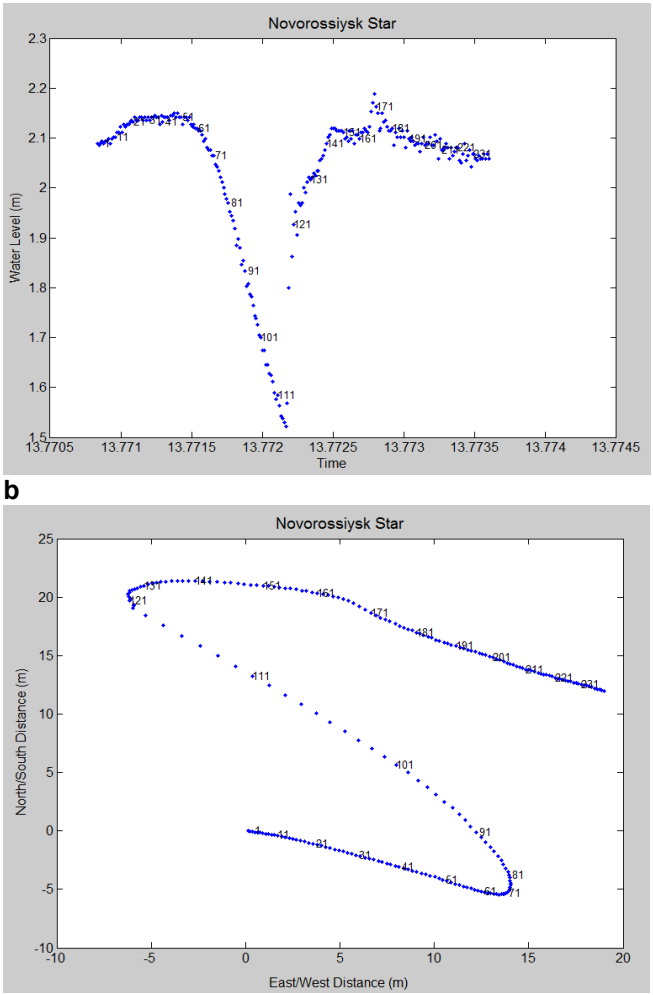

Figure 19a, 19b: S4 water level record on top (a), distance plot on bottom (b) for outbound ship, Novorossiysk Star (13.813). Plots have the same start and stop times for the event, therefore each data point is a function of time on both plots. The data points have been labeled with successive numbers so that the wave progress can be tracked in the progressive vector plot. All water level and distance plots for ships recorded by the S4 are located in Appendix IV.

5.4 Suspended Sediment Concentrations

Suspended sediment concentrations were observed to increase quickly to high levels if the trough depth was greater than about 0.15 m except when ships followed one another in quick succession. Ambient concentrations tended to be between 50 and 100 mg/L and concentrations reached values over 380 mg/L (the saturation value of the instrument) after the passage of the largest wakes.

These two vessels generated waves with the highest boundary shear stress, well above the critical erosion stress: Grande Sicilia (8.304) and Novorossiysk Star (13.813). The suspended sediment concentration recorded by the S4 was above the detection limit for 4 minutes after the passing of Grande Sicilia (8.304), meaning that concentrations were greater than 380 mg/L for that time. After this maximum, the sediment concentration decreased to 100 mg/L over a period of about 10 minutes, which was the previous ambient concentration prior to the wave passage. Maximum boundary stress and recorded suspended sediment values for each wave event are tabulated in Table 2 and plotted in Figure 20.

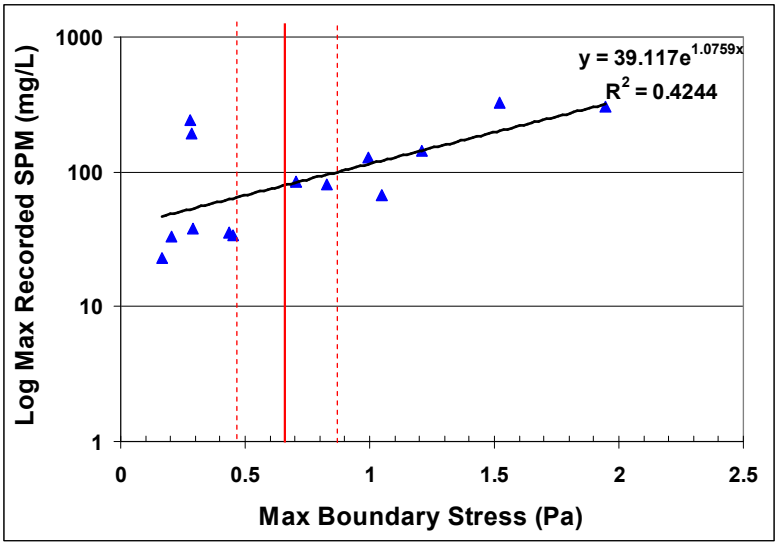

Figure 20: Maximum boundary stress (Pa), calculated using recorded water velocity, versus the maximum recorded suspended sediment concentration (mg/L). The two wake events that maxed out the sensor are not included, as they do not represent an accurate measurement of SPM. The solid red line indicates the critical stress Amos et al. (2004) concluded for this region of the Venice Lagoon, 0.68 Pa, and the dotted lines indicate the range of error the y also suggest, ± 0.20 Pa.

Theoretical sediment resuspension was calculated using shear stresses derived from recorded water velocity based on the sediment-flux relationships determined by Amos et al. (2004), described on page 9. The largest calculated stress value was 11.58 Pa, created by Grande Sicilia (8.304) when the water speed reached a maximum at 2.13 m/s. The plot of the stress was very erratic at its peak, a possible indication that the instrument was moving during the passage of the wake. The smallest stress value was 0.09 Pa, created by TK Istanbul (15.697).

Sediment flux was calculated for ship wakes that exceeded 0.68 Pa boundary stress (Appendix V), the critical stress for sediment movement discussed by Amos et al. (2004). This value seemed reasonable for this location, given the data in Table 2 (Figure 20). For example, the predicted concentration was produced for the wake of Grande Sicilia (8.304), shown in Figure 21a, using the relationship from Amos et al. (2004) and a settling velocity of 0.00041 m/sec, also from Amos et al. (2004). The initial rapid increase in concentration is well represented, but the predicted concentrations do not seem to reach the high concentrations observed, nor did the concentrations go down fast enough after the passage of the wake. A better fit was produced using the following relationship:

$$\log_{10}(F) = 0.6\ln(\tau) - 2.5846 \qquad (14)$$

shown in Figure 21a.

Table 2: Trough displacement, maximum water speed, maximum boundary stress and maximum recorded suspended sediment concentrations at the S4, located 100 m from the channel. Maximum recorded SPM values with an * after them indicate that the sensor reached its limit, therefore these are underestimates of the suspended sediment concentration actually in the water column. [S4 data includes the first 16 of the 22 wakes.]

Ship ID	Name	Trough Displacement, H (m)	Max Water Speed (m/s)	Max Boundary Stress (Pa)	Max Recorded SPM (mg/L)
Inbound:					
8.304	Grande Sicilia	0.6	2.12	11.58	381.46*
8.510	Lia Ievoli	0.20	0.33	0.286	191.85
8.562	East Coast	0.04	0.28	0.208	33.41
13.707	Clipper Karina	0.23	0.42	0.453	33.67
Outbound:					
8.365	Tucana	0.16	0.64	1.046	67.92
8.440	Coral Leaf	0.30	0.87	1.944	302.93
8.443	MV Nurettin Amca	0.09	0.33	0.281	241.96
8.647	Jia Xing	0.17	0.52	0.702	83.68
8.659	Ain Zeft	0.23	0.41	0.437	35.47
13.743	St. Constantine	0.12	0.26	0.169	22.96
13.785	MSC Mirella	0.25	0.57	0.828	81.66
13.813	Novorossiysk Star	0.65	1.28	4.24	381.46*
15.697	TK Istanbul	0.15	0.33	0.29	38.21
15.726	Uni Assent	0.32	0.62	0.99	127.45
15.984	Salerno Express	0.37	0.68	1.20	142.52
16.042	M/T Tigullio	0.38	0.77	1.52	328.18

This is only a slight alternative of the equation originally deduced from the graphs of Amos et al. (2004) and this new relationship could easily be consistent with the data because the actual data were not given in Amos et al. (2004). To get the concentrations to decline as quickly as observed, a settling velocity of 0.0035 m/s, ten times that measured by Amos et al. (2004), had to be used. It is possible that newly resuspended particles in high concentrations do, in fact, have a much higher settling velocity. It should be pointed out, however, that the observed decrease included not only settling but also advection of the suspended sediment cloud past the sensor; the calculated values assume only vertical settling and the settling speed used in the prediction therefore may be artificially high.

Figure 21b illustrates the suspended sediment after the passage of Novorossiysk Star (13.813), again using Equation 13 and a settling velocity of 0.0035 m/s. There is a noticeable time lag of about 25 seconds. At lower shear stress, and hence lower rates of resuspension, the time lag was likely due to the time it takes the resuspended cloud to reach the elevations of the turbidity sensor from the sea floor. These two ships created the highest water velocities, with Grande Sicilia producing twice

the velocity of Novorossiysk Star, and Novorossiysk Star producing a velocity at least twice that of any other ship that passed. All predictions for suspended sediment concentrations are shown in Appendix V.

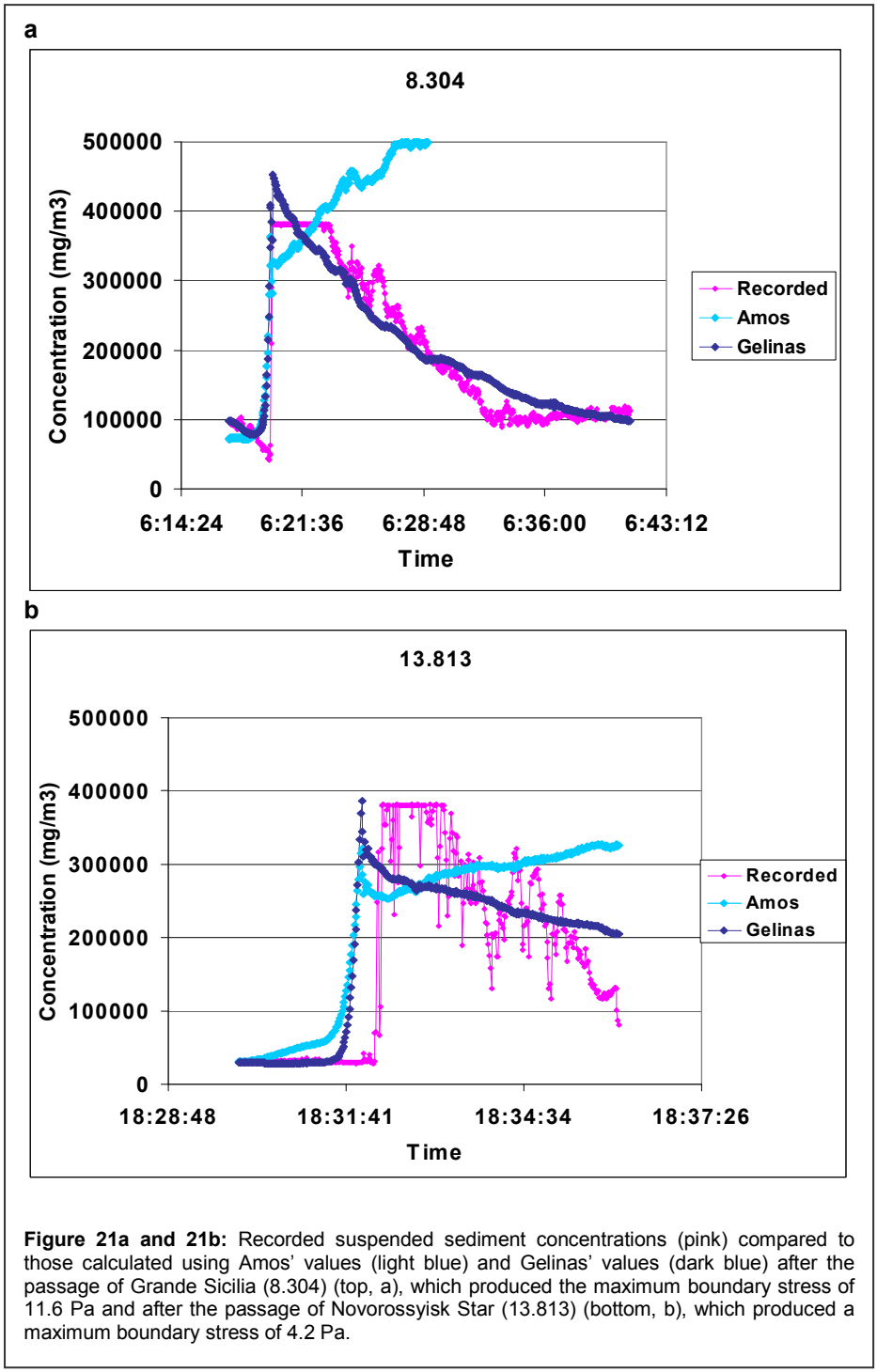

Figure 21a and 21b: Recorded suspended sediment concentrations (pink) compared to those calculated using Amos' values (light blue) and Gelinas' values (dark blue) after the passage of Grande Sicilia (8.304) (top, a), which produced the maximum boundary stress of 11.6 Pa and after the passage of Novorossyisk Star (13.813) (bottom, b), which produced a maximum boundary stress of 4.2 Pa.

5.5 Modeling the Water Level

Although a single, inverted solitary wave (Equation 4) captures the dominant, leading trough of these wakes, a better description of the water level seemed to be that of an N-wave, in particular, a double N-wave as described by equation 5.1 from Madsen and Schaeffer (2010). A double N-wave was used to model the water levels of 4 wakes at 10 sensors, for a total of 40 waves:

$$\eta_i\,(x_0,\,t) = A_1\mathrm{sech}^2\Omega_1(t - t_1) - A_2\mathrm{sech}^2\Omega_2(t - t_2) \qquad (7)$$

This is only one of many possible solutions to the Korteweg de Vries wave equation and the most appropriate solution would depend on the initial conditions. The initial conditions were not known for these observations, however, this equation produced fairly accurate representations of the observed wakes capturing not only the leading trough but some minor features as well. The highest calculated summed square error was 0.22.

The principal aspects of the wakes can all be produced using this equation: The small leading crest followed by a dominant trough was readily produced, as shown after the passing of Tucana (8.365) in Figure 22.

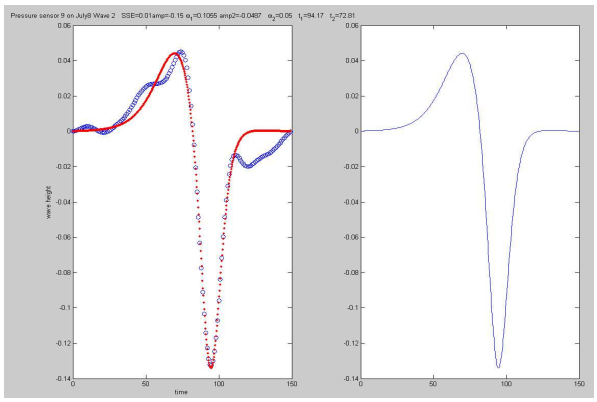

Figure 22: Plot of Tucana (8.365) wake shape at PS9, modeled wake shape highlighting the leading crest. In left panel, the blue circles show recorded water level and red shows modeled wake using parameters. Right panel shows modeled wake shape only.

In addition, the small, trailing crest can also be modeled (Figure 23).

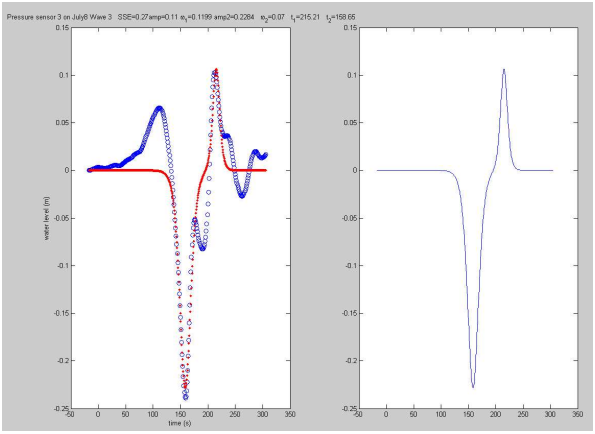

Figure 23: Plot of Coral Leaf (8.440) wake shape at PS3 with model highlighting the trailing crest. In left panel, the blue circles show recorded water level and red shows modeled wake using parameters. Right panel shows modeled wake shape only.

A slight infliction was sometimes seen in the leading edge of the trough as the water level decreased, which the double N-wave could also reproduce (Figure 24). However, the waves are too complex and the equation has too many parameters to deduce an exact equation at each pressure sensor. In fact, with the same input of recorded data, the procedure could produce two completely different solutions, as seen in Figure 25a and 25b. The same start and stop times were given for the wave of Coral Leaf (8.440), at PS3, however, when the amplitude and time parameters were altered in the program, the equation fit either the first or ending crest of the wave. The time parameters can be used to resolve crests and troughs in the wave to be modeled and the program adjusted the other parameters to create the best fit around those times. The ranges of fits are shown in Appendix VI and the values of the fitted parameters tabulated (Table 3).

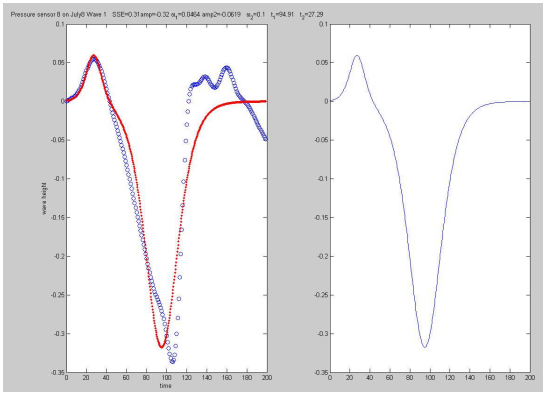

Figure 24: Plot of Grande Sicilia (8.304) wake shape at PS8 with model highlighting inflection sometimes seen after leading crest. In left panel, the blue circles show recorded water level and red shows modeled wake using parameters. Right panel shows modeled wake shape only.

There were instances where start and stop times had to be altered to get the program to model the desired aspects of the wave. For example, the program detected a small second trough that started to form in the wave from Coral Leaf (8.440) at PS4, Figures 26a-26c. This signal was so strong that the start and stop times had to be altered to get the program to fit the larger form of the wave. The start time was increased to 90 seconds and the end time truncated at 240 seconds, producing the form in Figure 26b.

When the start time was changed to 110 seconds and the end time truncated at 250 seconds, the program preferably modeled the ending crest of the wave, Figure 26c. Adjusting the start and stop times redefined the wave shape for Matlab program to fit. Doing this forced the program to produce the lowest SSE possible relative to the data it was given. Nevertheless, it seemed that the Korteweg de Vries wave equation was the proper one to apply to the wakes of large ships in confined channels and that a double N-wave solution might be adequate to describe the wakes.

a

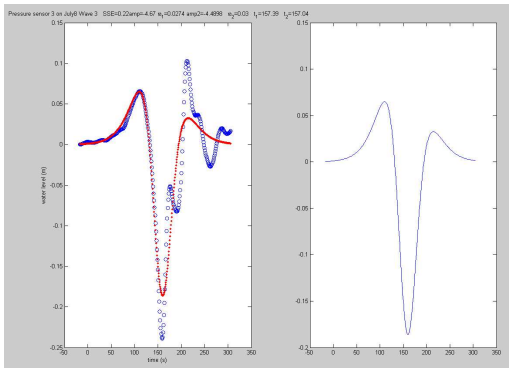

b

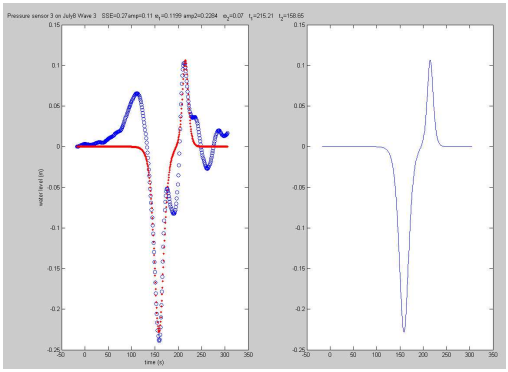

25a and 25b: Matlab analysis of water level at PS 3 for the wake produced by Coral Leaf (8.440). In the top figure, the blue circles are the recorded water levels from the pressure sensor and the red dots are the program's best fit. The best fit is plotted by itself on the right. In 25b (bottom), amplitude and t were altered to get Matlab to fit the ending crest of the wave.

Table 3: Tabulated parameters used for N-wave fits to wave data.

Ship ID	PS #	Start Time	End Time	Amp 1	Ω1	Amp2	Ω2	t1	t2	SSE	Notes
8.304	1	100	270	-0.69	0.071	-0.16	0.02	110.04	94.3	0.09	
	2	100	290	-0.53	0.084	-0.14	0.03	123.37	64.75	0.51	
	3	150	350	-0.36	0.058	-0.12	0.05	110.02	38.05	0.35	
	4	150	350	-0.22	0.061	-0.13	0.05	140.09	61.28	0.28	Fit to leading peak
	4.1	200	350	-0.3	0.029	-0.17	0.11	92.62	118.17	0.06	Fit to trailing trough
	5	175	375	-0.19	0.069	-0.08	0.07	95.61	29.98	0.14	
	7	150	300	-0.29	0.076	-0.12	0.06	90.38	28.36	0.29	
	8	200	400	-0.32	0.046	-0.06	0.1	94.91	27.29	0.31	
	9	125	250	-0.46	0.090	-0.11	0.08	80.57	30.62	0.32	
8.365	1	100	250	-0.15	0.111	-0.05	0.06	62.48	43.31	0.03	
	2	100	250	-0.14	0.115	-0.05	0.05	69.61	44.89	0.02	
	3	100	250	-0.13	0.110	-0.04	0.04	97.71	63.63	0.01	
	4	100	250	-0.1	0.096	-0.04	0.04	128.28	89.15	0.03	
	5	150	300	-0.11	0.092	-0.03	0.03	106.33	65.18	0.11	
	7	150	300	-0.13	0.098	-0.04	0.04	74.42	41.7	0.03	
	8	100	300	-0.12	0.101	-0.03	0.04	90.57	57.48	0.09	
	9	100	250	-0.15	0.106	-0.05	0.05	94.17	72.81	0.01	
	10	100	200	-0.14	0.106	-0.03	0.05	62.66	37.96	0.01	Fit to leading peak
	10.1	100	250	-0.14	0.130	0.06	0.05	63.07	115.62	0.05	Fit to trailing trough
8.440	1	x	x	-0.3	0.083	-0.07	0.03	129.03	96.18	0.07	Fit to leading peak
	1.1	x	x	0.05	0.130	0.29	0.1	202.29	129.71	0.19	Fit to trailing peak
	2	x	x	-0.27	0.074	0.07	0.03	134.51	97.49	0.14	Fit to leading peak
8.440	2.1	x	x	0.09	0.154	0.27	0.09	202.2	135.25	0.21	Fit to trailing peak
	3	x	x	-4.67	0.027	-4.49	0.03	157.39	157.04	0.22	Fit to leading peak

Ship ID	PS #	Start Time	End Time	Amp 1	Ω1	Amp2	Ω2	t1	t2	SSE	Notes
8.440	3.1	x	x	0.11	0.120	0.23	0.07	215.21	158.65	0.27	Fit to trailing peak
	4	90	240	14.48	0.023	14.64	0.02	96.35	96.37	0.06	Fit to leading peak
	4.1	x	x	0.06	0.066	0.15	0.05	241.58	186.51	0.22	Fit to trailing peak
	4.2	x	x	0.27	0.104	0.36	0.07	193.04	190.72	0.27	Fit to secondary trough
	5	x	x	-12.44	0.025	-12.28	0.02	211.09	211.04	0.1	Fit to leading peak
	5.1	x	x	0.07	0.079	0.16	0.05	260.67	213.51	0.21	Fit to trailing peak
	5.2	100	300	-0.19	0.064	0.10	0.18	110.77	137.35	0.11	Fit to secondary trough
	7	x	x	0.1	0.135	0.24	0.08	240.74	186.29	0.18	Fit to trailing peak
	8	x	x	0.07	0.096	0.17	0.05	218	150.18	0.22	Fit to trailing peak
	9	x	x	0.3	0.081	0.05	0.03	160.13	121.75	0.07	Fit to leading peak
	9.1	x	x	0.06	0.140	0.29	0.09	227.63	160.79	0.14	Fit to trailing peak
	10	x	x	0.09	0.112	0.24	0.08	188.32	124.57	0.44	Fit to trailing peak

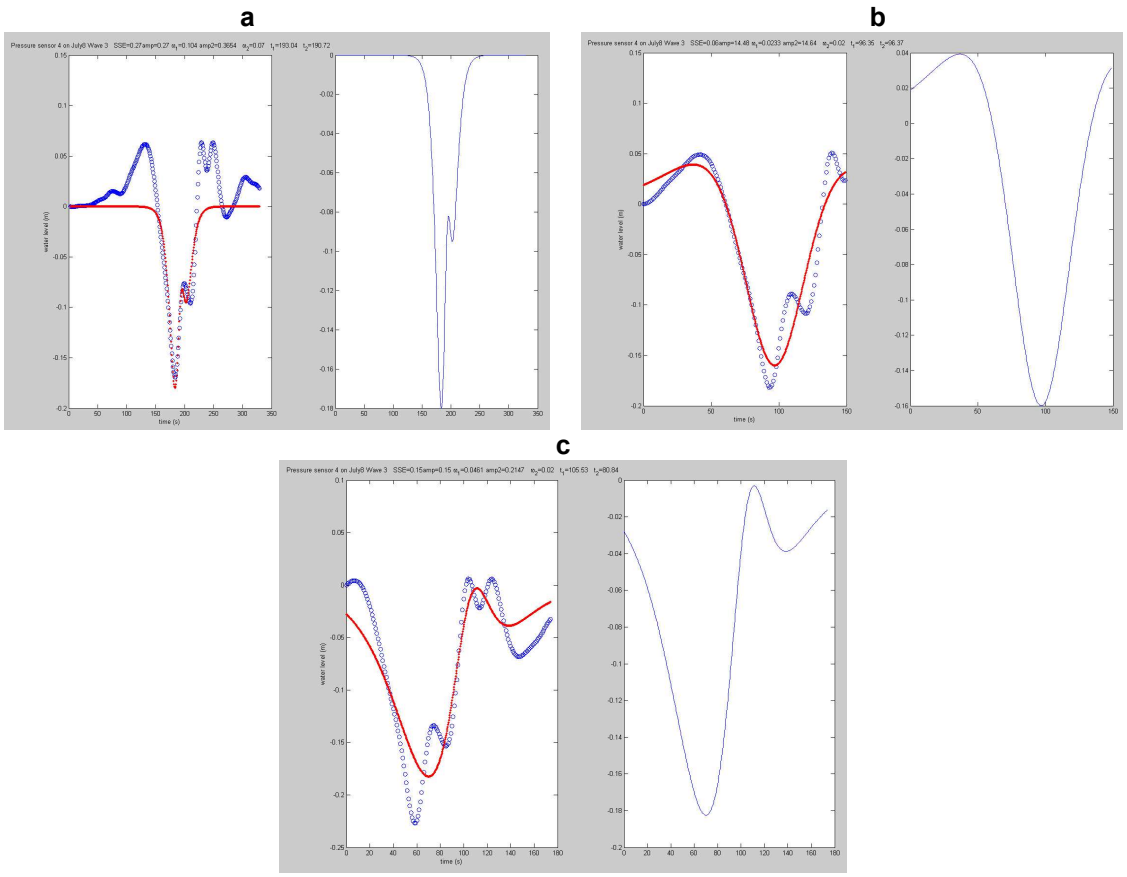

Figures 26a - 26c: Wake from Coral Leaf (8.440), as seen in Figure 26a and 26b, but now at PS4. In 26a (upper left), a small second trough has formed and is strong enough to be picked up by the Matlab program. In the left panel, the blue circles are recorded water level data and the red is the Matlab program best fit, the right panel is a plot of the modeled/best fit by itself. 26b (upper right) shows that the program cannot model the larger wave form until the start time is increased by 90 seconds and the stop time is truncated at 240 seconds because the secondary trough signal is so strong. In the left panel, the blue circles are recorded water level data and the red is the Matlab program best fit, the right panel is a plot of the modeled/best fit by itself. In 26c, (bottom middle) the start time is increased to 110 seconds but the end time is extended a bit longer, truncated at 250 seconds, and the program fits the trailing crest of the wave.

6. DISCUSSION

The wakes in this study are characterized by a solitary, asymmetrical trough that propagates up to 800 m along the shallow adjacent shoals of the Malamocco-Marghera shipping canal (Rapaglia et al. 2011), generating water velocities that exceed erosion thresholds in the Venice Lagoon**.** Wave impacts may, therefore, be responsible for the high erosion rates documented in the lagoon, 0.5m over 30 years (Molinaroli et al. 2009); however, wave action was not considered as a cause. The results of this study suggest that wakes from large industrial ships could have a substantial role in this erosion. Furthermore, a recent proposal to reroute cruise ships through this canal could enhance

this erosion, as cruise ships are larger than the industrial ships studied here. Additionally, these shoals are known to have high concentrations of POPs, toxic, sediment-bound contaminants. It is, therefore, valuable to be able to predict how a ship will affect sediment dynamics based on its wake size and propagation direction. Different aspects of the wake will be discussed separately to best analyze how to predict them.

6.1 Wake Characteristics

Trough displacements tend to decrease with distance from the channel, as shown in Figure 11. As previously discussed, Rapaglia et al. (2011) correlated suspended sediment concentrations to the blocking coefficient, S, and depth-based Froude number, F_D, raised to 1.6 and 3.5, respectively. This same relationship was used for the trough height at pressure sensor 1 (Figure 13) and produced an R-squared value of 0.81. This prediction could be useful to forecast the effect of rerouting cruise ships through this area, as proposed by the Port Authority of Venice. At the end of this field campaign a cruise ship, MSC Poesia, did actually pass the study site; it was being rerouted due to an event in the city of Venice. There is not a complete data set for this wake; however, there were pressure sensors still in the water as the ship passed and its dimensions and speed were obtained from the AIS, allowing calculation of its blocking coefficient and Froude number (Table 4). Equation 11 was used to predict the trough displacement this ship would make, yielding a value of 0.68 m at PS1. The recorded pressure sensor data at that

Table 4: Data for MSC Poesia, a cruise ship that passed at the end of sampling campaign. Only pressure sensor and AIS data were obtained.

Ship ID	Name	Speed (m/s)	Length (m)	Width (m)	Draft (m)	Displace. (m3)	S	Fr_D
18.301	MSC Poesia	4.1	293	36	7.8	82274.4	0.113	0.37

location showed a trough displacement of 0.73 m. This is a fairly accurate prediction and proves that the relationship between S and Fr_D is consistent when applied to cruise ships. In addition, both the predicted and actual trough depths were larger than anything created by the industrial ships studied at this location.

These two parameters do not correlate as well when considered separately. The blocking coefficient determines the displacement of water relative to the channel, which will dictate the extent of the pressure gradient setup by the ship's passage. This pressure gradient will in turn affect the water velocity around the ship. However, the ship speed is already affecting water velocity; therefore Froude number cannot be ignored. The exponential relationship indicated that, while both ship speed and size influence the size of trough displacement, speed plays a larger role. It should be noted that the draft used to calculate the blocking coefficient was obtained through the AIS. This value is

automatically set to a ship's nominal draft. It can be updated once the ship is loaded or unloaded, however, this is not always the case. Therefore the draft used to calculate the blocking coefficient may not be accurate at the time the ship passed the study site. The changes in wave shape as it propagates onto the shoals were likely due to differences in wave celerity between the trough and the crest. The trough moves more slowly than the trailing crest. As the wave propagates away from the channel, the time between the lowest point of the trough and the following crest should decrease because the crest would be overtaking the trough without passing it. This can be seen as the trailing edge of the trough becomes steeper with distance from the channel. After the passage of the trough, secondary, possibly transverse, waves followed (Figure 12).

6.2 Plane Wake Geometry

The wake's plane shape is best determined from an array of pressure sensors set in a single line perpendicular to the channel. This allows the best resolution to see how the wake changes as it propagates onto the shoals. From the ship's speed and the arrival time at sequential sensors, the wake shape can be described well as a second order polynomial. In contrast to other types of wakes, the angle that the wake makes with the channel is initially high, almost 90°, and then decreases to values that can be less than 20°. The original intention for calculating the angle of propagation was to correlate the numbers to the typical Kelvin wedge values, possibly identifying whether the propagating waves were from the divergent or transverse wave trains. However, the wakes were already altered at the study site 50 m outside the canal, assumedly due to the extreme shoaling bathymetry between the channel and the shoals. It became clear that the wake could not be attributed to the Kelvin wedge, particularly because of the strong nonlinearity in its shape.

The nonlinearity of the wake propagation can be best attributed to the shoaling water depths as the wave moves away from the shipping channel. This causes variations in propagation speed and creates non-linear plane wake geometry. The wave celerity, c, is defined as $c = \sqrt{g(h+H)}$. In this case, H is less than zero because each wave event is characterized by a trough. The absolute value of H decreased with distance from the channel, which would cause the celerity to increase if h remained the same. However, the still water height, h, also decreases from 2.5 m to 1.6 m in the first 200 m from the channel, and then remains relatively the same from 200-350 m. The ratio of H/h tended to increase to a maximum at 200 m from the channel, and then decrease (Figures 27a and 27b).

It appeared that although the absolute value of H is decreasing, the trough was deepening relative to the still water height until 200 m from the channel. This was consistent with the celerity changes seen as the wave propagates away from the channel, as shown in Figures 27a and 27b. For outbound Coral Leaf (8.440), the celerity decreased from 4.6 m/s to 3.5 m/s in 200 m, and then remained relatively constant from 200m to 350m. The same pattern occurred for inbound Mar Elena (16.494), where the

celerity decreased from 4.5 m/s to 3.1 m/s in the first 200 m, then remained relatively constant. Beyond 200 m, the trough depth appeared to be bounded by the bathymetry and loses energy due to friction, as expected. The H:h ratio decreases as the trough slowly returns towards the still water height. The distinct change in the wave celerity and H:h ratio as the wave propagates away from the channel create the nonlinear plane geometry I calculated. In the first 200 m, the wave travels farther than it does from 200 m to 350 m, creating a stronger non-linear effect closer to the channel and then becoming less as distance increases. The wave slows down significantly after it reaches 200 m due to frictional effects and possible breaking.

The discrepancies between the wake angles determined by the second-order polynomial and those calculated from the theoretical celerity (Figures 17a, 17b) suggest

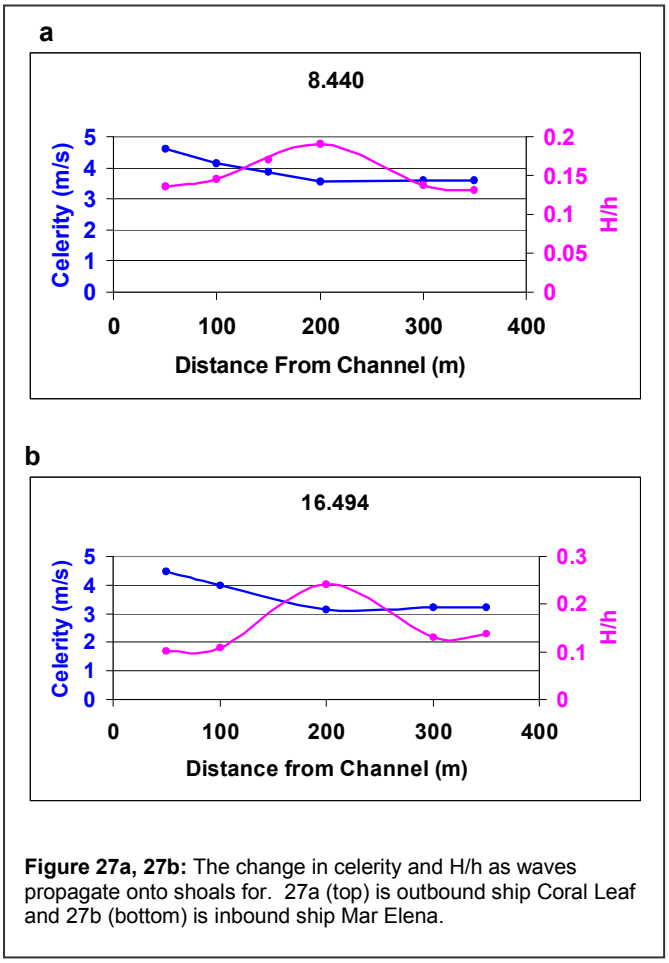

Figure 27a, 27b: The change in celerity and H/h as waves propagate onto shoals for. 27a (top) is outbound ship Coral Leaf and 27b (bottom) is inbound ship Mar Elena.

that these wakes cannot be described by the solitary wave celerity equation. Further work should be done to determine a more accurate velocity formula.

There appear to be real differences in the wake characteristics of inbound and outbound ships. These may be due to slight differences in ship speed of inbound versus outbound ships – inbound ships are typically slowing down while outbound ships are speeding up. However, it is more likely due to differences in bathymetry between the southward approaching wakes and the northern approaching wakes. There was no evidence in the available data to explain the differences.

6.3 Water Velocity

Water level and wake-distance plots were constructed using time series data from the S4, located 100 m from the channel at a height of 0.5 m off of the bottom. Numbering the data points allowed precise correlation between velocity direction and wave phase. Regardless of ships' headings, water particles traveled away from the channel, reversed direction back towards the channel as the trough deepened, then reversed away from the channel as the water level returned. This pattern is consistent with the velocity changes and subsequent pressure gradient created during a Bernoulli wake. The water is still attempting to fill in the displacement of the ship, and this is carried onto the shoals.

There appeared to be a time lag between the lowest point of the trough and the reversal of water velocity direction. The falling leg of the wake might be expected to be in one direction and the returning leg to be in the opposite direction; however in the progressive vector plots (Appendix IV) the velocity changed direction midway through the returning leg. This could be because of the superposition of the wake-generated water velocities on a regional flow or because the S4 was located about 1 m off of the bottom, meaning it was recording water velocity between 1 to 1.5m from the surface, depending on the tide. It therefore recorded surface water level in real time on an upward facing OBS; however, surface water velocity had to be advected through the water column before being recorded on the current meter.

6.4 Suspended Sediment Concentrations

Water column suspended sediment concentrations, recorded on the S4 100 m from the channel, were compared to predicted suspended sediment concentrations using the relationship between boundary stress and associated sediment flux, from Amos et al. (2004). This relationship was adapted to the study location, using values within a possible range of error from interpreting Amos et al.'s findings. This was only done for wakes that created a boundary stress greater than 0.68 Pa, the value Amos et al. (2004) concluded to be critical for sediment flux in this area of the Lagoon (Figure 20). There were two significant outliers, Lia Ievoli (8.510) and MV Nurettin Amca (8.443). These ships created maximum suspended sediment concentrations of 191.85 mg/L and 241.96 mg/L, respectively. These concentrations are three to four times the amount expected from the boundary stress each wake created, 0.3 Pa. This anomaly can be attributed to ships passing in close succession. MV Nurettin Amca (8.443) passed about five minutes after Coral Leaf (8.440). Coral Leaf's (8.440) wake produced a boundary stress of 1.9 Pa, resuspending 242 mg/L. This material may not have had time to settle out of suspension before the wake from MV Nurettin Amca (8.443) passed, causing the suspended sediment recorded for this ship passage to be artificially high.

Lia Ievoli (8.510) passed an hour and a half after four ships passed in close succession. The first of these ships, Grande Sicilia (8.304), created the second-largest

wake recorded and resuspended a massive amount of material. This material did not completely settle after this ship passed because the following wakes kept it in suspension. Sediment that did settle may have been much more easily resuspended because it was still unconsolidated. When Lia Ievoli (8.510) passed, the settled sediment was thoroughly reworked by earlier wakes and the initial suspended concentration was still relatively high, 100 mg/L. The wake actually caused a change of only 91 mg/L in suspended sediment, which was an amount typically seen at the boundary stress it created.

Aside from these two anomalies, not all of the resuspension events could be accurately predicted using the equation for two reasons: the settling velocity from Amos et al. (2004) was too low to accurately show the decrease in suspended sediment after a wake passed, yet the recorded suspended sediment was consistently higher than what was predicted by the equation (Appendix V). Amos et al. (2004) measured settling velocity at all of their sites, and while there were three sites close to this study location, they were not close to the Malamocco-Marghera shipping canal. They were in the central lagoon, but much further east of the canal than this study. As previously discussed, sediment grain size decreases with distance from the canal. Therefore, the suspended sediment at this study site could be larger and therefore settle more quickly than what Amos et al. (2004) saw at their sites. Additionally, a large resuspension event could mobilize aggregated particles from depth in the sediment which would have a greater settling speed than the surface layer. These sediments are compacted at depth and will readily flocculate once resuspended, increasing their settling velocity.

Regarding the higher recorded suspended sediment values than predicted, in a lagoon this shallow, wind waves can affect the bottom, increasing background turbidity and making sediments easier to suspend. Small pleasure boats crossed this shoal frequently, further increasing wave energy and current velocities. This increased wave activity could enhance local currents and advect suspended sediment from other locations. In addition, sediment that is frequently resuspended does not have time to reconsolidate on the seafloor. Its resuspension threshold therefore decreases with increased wave activity.

Resuspension seems to be an important factor contributing to shoaling in the navigation channels and the need for maintenance dredging (Sarretta et al. 2010). Some of this resuspension is due to ships' wakes. The direct return flow back towards the channel under the wake, however, is short-lived and travels only a few tens of meters (Figures 18b, 19b) . In addition, although the tides had been removed from the velocity measurement, there seemed to be a net, perhaps wind-driven, drift to the southeast, away from the channel during this study period. As a result, the net drift of resuspended sediment from these events was away from the channel at the location on the current meter, 100 meters from the channel. Sediment resuspended by the wake within a few tens of meters from the channel's edge could be driven directly back into the channel, however, or under different conditions of wind-driven circulation and tides, resuspended sediment from farther afield could be returned to the chann

6.5 Modeling the Water Level

The equation used to model these wakes was proposed as a model for tsunamis. The wakes in the Venice Lagoon appear to behave similarly to the tsunami characteristics described in Madsen and Schaeffer (2010). While the wakes in the Venice Lagoon are on a substantially smaller scale, they are also created by a displacement of water, and are propagating into shallower water. Their asymmetry increases as they propagate, and steep transient waves can be seen as they move farther away from the channel (Figure 12).

The overall wake shape was accurately modeled using a double N-wave equation from Madsen and Schaeffer (2010) (Appendix IV). Discrete and secondary aspects of the wake could also be produced by manipulating parameters in the equation or adjusting start and stop times for the wake (Figures 24, 26a). The initial conditions were not known for the wakes in this study, therefore an exact equation cannot be determined for each wave. However, it is clear that the equation allows for all wave shapes seen at this location, suggesting that this is a model worth investigating further in future studies to better understand Bernoulli wake propagation in shallow settings.

7. CONCLUSIONS and FUTURE WORK

Bernoulli wakes were recorded and analyzed for 22 passing ships in the industrial Malamocco-Marghera shipping canal in the Venice Lagoon. As they propagated onto the adjacent shoals, these wakes were characterized by a leading-trough, asymmetrical, inverted solitary wave. They created water velocities high enough to resuspend large amounts of sediment.

The angle of propagation changed as the wakes moved onto the adjacent shoals due to bathymetric changes and frictional energy loss. This angle was calculated three different ways. When combined with trough changes and subsequent water velocity changes, trends in the angles of wake propagation suggest where maximum sediment resuspension will occur as the trough moves along the shoals. This angle of propagation was calculated three different ways. The calculation done using the theoretical solitary shallow water wave velocity did not match the calculation done using arrival time at the pressure sensors. This suggests that these waves' propagation speed cannot be described by this theoretical velocity. Further work needs to be done to analyze the wave speed and formulate a more accurate velocity equation.

Although Bernoulli wakes have typically been described as inverted solitary waves, it is proposed that a better description of them is to use a positive and negative N-wave for a model. This model produced accurate wake shapes and could highlight secondary attributes of the wakes; however, further work needs to be done to determine initial conditions. Without them, the equation used to model the wakes has multiple

parameters and can be manipulated to model many different aspects of the wake. This equation has been used in the past to describe tsunami propagation. While the waves in the Venice Lagoon are not a result of a natural disaster, this location may provide a model for tsunami propagation due to its unique bathymetry.

References

Amos, C.L., Bergamasco, A., Umgiesser, G., Cappucci, S., Cloutier, D., DeNat, L., Flindt, M., Bonardi, M., and Cristante, S., 2004. The stability of tidal flats in Venice Lagoon—the results of in-situ measurements using two benthic, annular flumes. *Journal of Marine Systems*, 51, 211–241.

Associated Press, 2009. Venice port expansion threatens city, environmentalists warn. *The Guardian* Sept. 7 http://www.guardian.co.uk/world/2009/sep/07/venice-portperil-Sea 2009.

Bauer, B.O., Lorang, M.S., and Sherman, D.J., 2002. Estimating boat-wake-induced levee erosion using sediment suspension measurements. *Journal of Waterway, Port, Coastal, and Ocean Engineering*, 128, 152–162.

Bellucci, L. G., Frignani, M., Paolucci, D., and Ravanelli, M., 2002. Distribution of heavy metals in sediments of the Venice Lagoon: the role of the industrial area. *The Science of the Total Environment*, 295, 35-49.

Bernadello, M., Secco, T., Pellizzato, F., Chinellato, M., Sfriso, A., and Pavoni, B., 2006. The changing state of contamination in teh Lagoon of Venice. Part 2: Heavy metals. *Chemosphere*, 64, 1334-1345.

Brambati, A., Carbognin, L., Quaia, T., Teatini, P., and Tosi, L., 2003. The Lagoon of Venice: geological setting, evolution and land subsidence. *Episodes*, 26, 264-268.

Cairns, W.R., 2005. AIS and long range identification & tracking. *Journal of Navigation*, 58, 181–189.

Coraci, E., Umgiesser, G., and Zonta, R., 2007. Hydrodynamic and sediment transport modeling in the channels of Venice (Italy). *Estuarine and Coastal Shelf Science,* 75, 250–260.

Didenkulova, I., Parnell, K.E., Soomere, T., Pelinovsky, E., and Kurrenoy, D., 2009. Shoaling and runup of long waves induced by high-speed ferries in Tallinn Bay. *Journal of Coastal Research*, 56, 491–495.

Erm, A., Alari, V., and Listak, M., 2009. Monitoring wave-induced sediment resuspension. *Estonia Journal of Engineering*, 15, 196–211.

Ferrarin, C., Cucco, A., Umgiesser, G., Bellafiore, D., and Amos, C.L., 2010. Modelling fluxes of water and sediment between Venice Lagoon and the sea. *Continental Shelf Research*. 30, 904-913.

Gaĉić, M., Kovaĉević, V., Mazzoldi, A., Paduan, J., Mancero, I., Arena, F., and Gelsi, G., 2002. Measuring water exchange between the Venetian Lagoon and the open sea. *EOS Trans. A.G.U.* 83, 217–222.

Goldberg, E.D., 1995. Emerging problems in the coastal zone for the twenty-first century. *Marine Pollution Bulletin,* 31, 152–158.

Gourlay, T.P., 2006. A simple method for predicting the maximum squat of a high-speed displacement ship. *Marine Technology*, 43, 146–151.

Gourlay, T.P., 2008. Slender body methods for predicting ship squat. *Ocean Engineering,* 35, 191–200.

Hayes, K.R., and Sliwa, C., 2003. Identifying potential marine pests—a deductive approach applied to Australia. *Marine Pollution Bulletin*, 46, 91–98.

Hennings, I., Romeiser, R., Alpers, W., and Viola, A. 1999. Radar imaging of Kelvin arms of ship wakes. *International Journal of Remote Sensing*, 20, 2519-2543.

Hjulström. 1935. Studies in the morphological activity of rivers as illustrated by the river Fyris. Geological Institute at the Univiversity of Uppsala Bulletin, 25, 221–528.
Hofmann, H., Lorke, A., and Peeters, F., 2008. The relative importance of wind and ship waves in the littoral zone of a large lake. *Limnology and Oceanography*, 53, 368–380.
Houser, C., 2010. Relative importance of vessel-generated and wind waves to salt marsh erosion in a restricted fetch environment. *Journal of Coastal Research*, 26, 230–240.
Komar, Paul D. *Beach Processes and Sedimentation*. New Jersey: Prentice-Hall, Inc. 1998.
Lin, Y.-H. and Hwang, H.-H., 2008. The Fission Process of N-Waves over a Mild Slope. *Journal of Fluid Mechanics*, 24, 205-214.
Madsen, Per A., and Schaeffer, Hemming A., 2010. Analytical solutions for tsunami runup on a plane beach: single waves, N-waves and transient waves. *Journal of Fluid Mechanics*, 543, 27-57.
MAV-CVN, 2004. Attivita di aggiornamento del piano degli interventi per il recupero morfologico in aplicazione della delibera de Consiglio del Minstri del 15 Marzo 2001. Studi di base, linee guida e proposte di intervento del piano morfologico. Magistrato alle Acque di Venezia. Consorzio Venezia Nuova, Venice Italy. Technical Report.
Molinaroli, E., Guerzoni, S., Sarretta, A., Masiol, M., and Pistolato, M., 2009. Thirty-year changes (1970 to 2000) in bathymetry and sediment texture recorded in the Lagoon of Venice sub-basins, Italy. *Marine Geology*, 258, 115–125.
Nanson, G.C., von Krusentierna, A., Bryant, E.A., and Renilson, M.R., 1994. Experimental measurements of river-bank erosion caused by boat generated waves on the Gordon River, Tasmania. *Regional Rivers Resource Management*, 9, 1–14.
Neil, D.T., Orpin, A.R., Ridd, E.V., and Yu, B.F., 2002. Sediment yield and impacts from river catchments to the Great Barrier Reef lagoon. *Marine and Freshwater Research*, 53, 733–752.
Oebius, H., 2000. Charakterisierung der einflussgrößen schiffsumströmung und propellerstrahl auf die wasserstraßen. Mitteilungsblatt der Bundesanstalt für Wasserbau Nr. 82. . 16 pp.
Osborne, P.D., and Boak, E.H., 1999. Sediment suspension and morphological response under vessel-generated wave groups: Torpedo Bay, Auckland, New Zealand. *Journal of Coastal Research*, 15, 388–398.
Parnell, K.E., Kofoed-Hansen, H., 2001. Wakes from large high-speed ferries in confined coastal waters: management approaches with examples from New Zealand and Denmark. *Coastal Management*, 29, 217–237.
Parnell, K., Delpeche, N., Didenkulova, I., Dolphin, T., Erm, A., Kask, A., Kelpšaite, L., Kurennoy, D., Quak, E., Räämet, A., Soomere, T., Terentjeva, A., Torsvik, T., and Zaitseva-Pärnaste, I., 2008. Far-field vessel wakes in Talinn Bay. *Estonian Journal of Engineering*, 14, 273–302.
PIANC, 2003. Guidelines for managing wake wash from high-speed vessels. Report of the Working Group 41 of the Maritime Navigation Commission. International Navigation Association (PIANC), Brussels. 32 pp.

Port of Venice Website, 2010. http://www.port.venice.it/pdv/Home.do?metodo=carica_home201027 May 2010.
Racanelli, S. and Bonamin, V., 2000. Dioxins in the Venice Lagoon: Present Situation, Projects and Recovering Hypotheses. *Environmental Science and Pollution Research*, 7, 125-129.
Rapaglia, J., Zaggia, L., Ricklefs, K., Gelinas, M., and Bokuniewicz, H., 2011. Characteristics of ships' depression waves and associated sediment resuspension in Venice Lagoon, Italy. *Journal of Marine Systems*, 85, 45-56.
Ravens, T.M., and Thomas, R.C., 2008. Ship wave-induced sedimentation of a tidal bore in Galveston Bay. *Journal of Waterway, Port, Coastal, and Ocean Engineering*, 134, 21–29.
Reed, A.M., and Milgram, J.H., 2002. Ship Wakes and their Radar Images. *Annual Review of Fluid Mechanics*, 34, 469-502.
Ricciardi, A., and Rasmussen, J.B., 1998. Predicting the identity and impact of future biological invaders: a priority for aquatic resource management. *Canadian Journal of Fishery and Aquatic Sciences,* 55, 1759–1765.
le Roux, J.P. 2001. A simple method to predict the threshold of particle transport under oscillatory waves. *Sedimentary Geology*, 143, 59-70.
Sarretta, A., Pillon, S., Molinaroli, E., Guerzoni, S., Fontolan, G. (2010). Sediment Budget in the Lagoon of Venice, Italy. *Continental Shelf Research*, 30, 934-949.
Schoellhamer, D.H., 1996. Anthropogenic sediment resuspension mechanisms in a shallow microtidal estuary. *Estuarine and Coastal Shelf Science*, 43, 533–548.
Secco, T., Pellizzato, F., Sfriso, A., and Pavoni, B., 2005. The changing state of contamination in the Lagoon of Venice. Part 1: organic pollutants. *Chemosphere*, 58, 279-290.
Small, C., Nicholls, R.J., 2003. A Global Analysis of Human Settlement in Coastal Zones. *Journal of Coastal Research,* 19, 584-599.
Smith, G., 2009. International shipping the lifeblood of global economic growth: as the global economy goes, so goes shipping and related industries. *The RMA Journal*, 4 pp.
Sternberg, R.W. "Predicting initial motion and bedload transport of sediment particles in shallow marine environments." In *Shelf Sediment Transport: Processes and Patterns*, edited by Swift, D.J.P., Duane, D.B., and Pilkey, O.H., 61-82. Stroudsburg, PA: Dowden, Hutchinson and Ross, Inc, 1972.
Soomere, T., 2007. Nonlinear components of ship wake waves. *Applied Mechanical Review*, 60, 120–138.
Soomere, T., Kask, A., Kask, J., and Nerman, R., 2007. Transport and distribution of bottom sediments at Pirita Beach. *Estonian Journal of Earth Science*, 56, 233–254.
Soomere, T., Parnell, K., and Didenkulova, I., 2009. Implications of fast-ferry wakes for semisheltered beaches: a case study at Aegna Island, Baltic Sea. *Journal of Coastal Research*, 56, 128–132.
Soomere, T., and Kask, J., 2003. A specific impact of waves of fast ferries on sediment transport processes in Tallinn Bay. *Proceeds of Esonian. Academy of Sciences, Biology and Ecology*, 52, 319–331.
Stewart, Robert H. *Introduction to Physical Oceanography*. Texas A&M: Open

University, 2004.
Tadepalli, S. and Synolakis, C.E., 1994. The run-up of N-waves on sloping beaches. *Proceedings: Mathematical and Physical Sciences*, 445, 99-112.
Tadepalli, S., and Synolakis, C.E., 1996. Model for the leading waves of tsunamis. *PhysicalReview Letters*, 77, 2141–2144.
Umgiesser, G., Sclavo, M., Carniel, S., and Bergamasco, A., 2004. Exploring the bottom stress variability in the Venice Lagoon. *Journal of Marine Systems*, 51, 161–178.
Velegrakis, A.F., Vousdoukas, M.I., Vagenas, A.M., Karambas, T., Dimou, K., and Zarkadas, T., 2007. Field observations of waves generated by passing ships: a note. *Coastal Engineering,* 54, 369–375.
Wiberg, P.L., and Sherwood, C.R., 2008. Calculating wave-generated bottom orbital velocities from surface-wave parameters. *Computational Geoscience*, 34, 1243–1262.
Zonta, R., Botter, M., Cassin, D., Pini, R., Scattolin, M., and Zaggia, L., 2007. Sediment chemical contamination of a shallow water area close to the industrial zone of Porto Marghera (Venice Lagoon, Italy). *Marine Pollution Bulletin*, 55, 529–5

Appendix I:

Ships, identified by ID number, with pressure sensor number, distance from channel, still water height, h, maximum trough depth, and the difference between the two, H. [Data obtained from pressure sensors for all 22 wakes.]

Ship Name Ship ID	Pressure sensor #	Distance From Channel (m)	Still Water Height, h (m)	Max Trough Depth (m)	Trough, H (m)
INBOUND:					
Grande Sicilia	1	50	1.77	1.119	0.65
8.304	2	100	1.33	0.73	0.60
	3	200	0.95	0.52	0.43
	4	300	0.98	0.66	0.32
	5	350	0.92	0.72	0.20
	7	250	0.95	0.61	0.34
	8	250	0.99	0.66	0.33
	9	150	1.19	0.7	0.49
	10	150	1.16	0.65	0.51
Lia Ievoli	1	50	2.67	2.48	0.19
8.510	2	100	2.29	2.09	0.20
	3	200	1.76	1.65	0.11
	4	300	1.76	1.67	0.09
	5	350	1.75	1.66	0.09
	7	250	1.8	1.67	0.13
	8	250	1.81	1.64	0.17
	9	150	2.12	1.97	0.15
	10	150	1.98	1.78	0.20
East Coast	1	50	2.77	2.73	0.04
8.562	2	100	2.36	2.32	0.04
	3	200	1.88	1.84	0.04
	4	300	1.83	1.8	0.03
	5	350	1.83	1.8	0.03
	7	250	1.88	1.84	0.04
	8	250	1.89	1.86	0.03
	9	150	2.2	2.16	0.04
	10	150	2.06	2.04	0.02
Clipper Karina	1	50	2.81	2.57	0.24
13.707	2	100	2.25	2.02	0.23
	3	200	1.77	1.49	0.28
	4	300	1.71	1.47	0.24

Ship ID	Pressure-sensor #	Distance From Channel (m)	Still Water Height, h (m)	Max Trough Depth (m)	Trough, H (m)
Clipper Karina	5	350	1.74	1.49	0.25
13.707	7	250	1.75	1.48	0.27
	8	250	1.77	1.53	0.24
	9	150	2.09	1.81	0.28
	10	150	1.92	1.7	0.22
Hellenic Voyager	1	50	2.41	1.73	0.68
16.278	2	100	1.82	1.14	0.68
	3	200	1.67	1.13	0.54
	4	300	1.33	0.9	0.43
	5	350	1.32	0.95	0.37
	7	250	1.28	0.8	0.48
	8	250	1.33	0.9	0.43
	9	150	1.63	1.1	0.53
	10	150	1.54	0.99	0.55
Wehr Elbe	1	50	2.43	1.92	0.51
16.292	2	100	1.94	1.44	0.50
	3	200	1.55	1.17	0.38
	4	300	1.29	1.06	0.23
	5	350	1.28	0.98	0.30
	7	250	1.32	1.12	0.20
	8	250	1.33	1.01	0.32
	9	150	1.74	1.25	0.49
	10	150	1.53	1.03	0.50
Mar Elena	1	50	2.28	2.05	0.23
16.494	2	100	1.83	1.63	0.20
	3	200	1.32	1	0.32
	4	300	1.23	1.07	0.16
	5	350	1.23	1.06	0.17
	7	250	1.24	1	0.24
	8	250	1.25	1.01	0.24
	9	150	1.62	1.41	0.21
	10	150	1.41	1.2	0.21
MSC Leader	1	50	2.3	2.08	0.22
16.508	2	100	1.85	1.67	0.18

Ship ID	Pressure-sensor #	Distance From Channel (m)	Still Water Height, h (m)	Max Trough Depth (m)	Trough, H (m)
MSC Leader	4	300	1.22	1.1	0.12
16.508	5	350	1.21	1.06	0.15
	7	250	1.2	1.04	0.16
	8	250	1.23	1.04	0.16
	9	150	1.63	1.44	0.19
	10	150	1.4	1.22	0.19
OUTBOUND:					
Tucana	1	50	2.11	1.97	0.14
8.365	2	100	1.7	1.54	0.16
	3	200	1.21	1.07	0.14
	4	300	1.19	1.06	0.13
	5	350	1.17	1.05	0.12
	7	250	1.21	1.06	0.15
	8	250	1.24	1.09	0.15
	9	150	1.55	1.38	0.17
	10	150	1.42	1.25	0.17
Coral Leaf	1	50	2.49	2.15	0.34
8.440	2	100	2.06	1.76	0.30
	3	200	1.58	1.28	0.30
	4	300	1.53	1.32	0.21
	5	350	1.52	1.32	0.20
	7	250	1.57	1.28	0.29
	8	250	1.578	1.36	0.22
	9	150	1.904	1.59	0.31
	10	150	1.77	1.46	0.31
MV Nurettin Amca	1	50	2.46	2.37	0.09
8.443	2	100	2.05	1.96	0.09
	3	200	1.57	1.46	0.11
	4	300	1.52	1.46	0.06
	5	350	1.53	1.47	0.06
	7	250	1.52	1.49	0.03
	8	250	1.6	1.53	0.07
	9	150	1.91	1.77	0.14
	10	150	1.78	1.67	0.11

Ship ID	Pressure-sensor #	Distance From Channel (m)	Still Water Height, h (m)	Max Trough Depth (m)	Trough, H (m)
Jia Xing	1	50	2.68	2.48	0.20
8.647	2	100	2.27	2.10	0.17
	3	200	1.77	1.65	0.12
	4	300	1.74	1.65	0.09
	5	350	1.73	1.65	0.08
	7	250	1.77	1.66	0.11
	8	250	1.78	1.68	0.10
	9	150	2.108	1.95	0.16
	10	150	1.96	1.83	0.13
Ain Zeft	1	50	2.63	2.39	0.24
8.659	2	100	2.22	1.99	0.23
	3	200	1.73	1.51	0.22
	4	300	1.7	1.52	0.18
	5	350	1.7	1.50	0.20
	7	250	1.73	1.49	0.24
	8	250	1.75	1.55	0.20
	9	150	2.05	1.82	0.23
	10	150	1.93	1.70	0.23
St. Constantine	1	50	2.69	2.56	0.13
13.743	2	100	2.13	2.01	0.12
	3	200	1.65	1.55	0.10
	4	300	1.58	1.51	0.07
	5	350	1.59	1.51	0.08
	7	250	1.64	1.51	0.13
	8	250	1.64	1.54	0.10
	9	150	1.96	1.84	0.12
	10	150	1.81	1.70	0.11
MSC Mirella	1	50	2.57	2.23	0.34
13.785	2	100	2	1.75	0.25
	3	200	1.53	1.34	0.19
	4	300	1.47	1.32	0.15
	5	350	1.47	1.32	0.15
	7	250	1.51	1.31	0.20
	8	250	1.52	1.36	0.16
	9	150	1.83	1.55	0.28

Ship ID	Pressure-sensor #	Distance From Channel (m)	Still Water Height, h (m)	Max Trough Depth (m)	Trough, H (m)
MSC Mirella	10	150	1.69	1.46	0.23
Novorossiysk Star	1	50	2.47	1.83	0.64
13.813	2	100	1.91	1.26	0.65
	3	200	1.47	0.91	0.56
	4	300	1.38	0.98	0.40
	5	350	1.4	1.03	0.37
	7	250	1.42	0.93	0.49
	8	250	1.43	0.99	0.44
	9	150	1.75	1.23	0.52
	10	150	1.59	1.00	0.59
TK Istanbul	1	50	2.87	2.71	0.16
15.697	2	100	2.18	2.03	0.15
	4	300	1.64	1.49	0.15
	5	350	1.67	1.54	0.13
	7	250	1.7	1.54	0.16
	8	250	1.72	1.55	0.17
	9	150	2.01	1.87	0.14
	10	150	1.91	1.74	0.17
Uni Assent	1	50	2.87	2.52	0.35
15.726	2	100	2.18	1.86	0.32
	4	300	1.66	1.44	0.22
	5	350	1.68	1.47	0.21
	7	250	1.71	1.44	0.27
	8	250	1.7	1.49	0.21
	9	150	2.02	1.67	0.35
	10	150	1.91	1.60	0.31
Salerno Express	1	50	2.34	1.99	0.35
15.984	2	100	1.66	1.29	0.37
	4	300	1.11	0.87	0.24
	5	350	1.12	0.92	0.20
	7	250	1.15	0.85	0.30
	8	250	1.2	0.91	0.29
	9	150	1.49	1.12	0.37
	10	150	1.38	1.03	0.35

Ship ID	Pressure-sensor #	Distance From Channel (m)	Still Water Height, h (m)	Max Trough Depth (m)	Trough, H (m)
M/T Tiguillo	1	50	2.32	1.95	0.37
16.042	2	100	1.61	1.23	0.38
	4	300	1.08	0.86	0.22
	5	350	1.11	0.89	0.22
	7	250	1.12	0.83	0.29
	8	250	1.11	0.88	0.23
	9	150	1.45	1.08	0.37
	10	150	1.34	0.98	0.36
Calajunco M	1	50	2.27	1.87	0.40
16.394	2	100	1.82	1.43	0.39
	3	200	1.21	1.03	0.18
	4	300	1.18	0.95	0.23
	5	350	1.19	0.92	0.27
	7	250	1.2	0.86	0.34
	8	250	1.18	0.90	0.28
	9	150	1.6	1.23	0.37
	10	150	1.39	0.96	0.43
Hokuetsu Ace II	1	50	2.27	1.79	0.48
16.410	2	100	1.82	1.38	0.44
	3	200	1.4	0.94	0.46
	4	300	1.17	0.94	0.23
	5	350	1.17	0.91	0.26
	7	250	1.19	0.84	0.35
	8	250	1.21	0.86	0.35
	9	150	1.6	1.20	0.40
	10	150	1.4	0.90	0.50

Appendix II

Plane wake view, linear fit

INBOUND SHIPS:

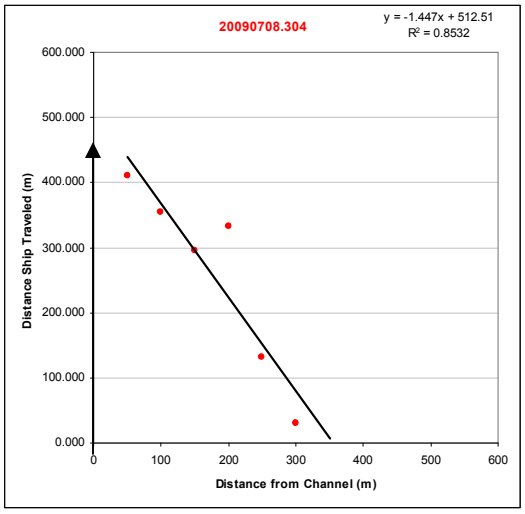

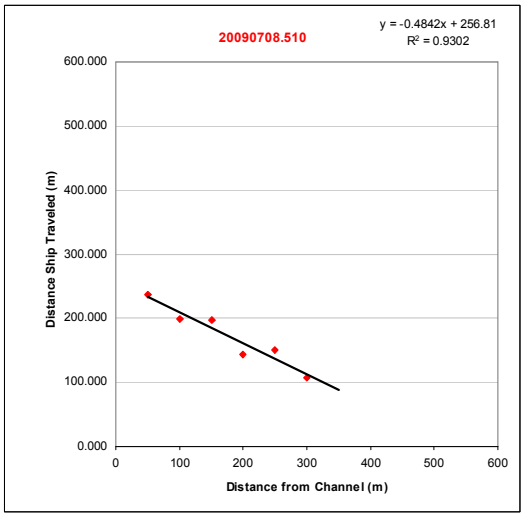

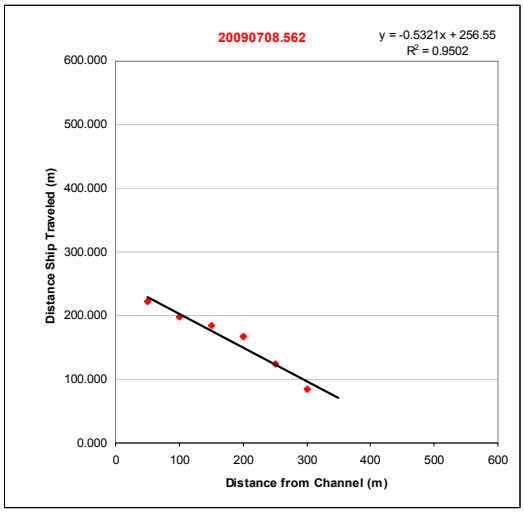

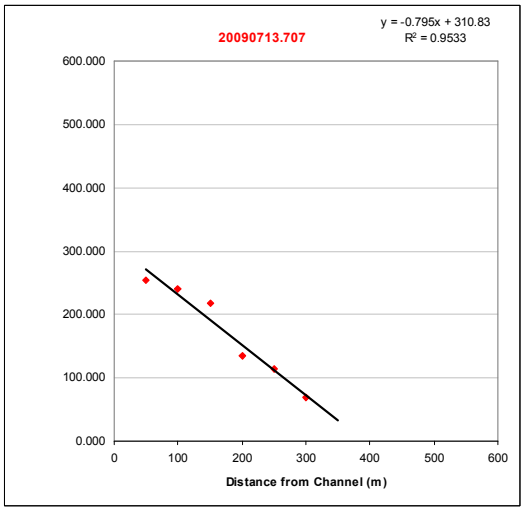

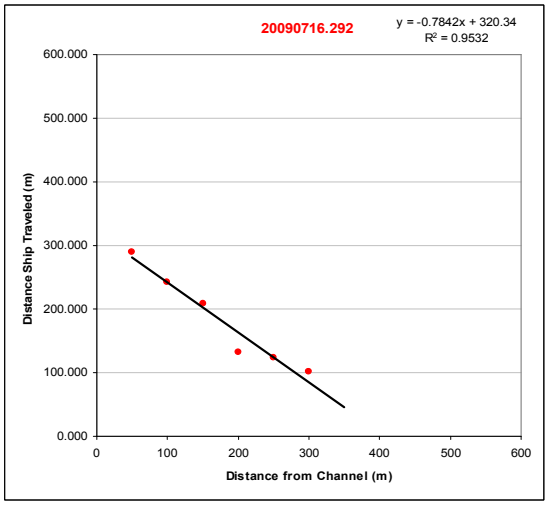

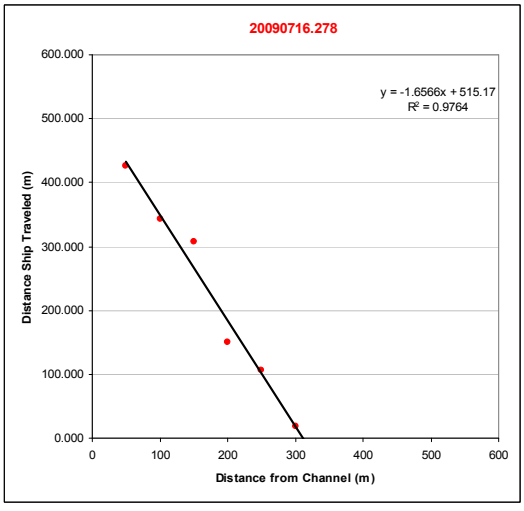

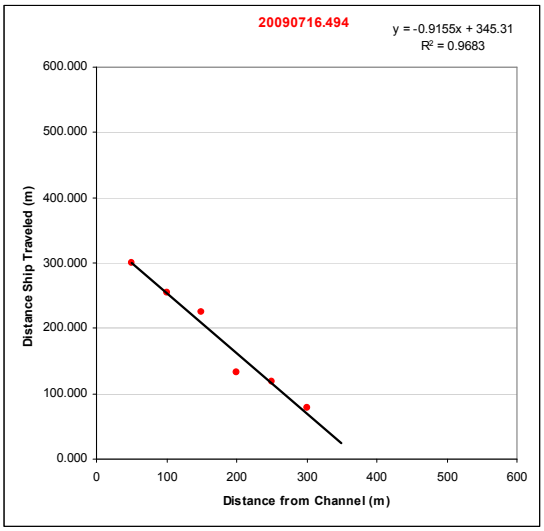
20090716.494
y = -0.9155x + 345.31
R² = 0.9683
600.000
500.000
400.000
300.000
200.000
100.000
0.000
Distance Ship Traveled (m)
0
100
200
300
400
500
600
Distance from Channel (m)

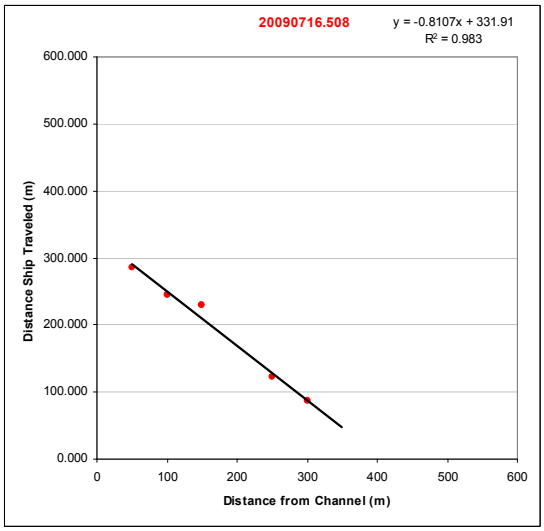
20090716.508
y = -0.8107x + 331.91
R² = 0.983
600.000
500.000
400.000
300.000
200.000
100.000
0.000
Distance Ship Traveled (m)
0
100
200
300
400
500
600
Distance from Channel (m)

OUTBOUND SHIPS:

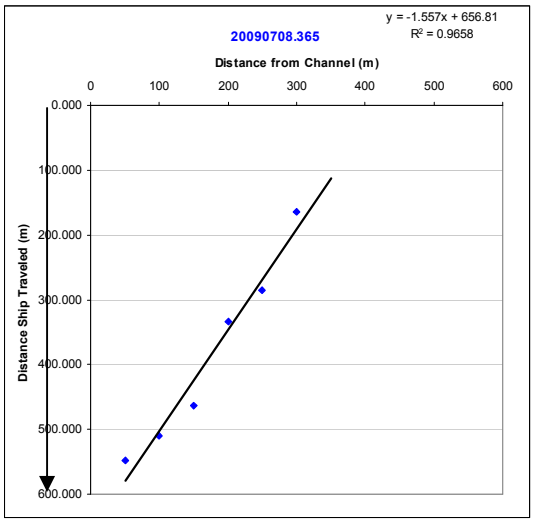

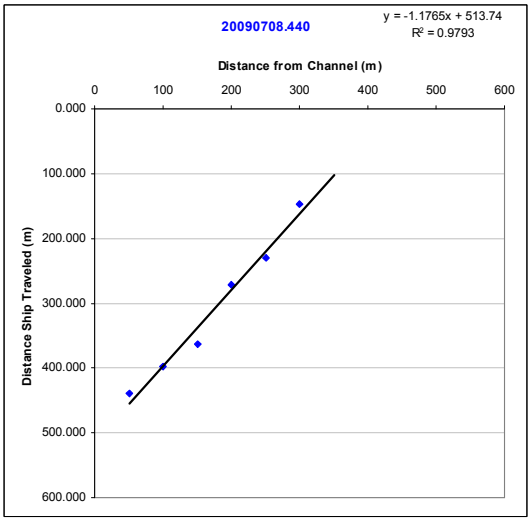

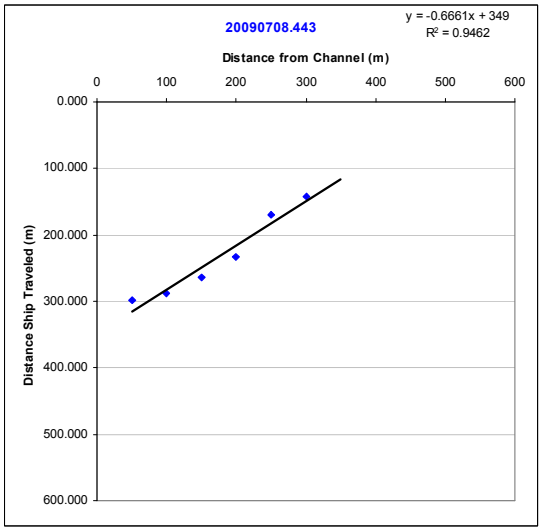

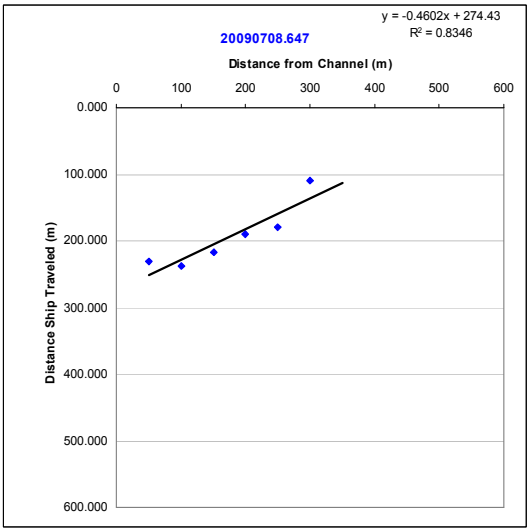

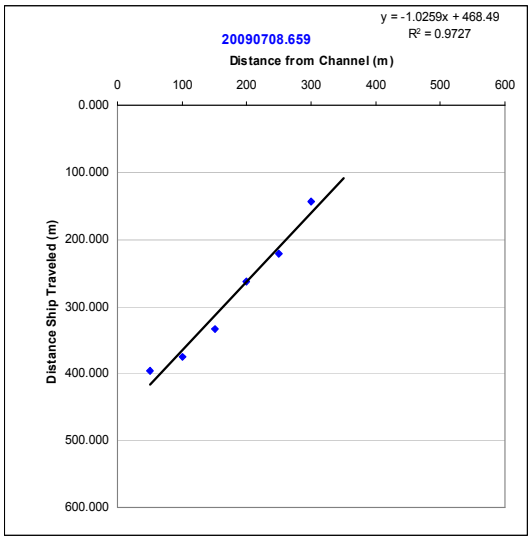
y = -1.0259x + 468.49
R² = 0.9727
20090708.659
Distance from Channel (m)
0
100
200
300
400
500
600
Distance Ship Traveled (m)
0.000
100.000
200.000
300.000
400.000
500.000
600.000

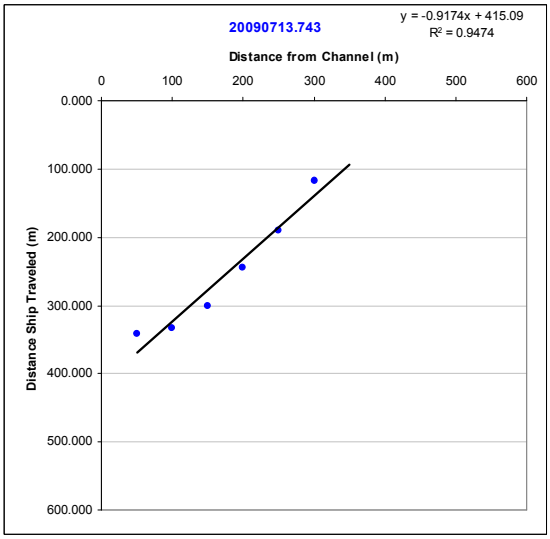
y = -0.9174x + 415.09
R² = 0.9474
20090713.743
Distance from Channel (m)
0
100
200
300
400
500
600
Distance Ship Traveled (m)
0.000
100.000
200.000
300.000
400.000
500.000
600.000

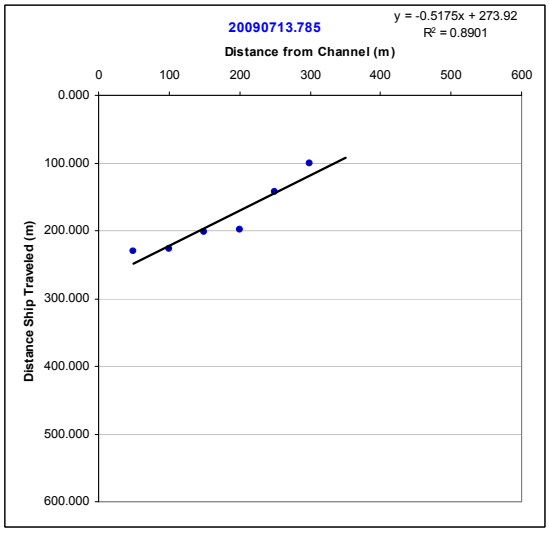
y = -0.5175x + 273.92
R² = 0.8901
20090713.785
Distance from Channel (m)
0
100
200
300
400
500
600
Distance Ship Traveled (m)
0.000
100.000
200.000
300.000
400.000
500.000
600.000

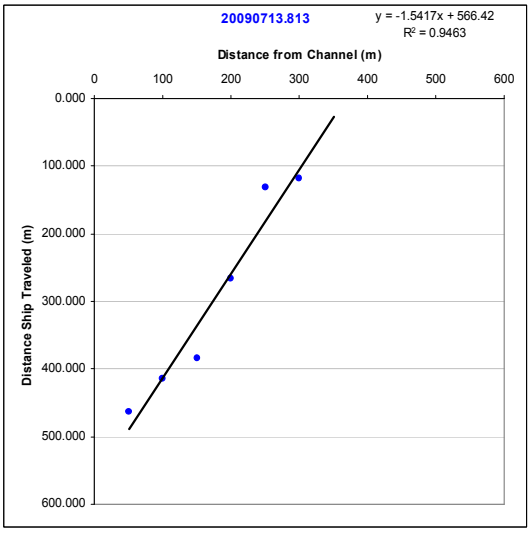
y = -1.5417x + 566.42
R² = 0.9463
20090713.813
Distance from Channel (m)
0
100
200
300
400
500
600
Distance Ship Traveled (m)
0.000
100.000
200.000
300.000
400.000
500.000
600.000

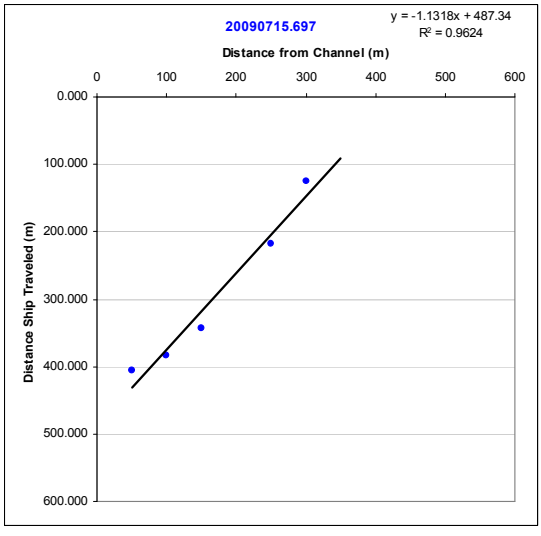
y = -1.1318x + 487.34
R² = 0.9624
20090715.697
Distance from Channel (m)
0
100
200
300
400
500
600
Distance Ship Traveled (m)
0.000
100.000
200.000
300.000
400.000
500.000
600.000

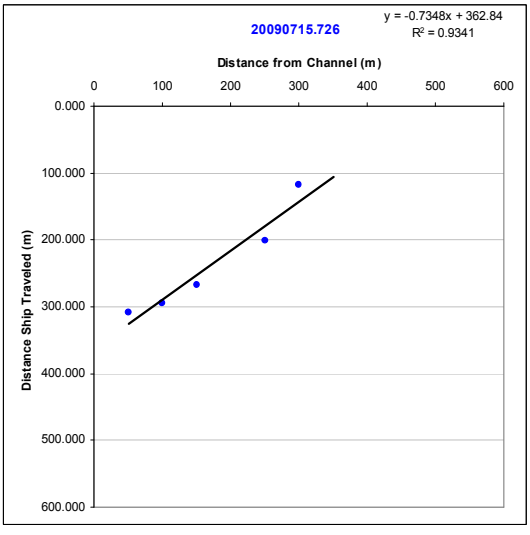
y = -0.7348x + 362.84
R² = 0.9341
20090715.726
Distance from Channel (m)
0
100
200
300
400
500
600
Distance Ship Traveled (m)
0.000
100.000
200.000
300.000
400.000
500.000
600.000

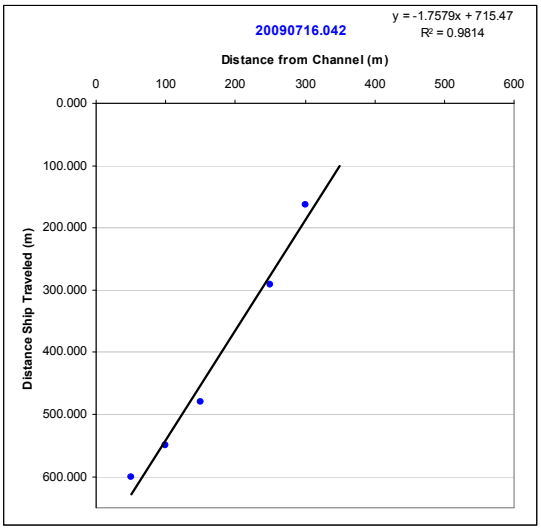
20090716.042
y = -1.7579x + 715.47
R² = 0.9814
Distance from Channel (m)
0
100
200
300
400
500
600
Distance Ship Traveled (m)
0.000
100.000
200.000
300.000
400.000
500.000
600.000

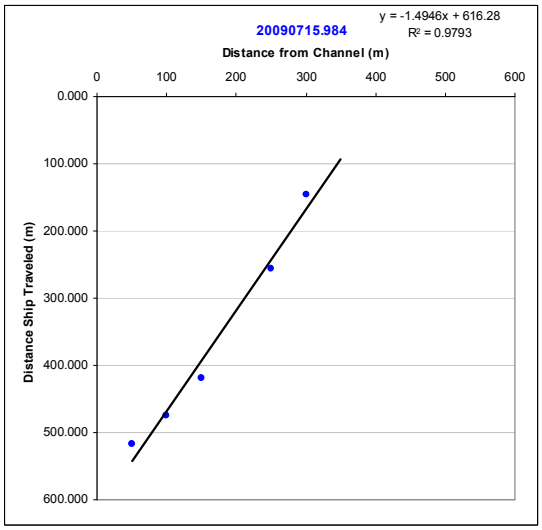
20090715.984
y = -1.4946x + 616.28
R² = 0.9793
Distance from Channel (m)
0
100
200
300
400
500
600
Distance Ship Traveled (m)
0.000
100.000
200.000
300.000
400.000
500.000
600.000

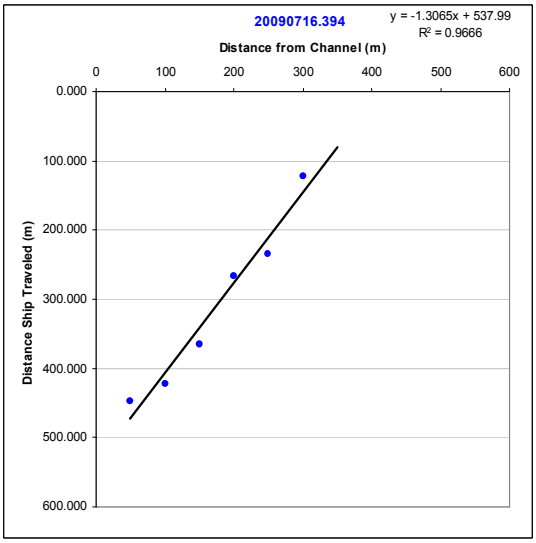
20090716.394
y = -1.3065x + 537.99
R² = 0.9666
Distance from Channel (m)
0
100
200
300
400
500
600
Distance Ship Traveled (m)
0.000
100.000
200.000
300.000
400.000
500.000
600.000

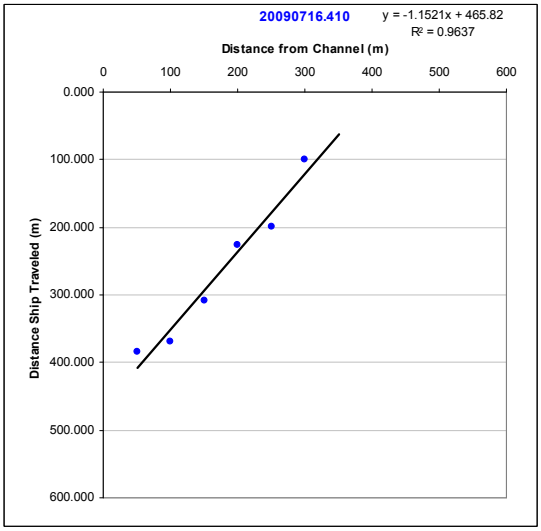
20090716.410
y = -1.1521x + 465.82
R² = 0.9637
Distance from Channel (m)
0
100
200
300
400
500
600
Distance Ship Traveled (m)
0.000
100.000
200.000
300.000
400.000
500.000
600.000

Appendix III

Plane wake view, polynomial fit

INBOUND SHIPS:

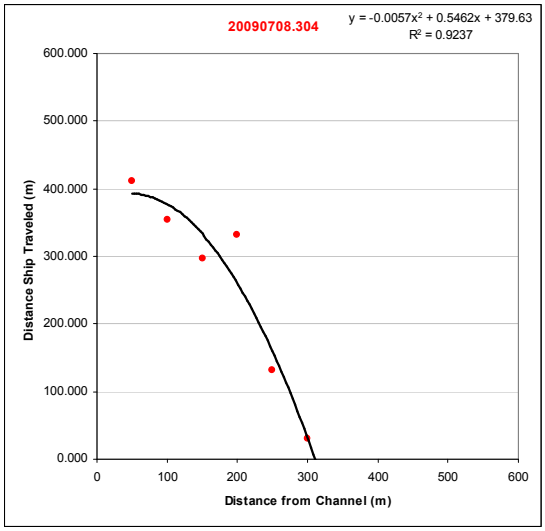

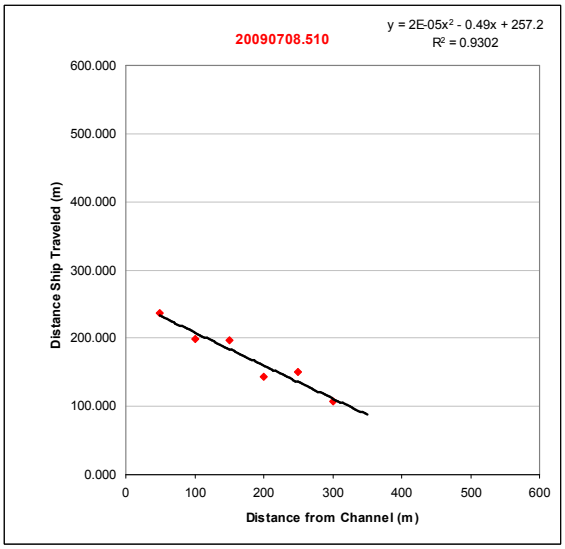

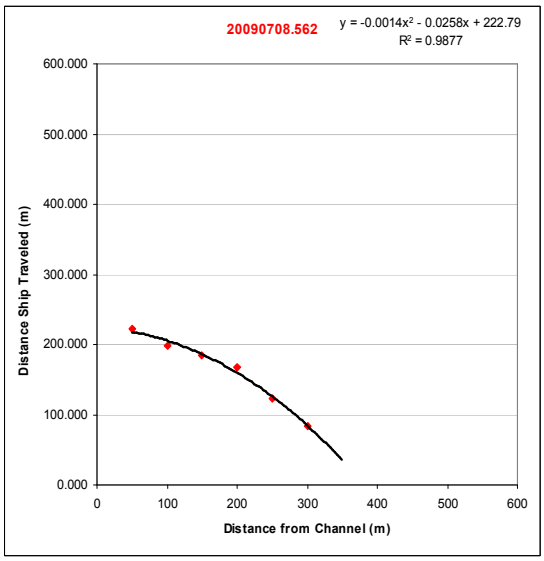

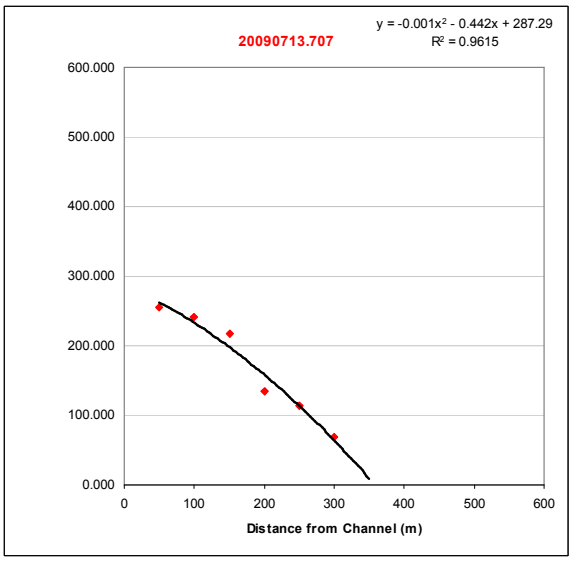

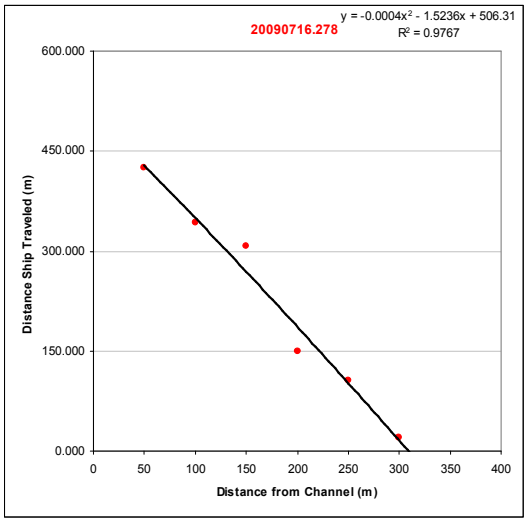
y = -0.0004x² - 1.5236x + 506.31
20090716.278
R² = 0.9767
600.000
450.000
300.000
150.000
0.000
Distance Ship Traveled (m)
0
50
100
150
200
250
300
350
400
Distance from Channel (m)

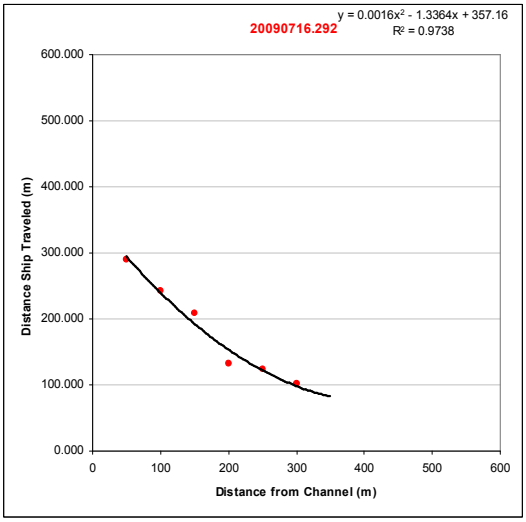
y = 0.0016x² - 1.3364x + 357.16
20090716.292
R² = 0.9738
600.000
500.000
400.000
300.000
200.000
100.000
0.000
Distance Ship Traveled (m)
0
100
200
300
400
500
600
Distance from Channel (m)

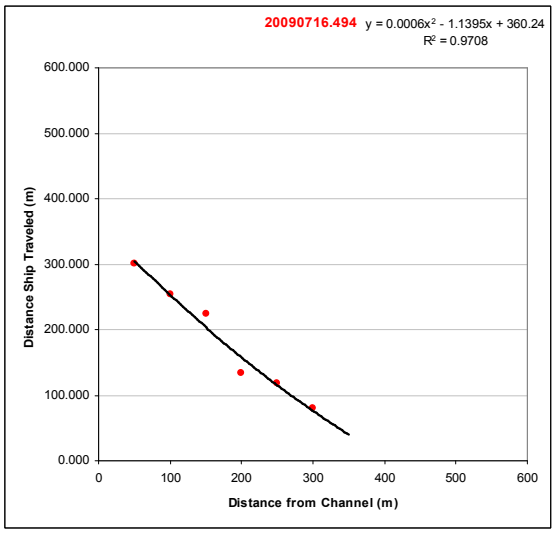
20090716.494
y = 0.0006x² - 1.1395x + 360.24
R² = 0.9708
600.000
500.000
400.000
300.000
200.000
100.000
0.000
Distance Ship Traveled (m)
0
100
200
300
400
500
600
Distance from Channel (m)

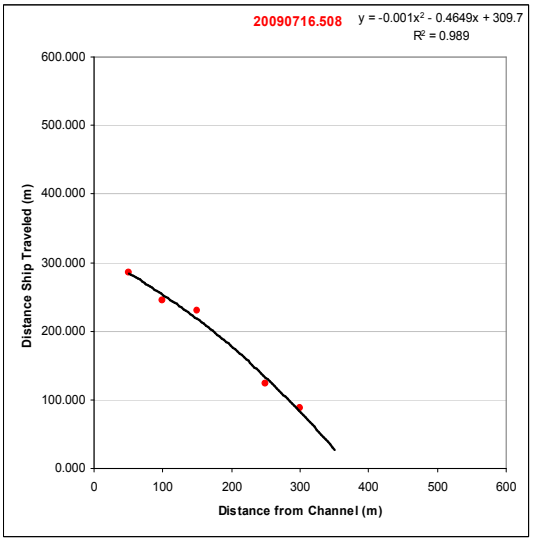
20090716.508
y = -0.001x² - 0.4649x + 309.7
R² = 0.989
600.000
500.000
400.000
300.000
200.000
100.000
0.000
Distance Ship Traveled (m)
0
100
200
300
400
500
600
Distance from Channel (m)

OUTBOUND SHIPS:

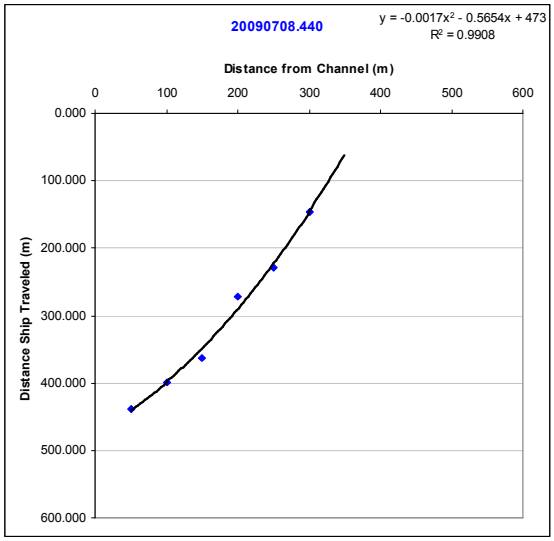

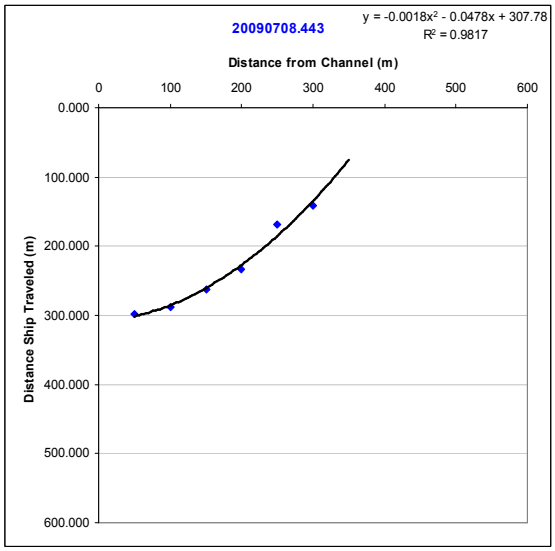

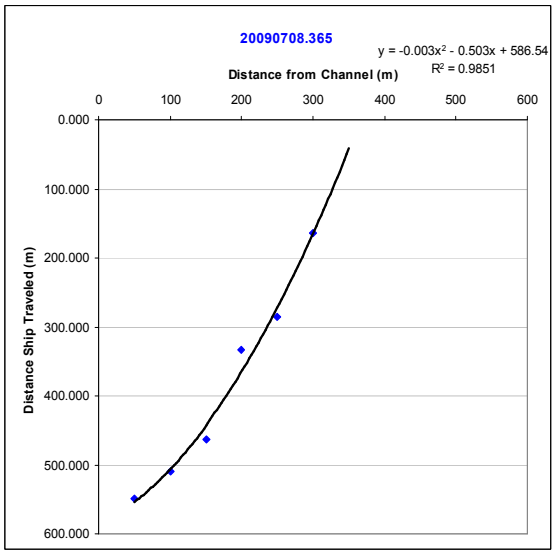

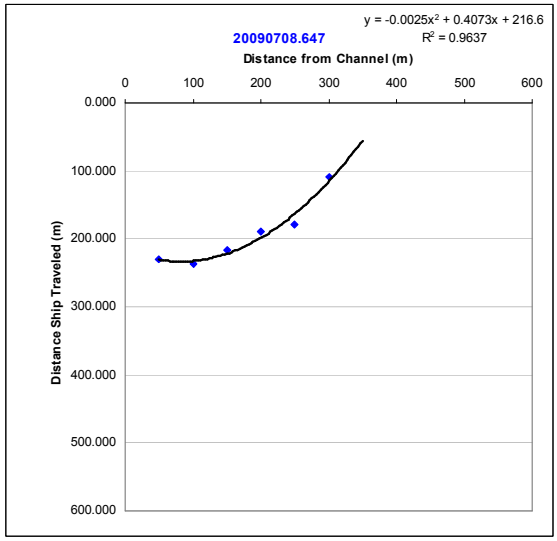

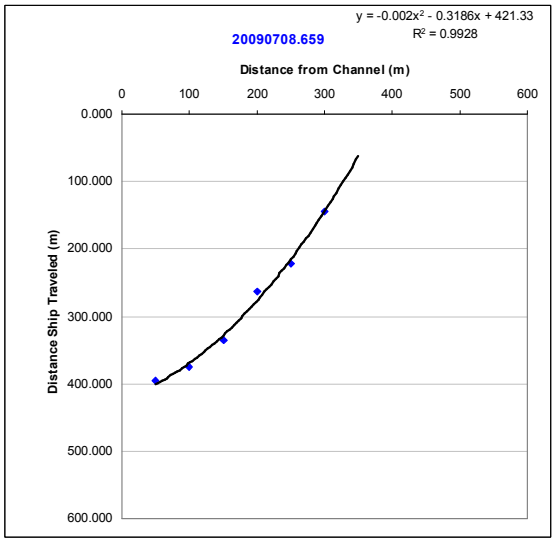

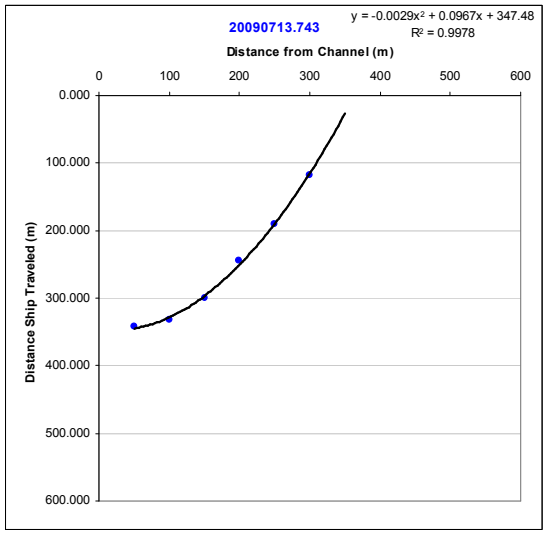

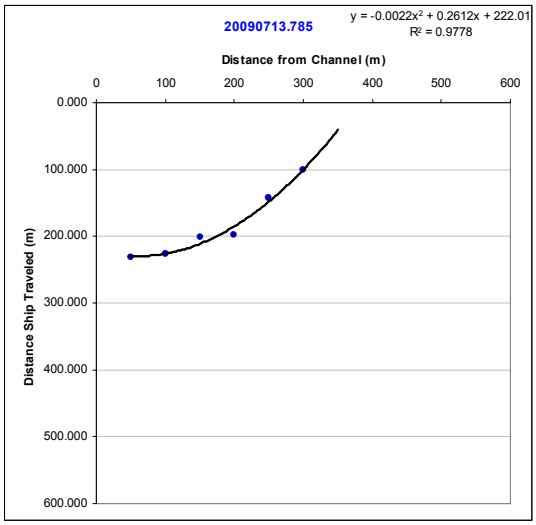
20090713.785
y = -0.0022x² + 0.2612x + 222.01
R² = 0.9778
Distance from Channel (m)
0
100
200
300
400
500
600
Distance Ship Traveled (m)
0.000
100.000
200.000
300.000
400.000
500.000
600.000

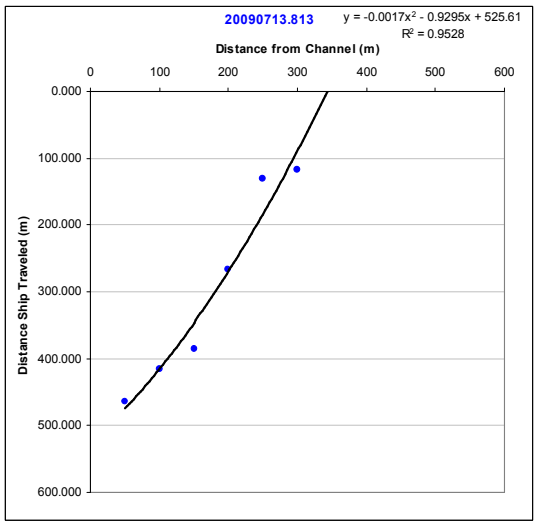
20090713.813
y = -0.0017x² - 0.9295x + 525.61
R² = 0.9528
Distance from Channel (m)
0
100
200
300
400
500
600
Distance Ship Traveled (m)
0.000
100.000
200.000
300.000
400.000
500.000
600.000

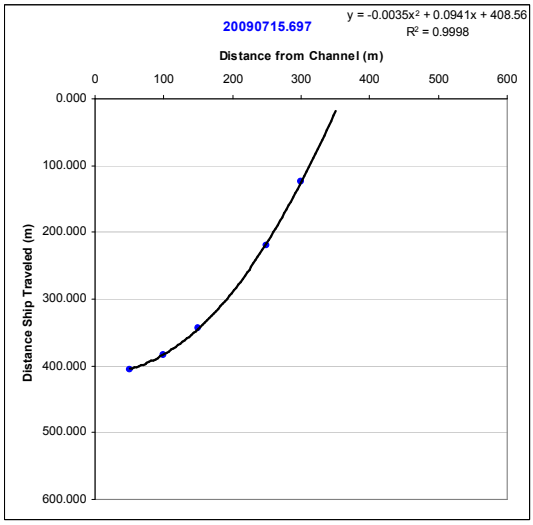
20090715.697
y = -0.0035x² + 0.0941x + 408.56
R² = 0.9998
Distance from Channel (m)
0
100
200
300
400
500
600
Distance Ship Traveled (m)
0.000
100.000
200.000
300.000
400.000
500.000
600.000

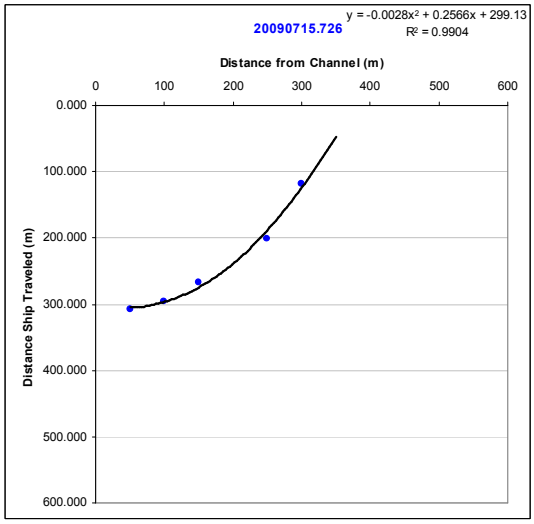
20090715.726
y = -0.0028x² + 0.2566x + 299.13
R² = 0.9904
Distance from Channel (m)
0
100
200
300
400
500
600
Distance Ship Traveled (m)
0.000
100.000
200.000
300.000
400.000
500.000
600.000

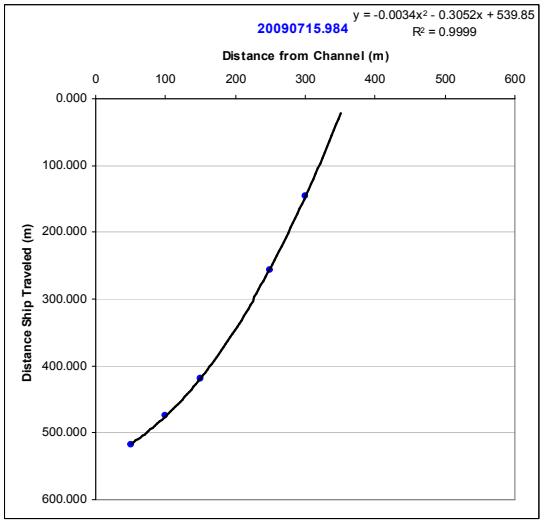
20090715.984
y = -0.0034x² - 0.3052x + 539.85
R² = 0.9999
Distance from Channel (m)
0
100
200
300
400
500
600
Distance Ship Traveled (m)
0.000
100.000
200.000
300.000
400.000
500.000
600.000

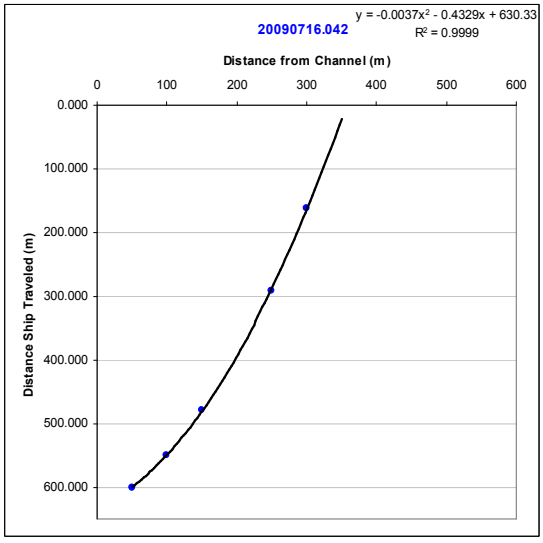
20090716.042
y = -0.0037x² - 0.4329x + 630.33
R² = 0.9999
Distance from Channel (m)
0
100
200
300
400
500
600
Distance Ship Traveled (m)
0.000
100.000
200.000
300.000
400.000
500.000
600.000

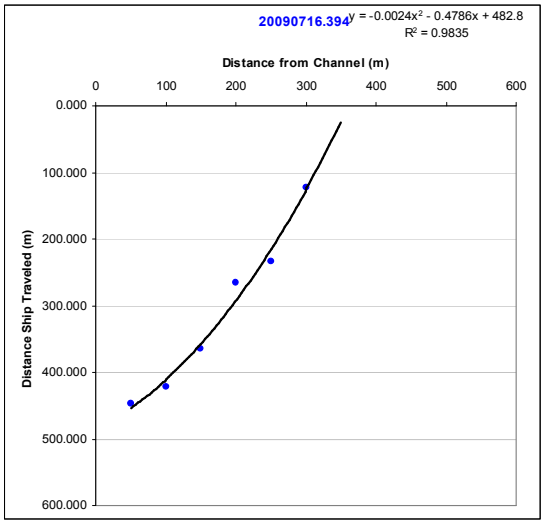
20090716.394
y = -0.0024x² - 0.4786x + 482.8
R² = 0.9835
Distance from Channel (m)
0
100
200
300
400
500
600
Distance Ship Traveled (m)
0.000
100.000
200.000
300.000
400.000
500.000
600.000

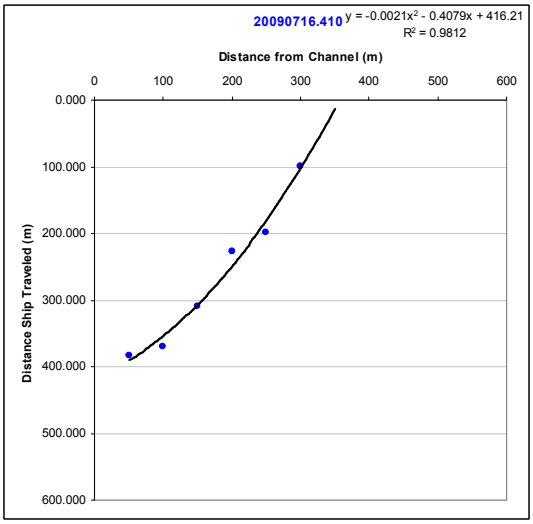
20090716.410
y = -0.0021x² - 0.4079x + 416.21
R² = 0.9812
Distance from Channel (m)
0
100
200
300
400
500
600
Distance Ship Traveled (m)
0.000
100.000
200.000
300.000
400.000
500.000
600.000

Appendix IV

Water level plots on left, distance plots on right

Inbound:

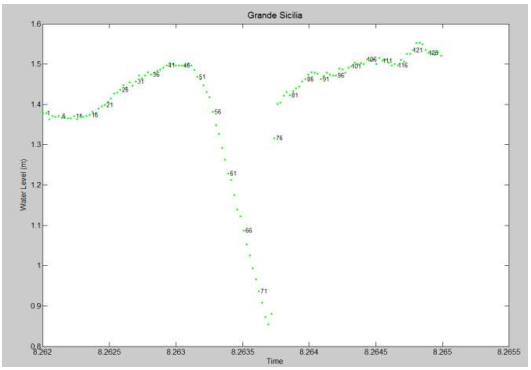

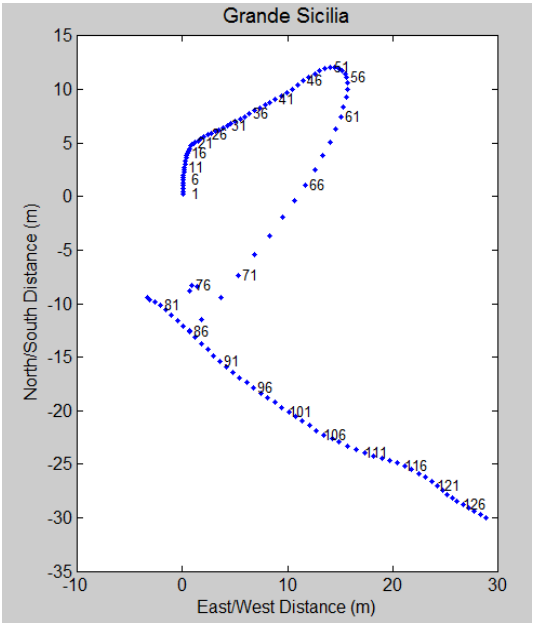

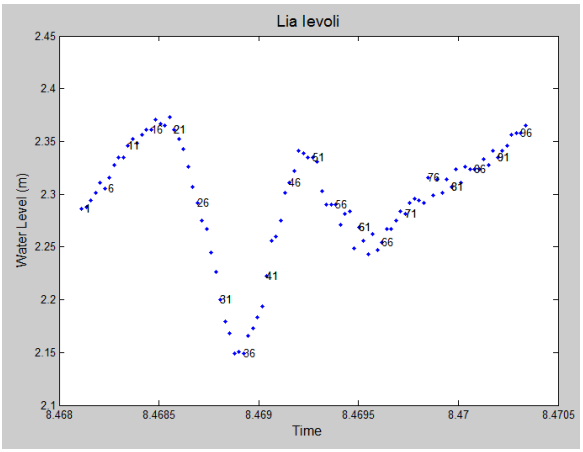

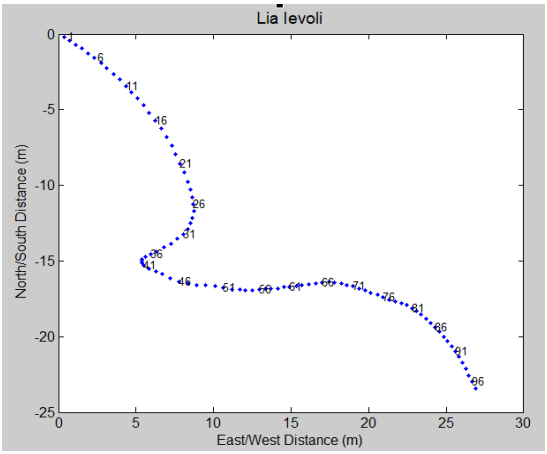

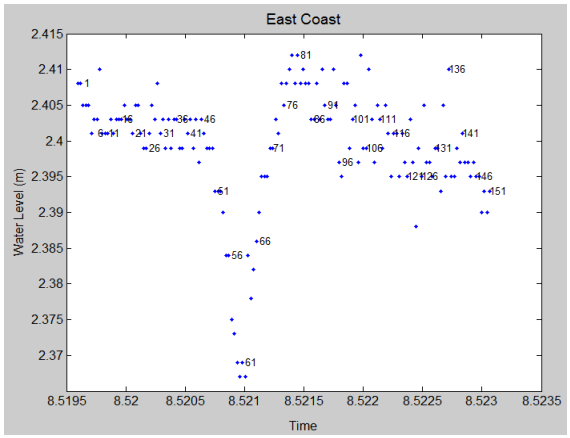
East Coast
Water Level (m)
Time

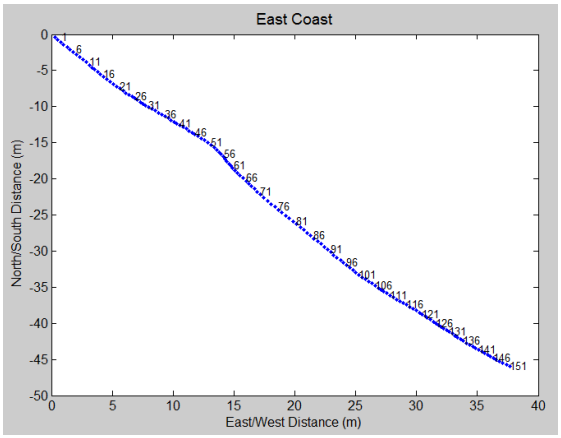
East Coast
North/South Distance (m)
East/West Distance (m)

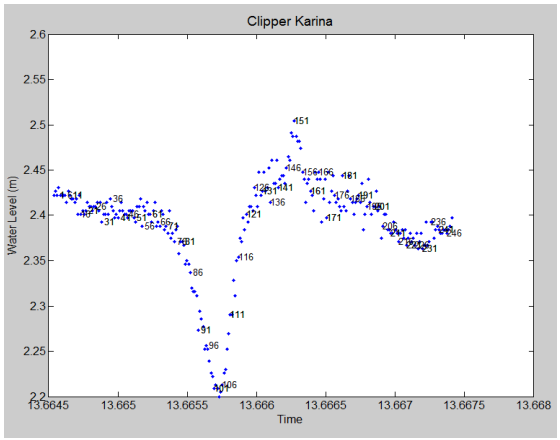
Clipper Karina
Water Level (m)
Time

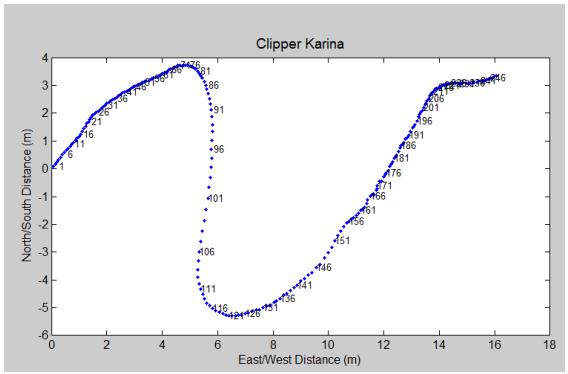
Clipper Karina
North/South Distance (m)
East/West Distance (m)

Outbound:

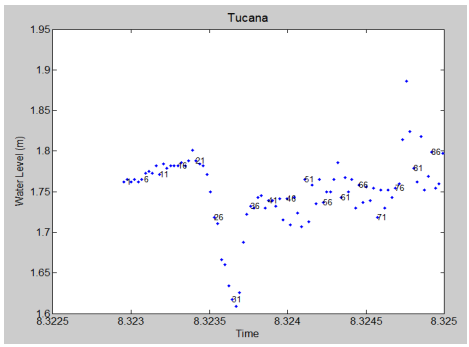
Tucana
Water Level (m)
Time

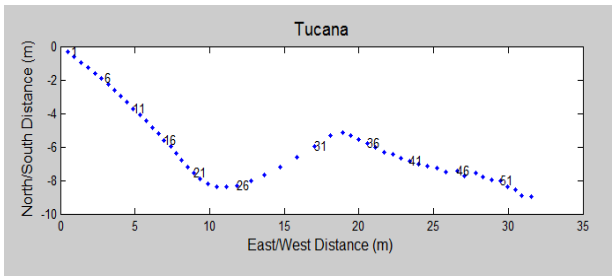
Tucana
North/South Distance (m)
East/West Distance (m)

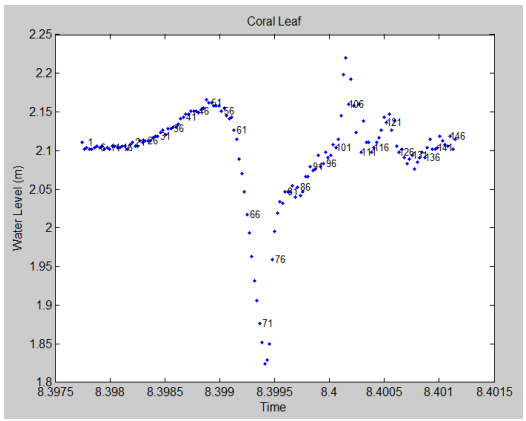
Coral Leaf
Water Level (m)
Time

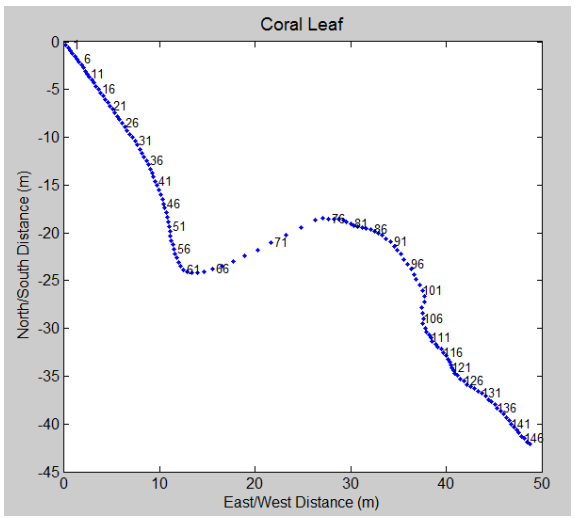
Coral Leaf
North/South Distance (m)
East/West Distance (m)

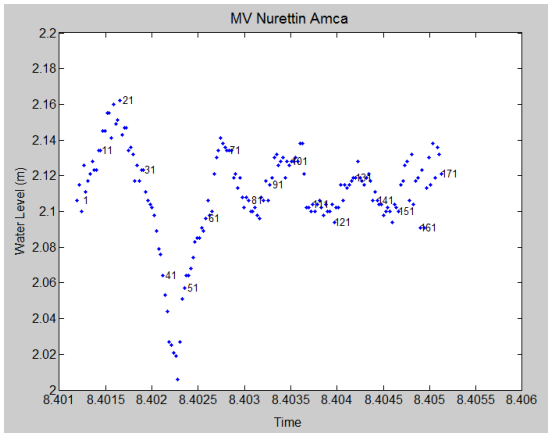
MV Nurettin Amca
Water Level (m)
Time

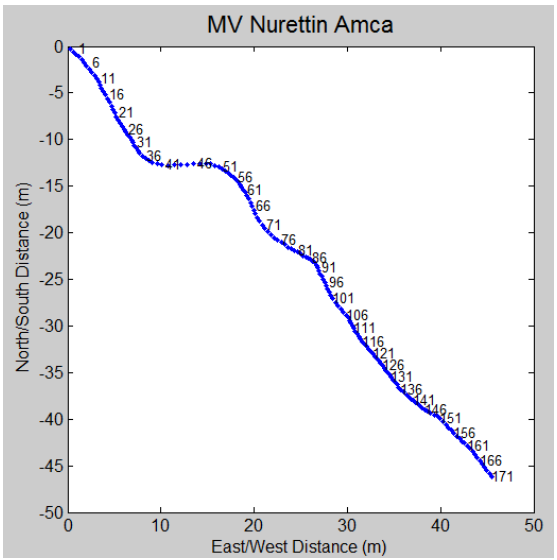
MV Nurettin Amca
North/South Distance (m)
East/West Distance (m)

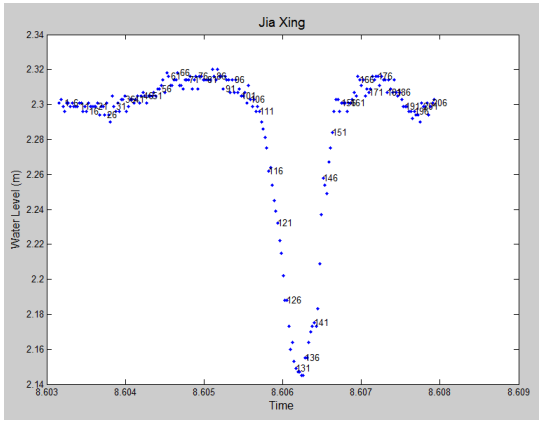
Jia Xing
Water Level (m)
Time
2.34
2.32
2.3
2.28
2.26
2.24
2.22
2.2
2.18
2.16
2.14
8.603
8.604
8.605
8.606
8.607
8.608
8.609

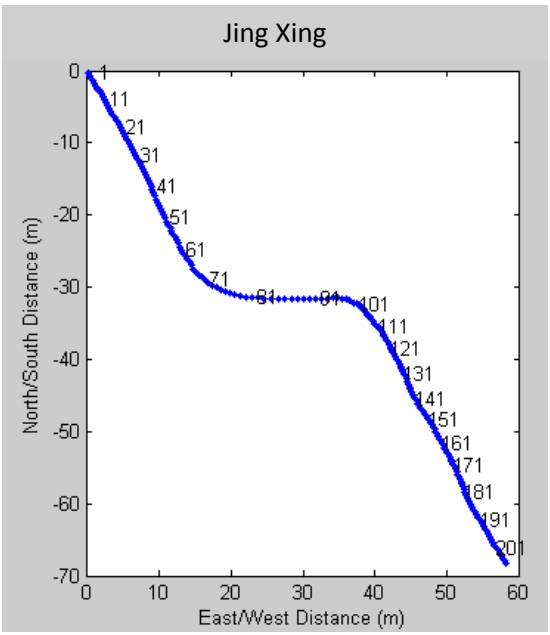
Jing Xing
North/South Distance (m)
East/West Distance (m)
0
-10
-20
-30
-40
-50
-60
-70
0
10
20
30
40
50
60
1
11
21
31
41
51
61
71
81
84
101
111
121
131
141
151
161
171
181
191
201

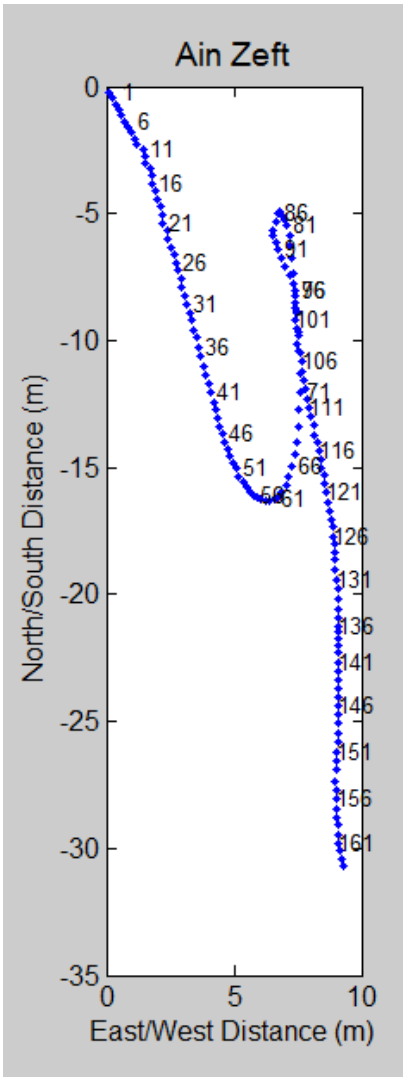
Ain Zeft
North/South Distance (m)
East/West Distance (m)

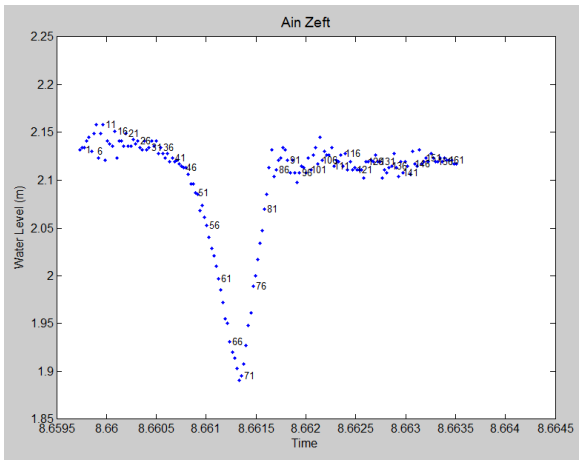
Ain Zeft
Water Level (m)
Time

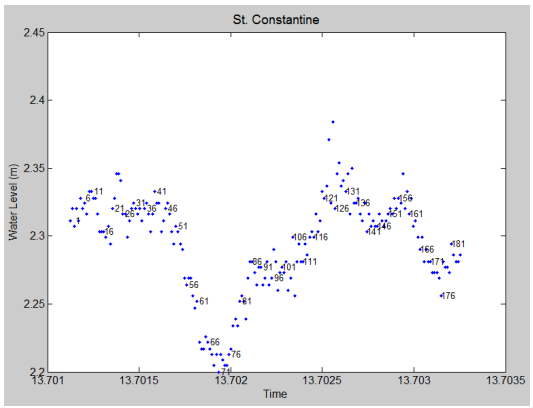
St. Constantine
Water Level (m)
Time

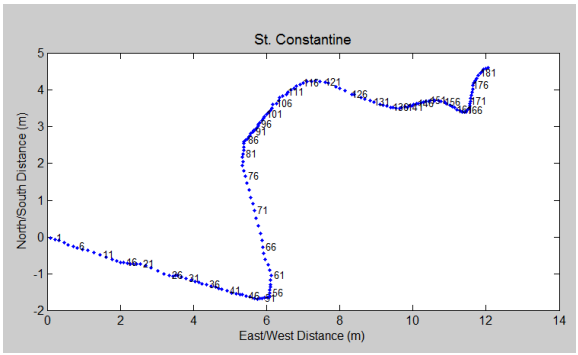
St. Constantine
North/South Distance (m)
East/West Distance (m)

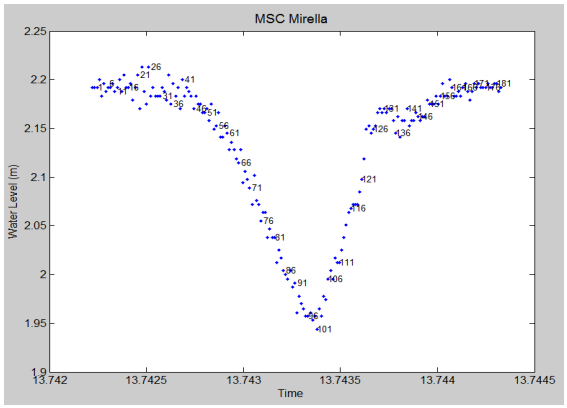
MSC Mirella
Water Level (m)
Time

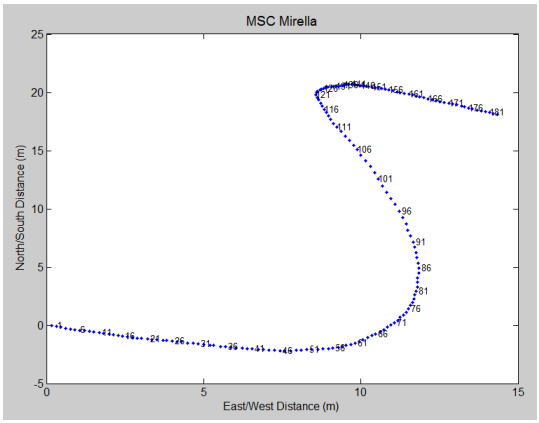
MSC Mirella
North/South Distance (m)
East/West Distance (m)

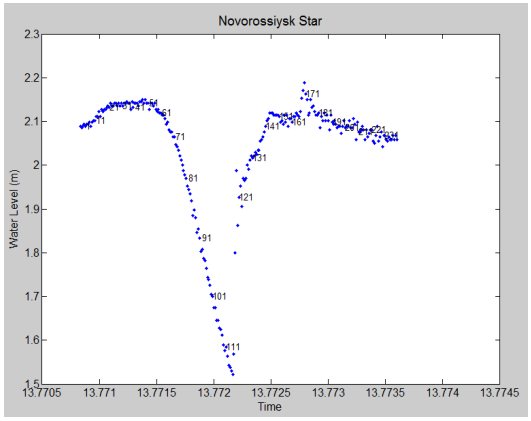
Novorossiysk Star
Water Level (m)
Time

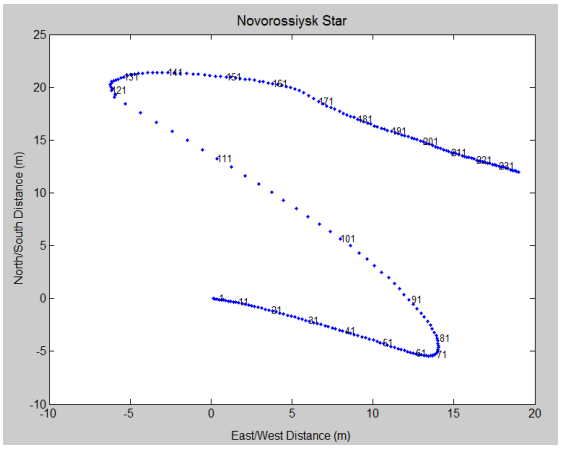
Novorossiysk Star
North/South Distance (m)
East/West Distance (m)

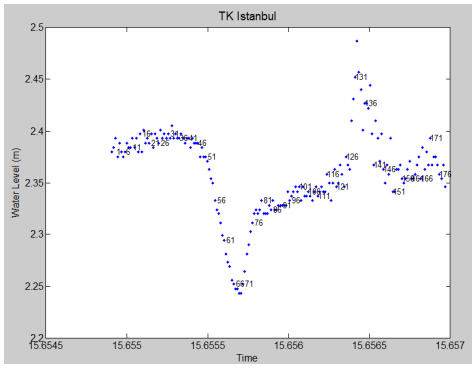
TK Istanbul
Water Level (m)
Time

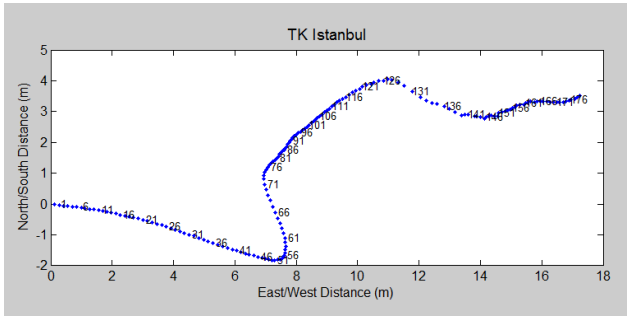
TK Istanbul
North/South Distance (m)
East/West Distance (m)

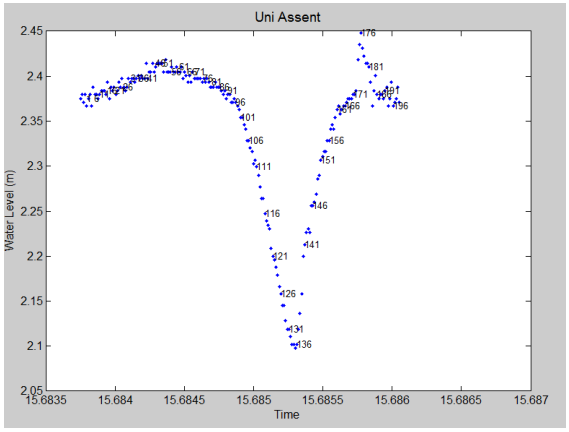
Uni Assent
Water Level (m)
Time

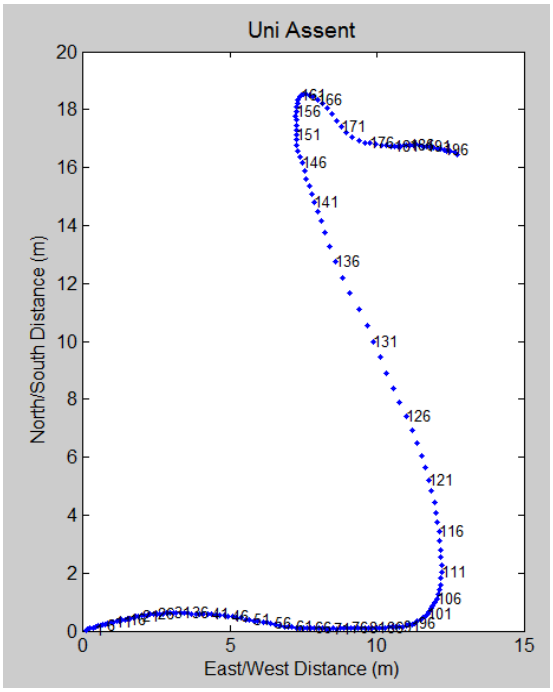
Uni Assent
North/South Distance (m)
East/West Distance (m)

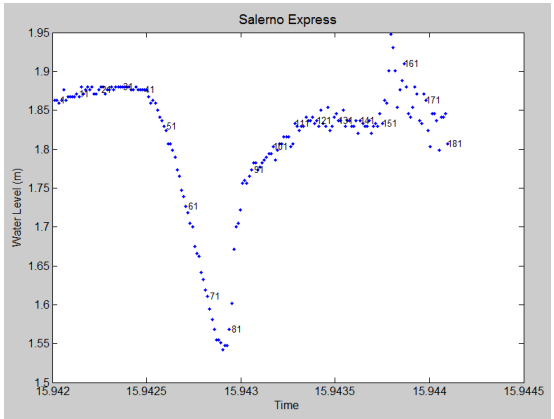
Salerno Express
Water Level (m)
Time

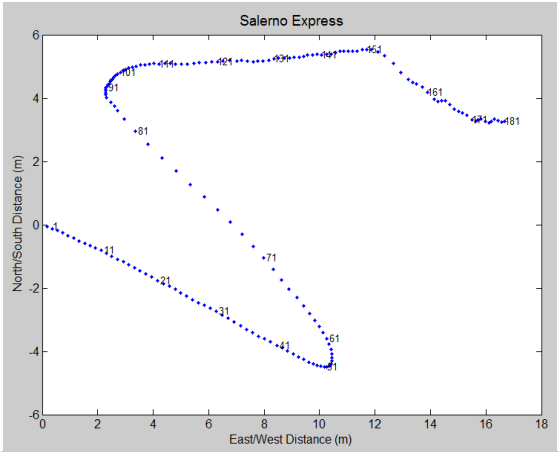
Salerno Express
North/South Distance (m)
East/West Distance (m)

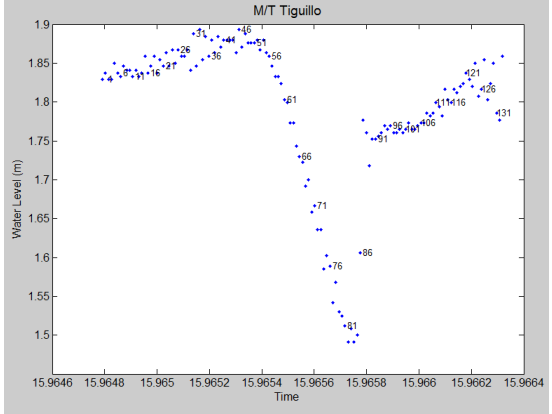
M/T Tiguillo
Water Level (m)
Time

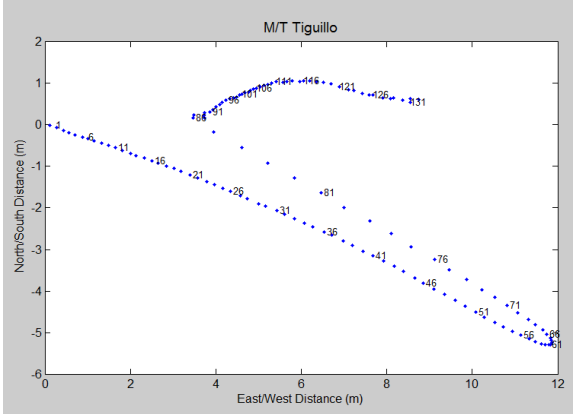
M/T Tiguillo
North/South Distance (m)
East/West Distance (m)

Appendix V

Calculated and recorded suspended sediment concentrations for ships that created a boundary stress greater than 0.68 Pa using Gelinas' equation:

$$\log_{10}(F) = 0.6\ln(\tau) - 2.5846 \qquad (12)$$

With $W_s = 0.0035$ m/s

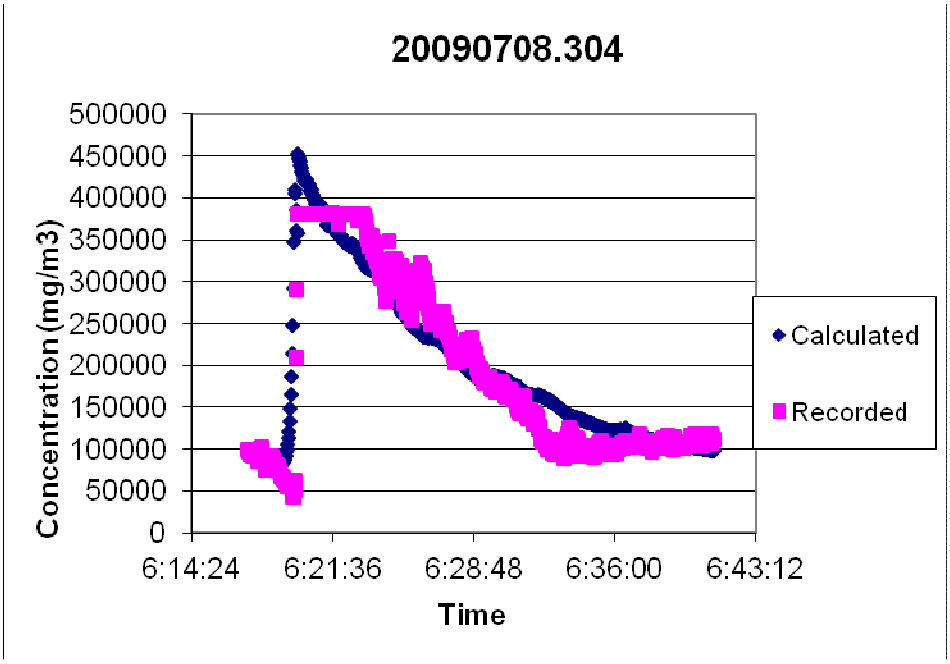

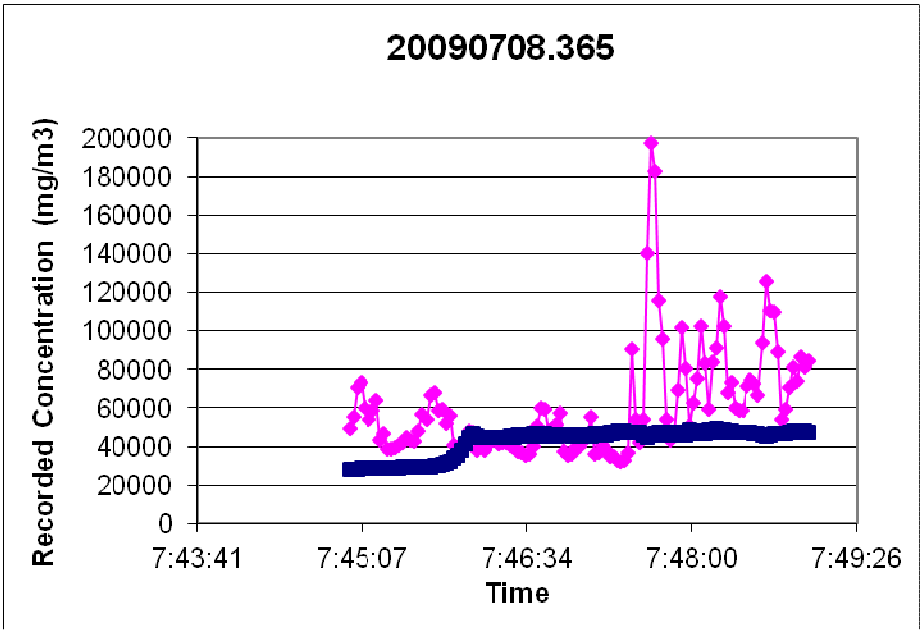

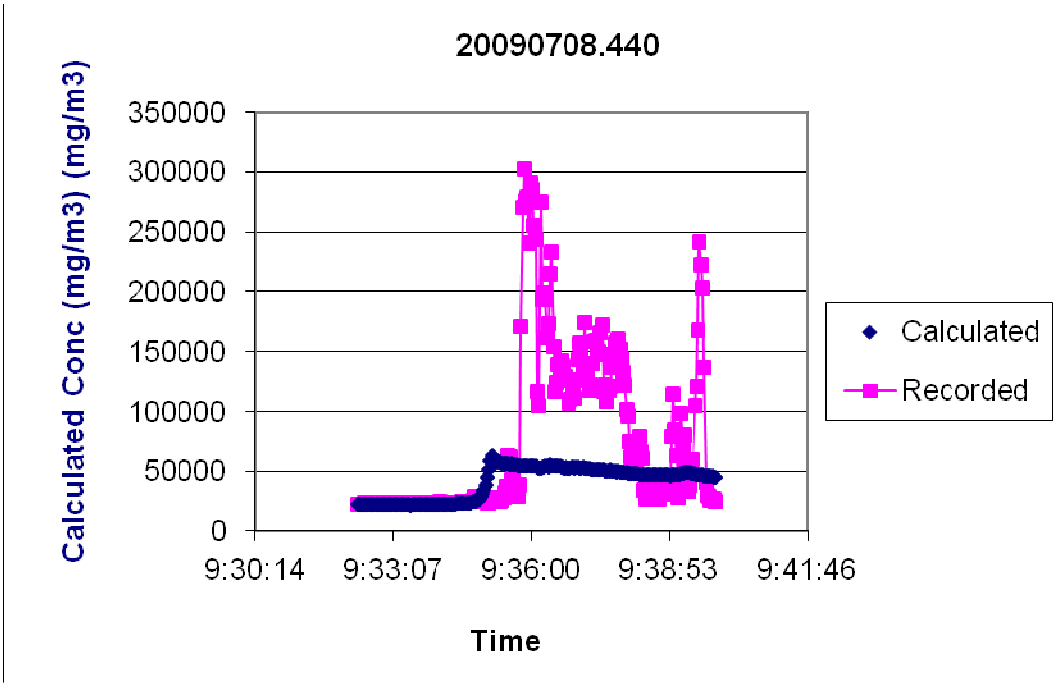
20090708.440
Calculated Conc (mg/m3) (mg/m3)
350000
300000
250000
200000
150000
100000
50000
0
9:30:14
9:33:07
9:36:00
9:38:53
9:41:46
Time
Calculated
Recorded

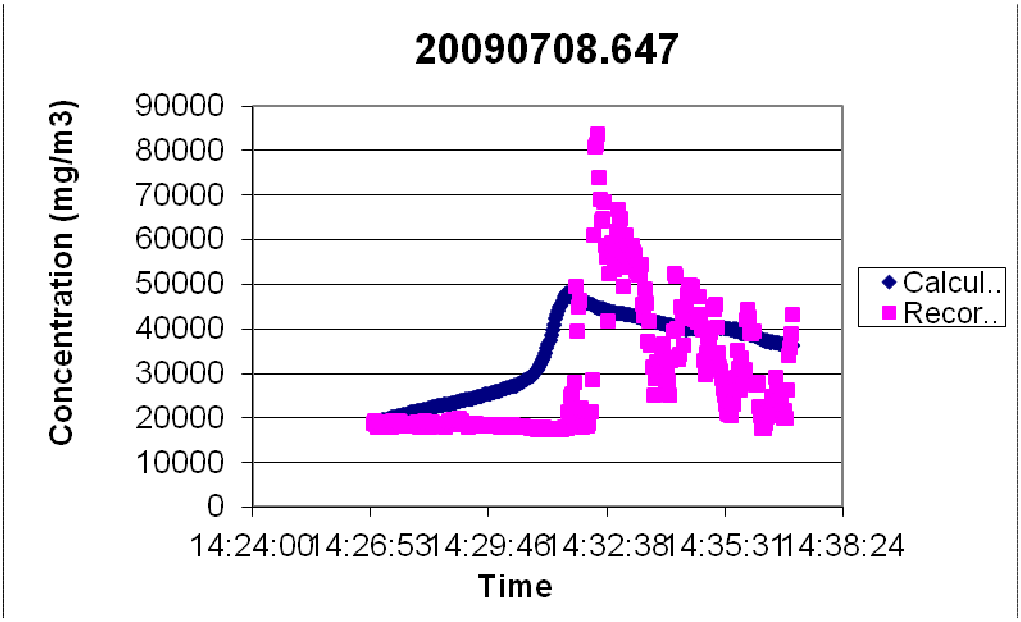
20090708.647
Concentration (mg/m3)
90000
80000
70000
60000
50000
40000
30000
20000
10000
0
14:24:00
14:26:53
14:29:46
14:32:38
14:35:31
14:38:24
Time
Calcul..
Recor..

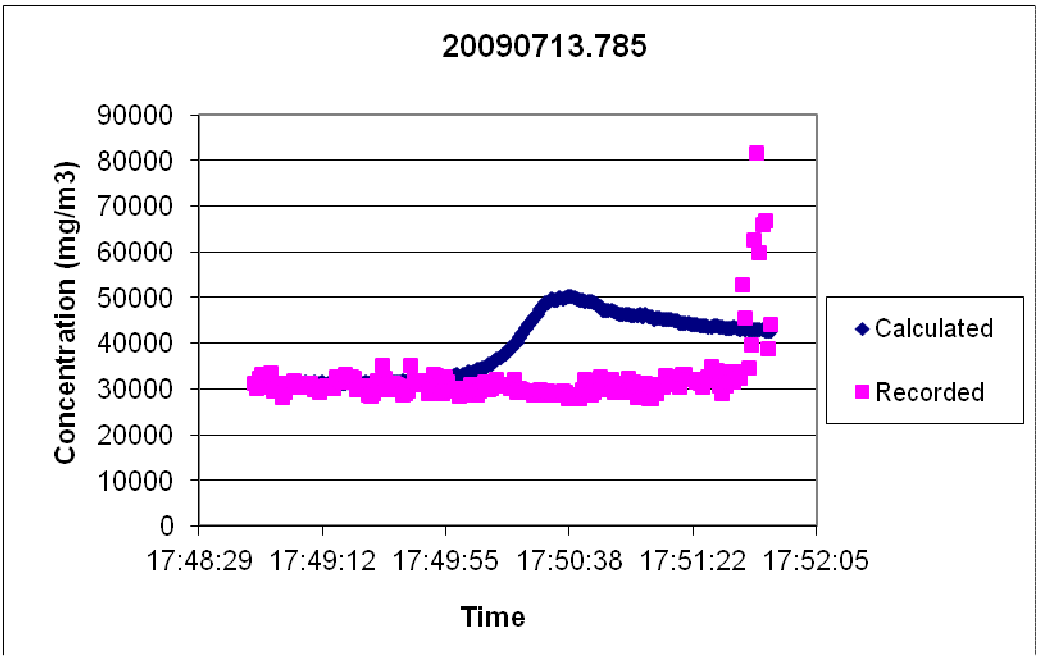
20090713.785
90000
80000
70000
60000
50000
40000
30000
20000
10000
0
Concentration (mg/m3)
17:48:29
17:49:12
17:49:55
17:50:38
17:51:22
17:52:05
Time
Calculated
Recorded

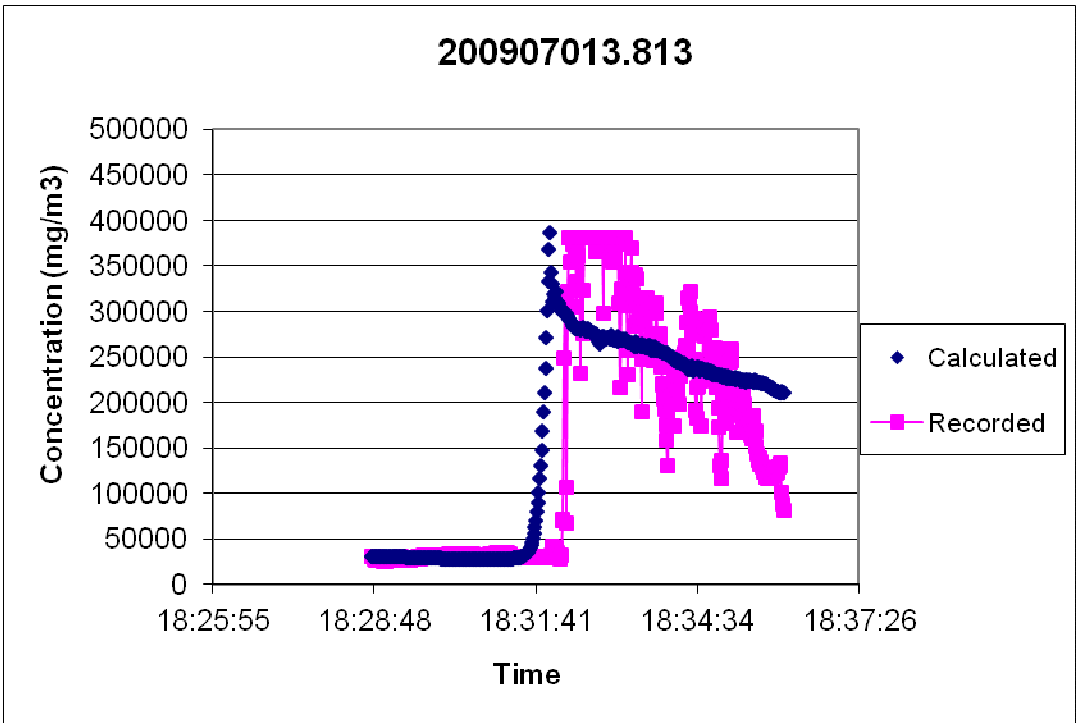
200907013.813
500000
450000
400000
350000
300000
250000
200000
150000
100000
50000
0
Concentration (mg/m3)
18:25:55
18:28:48
18:31:41
18:34:34
18:37:26
Time
Calculated
Recorded

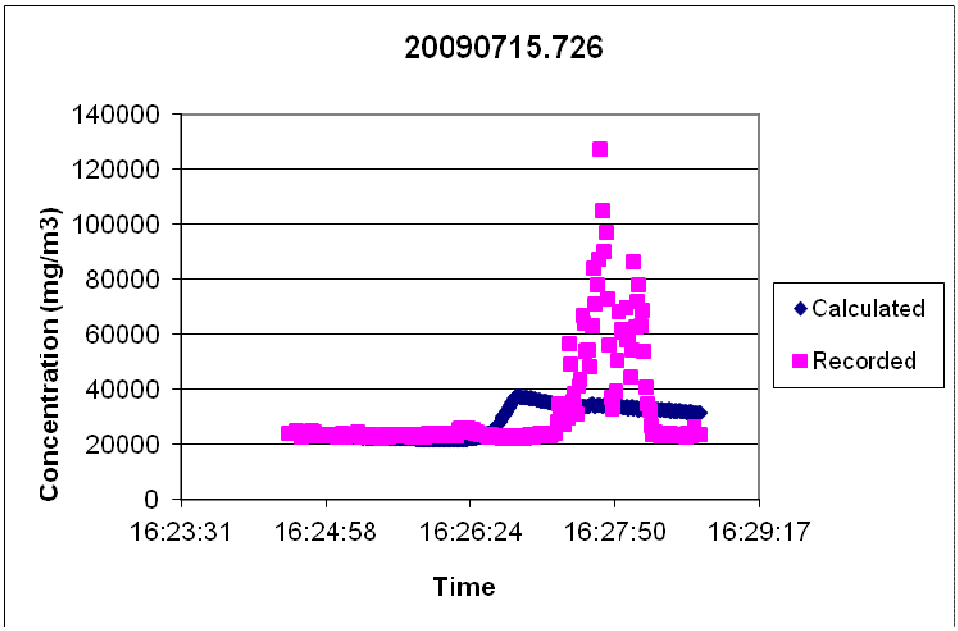
20090715.726
140000
120000
100000
80000
60000
40000
20000
0
Concentration (mg/m3)
16:23:31
16:24:58
16:26:24
16:27:50
16:29:17
Time
Calculated
Recorded

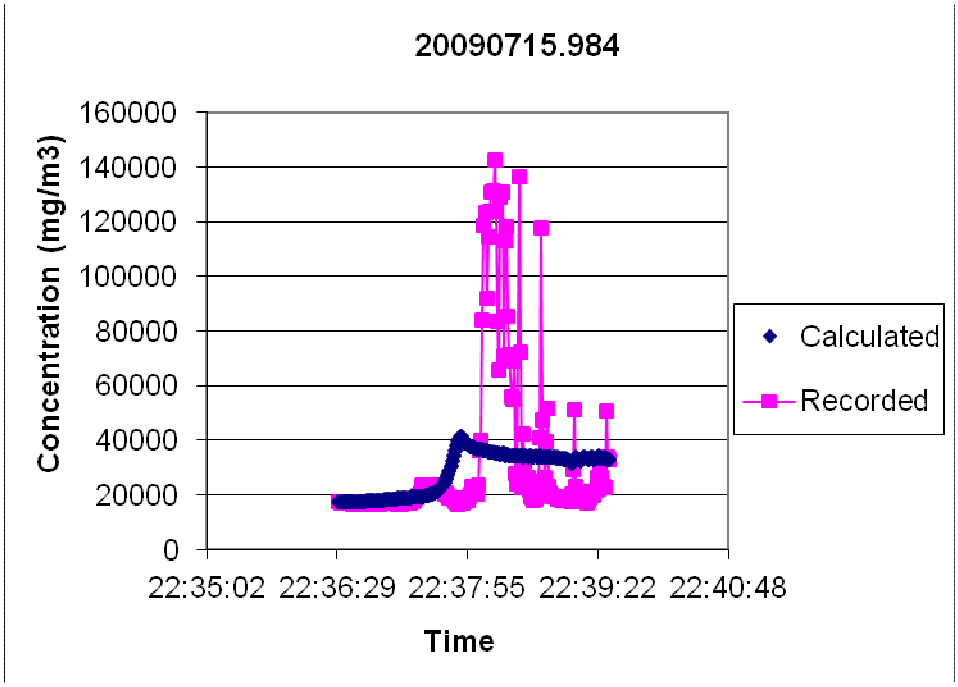
20090715.984
160000
140000
120000
100000
80000
60000
40000
20000
0
Concentration (mg/m3)
22:35:02
22:36:29
22:37:55
22:39:22
22:40:48
Time
Calculated
Recorded

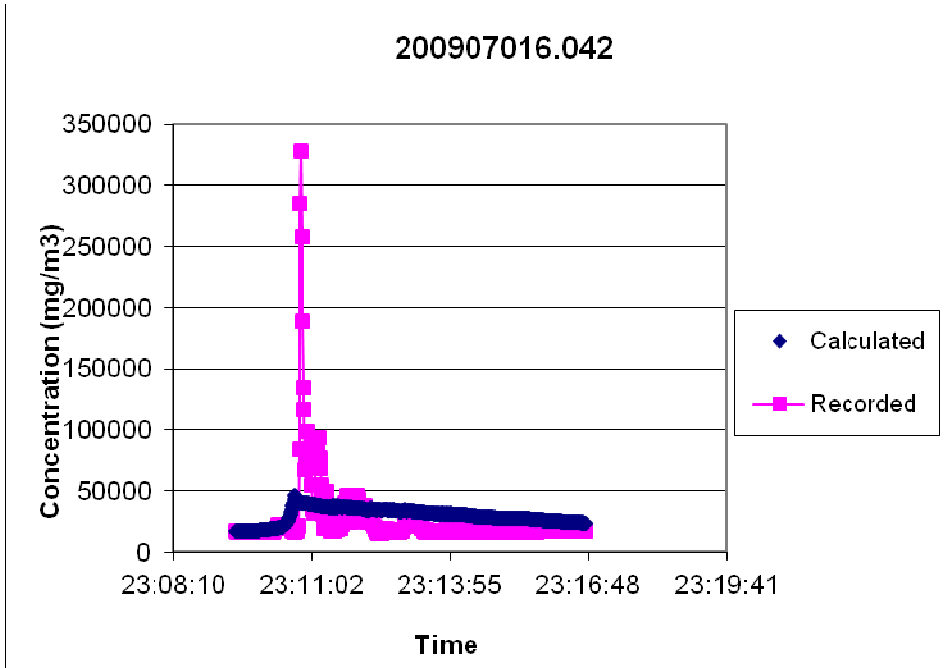
200907016.042
350000
300000
250000
200000
150000
100000
50000
0
Concentration (mg/m3)
23:08:10
23:11:02
23:13:55
23:16:48
23:19:41
Time
Calculated
Recorded

Appendix VI

Modeling the water level using Madsen and Schaeffer (2010) equation 5.1

$$\eta_i\,(x_0,\,t) = A_1 \mathrm{sech}^2\Omega_1(t - t_1) - A_2 \mathrm{sech}^2\Omega_2(t - t_2)$$

Grande Sicilia (8.304)

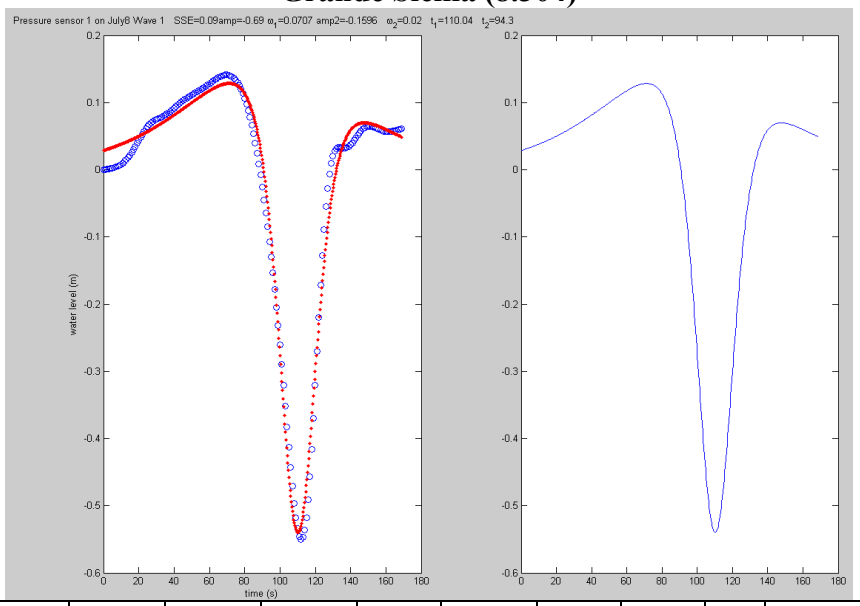

Ship ID	PS #	Start Time	End Time	Amp 1	Ω1	Amp 2	Ω2	t1	t2	SSE	Notes
8.304	1	100	270	-0.69	0.07	-0.16	0.02	110	94	0.09	

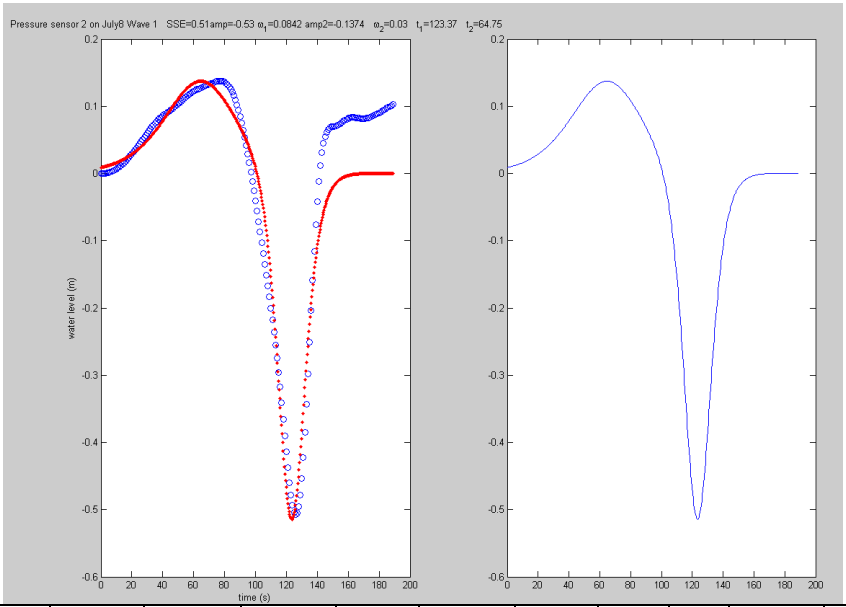

Ship ID	PS #	Start Time	End Time	Amp 1	Ω1	Amp 2	Ω2	t1	t2	SSE	Notes
8.304	2	100	290	-0.53	0.08	-0.14	0.03	123	65	0.51	

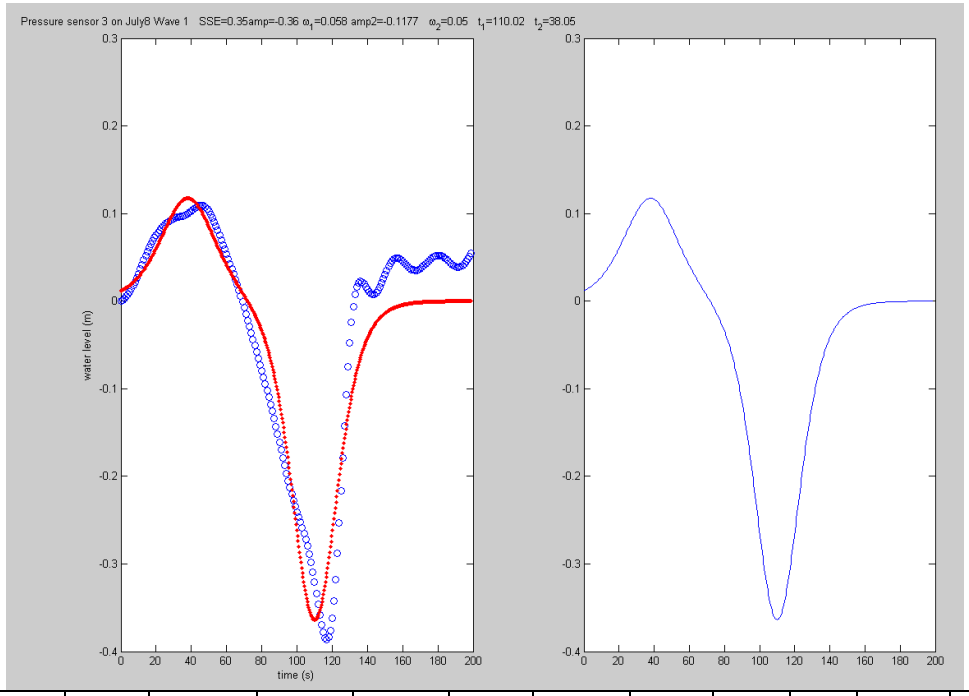

Ship ID	PS #	Start Time	End Time	Amp 1	Ω1	Amp 2	Ω2	t1	t2	SSE	Notes
8.304	3	150	350	-0.36	0.06	-0.12	0.05	110	38	0.35	

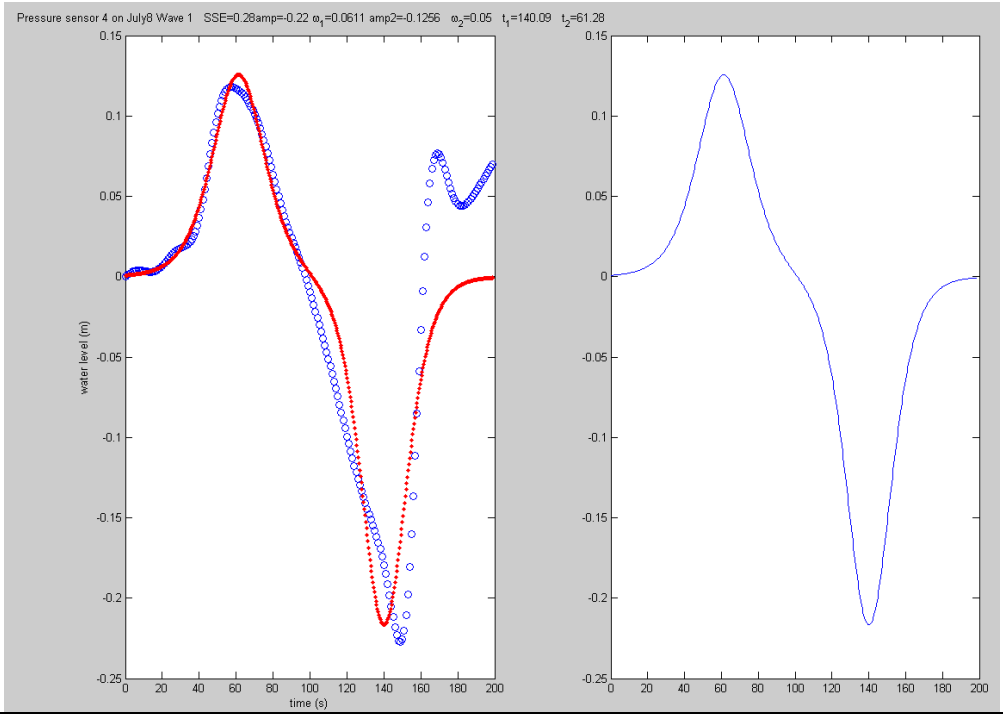

Ship ID	PS #	Start Time	End Time	Amp1	Ω1	Amp2	Ω2	t1	t2	SSE	Notes
8.304	4	150	350	-0.22	0.06	-0.125	0.05	140	61	0.28	

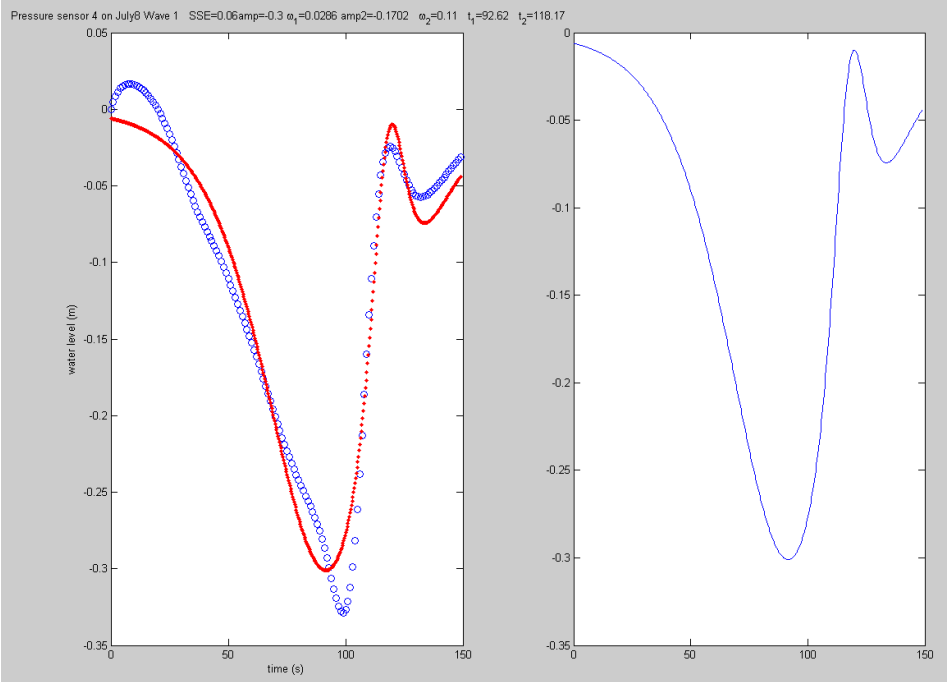

Ship ID	PS #	Start Time	End Time	Amp 1	Ω1	Amp 2	Ω2	t1	t2	SSE	Notes
8.304	4.1	200	350	-0.3	0.03	-0.17	0.11	92	118	0.06	Fit to trailing trough

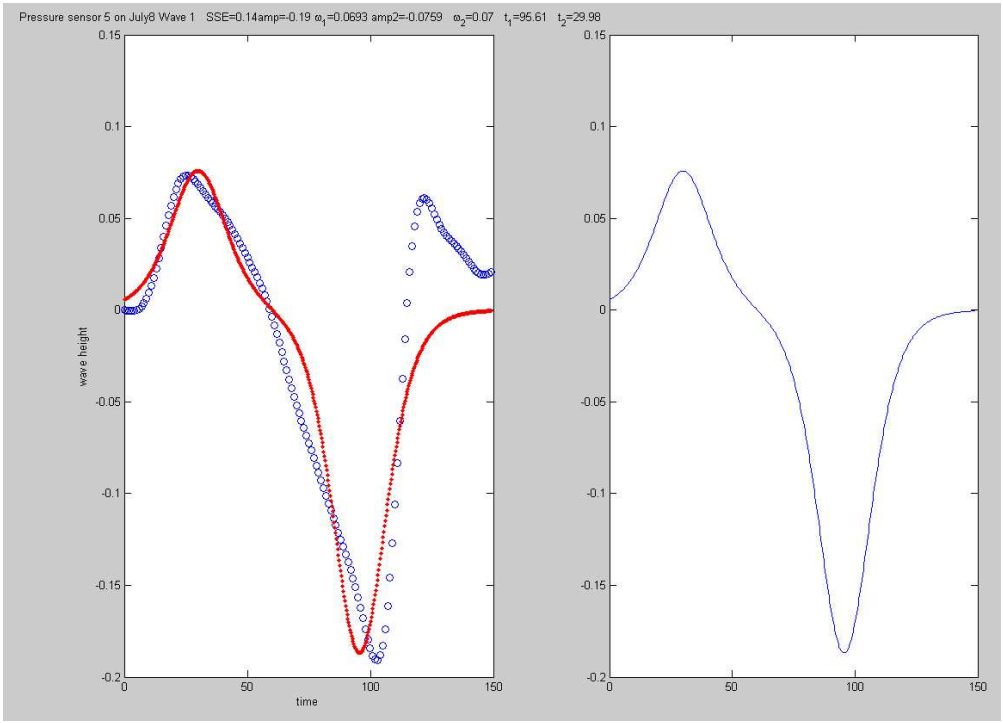

Ship ID	PS #	Start Time	End Time	Amp 1	Ω1	Amp2	Ω2	t1	t2	SSE	Notes
8.304	5	175	375	-0.19	0.07	-0.08	0.07	95	29	0.14	

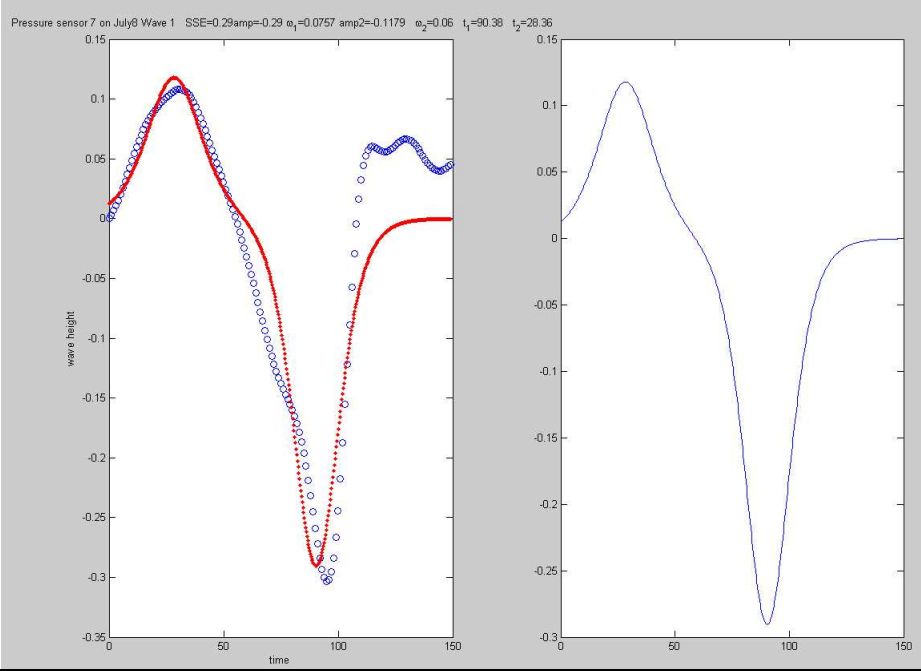

Ship ID	PS #	Start Time	End Time	Amp1	Ω1	Amp2	Ω2	t1	t2	SSE	Notes
8.304	7	150	300	-0.29	0.076	-0.118	0.06	90.38	28.36	0.29	

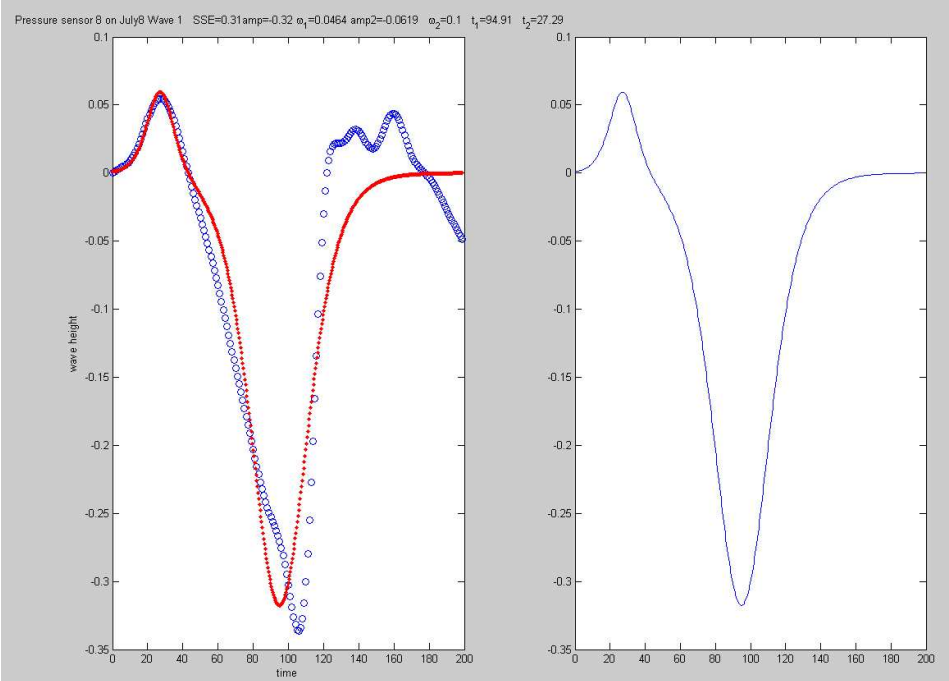

Ship ID	PS #	Start Time	End Time	Amp1	Ω1	Amp2	Ω2	t1	t2	SSE	Notes
8.304	8	200	400	-0.32	0.046	-0.06	0.1	94	27	0.31	

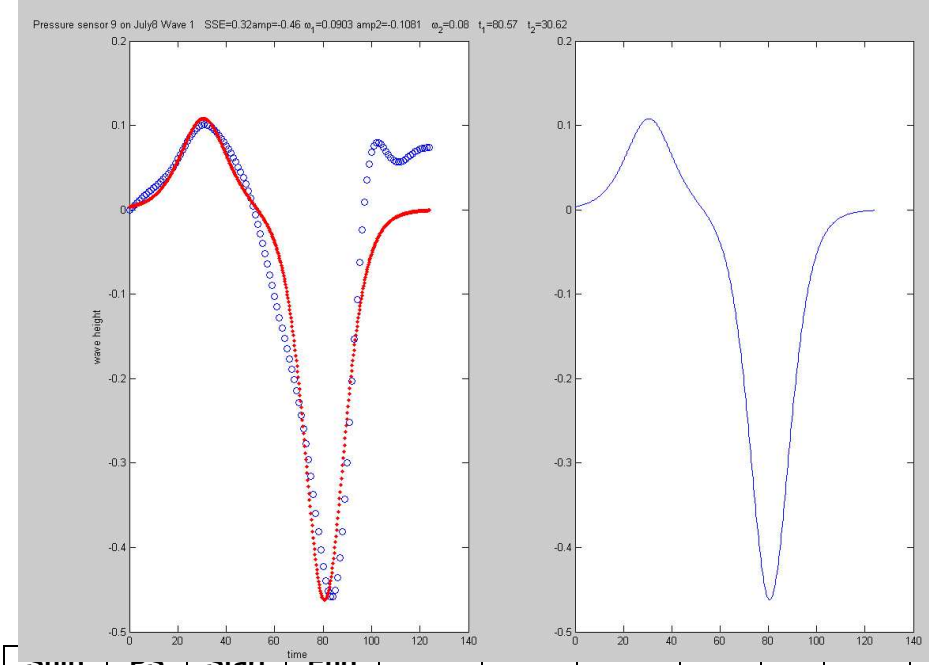

Ship ID	PS #	Start Time	End Time	Amp1	Ω1	Amp2	Ω2	t1	t2	SSE	Notes
8.304	9	125	250	-0.46	0.090	-0.108	0.08	80	30	0.32	

Tucana (8.365)

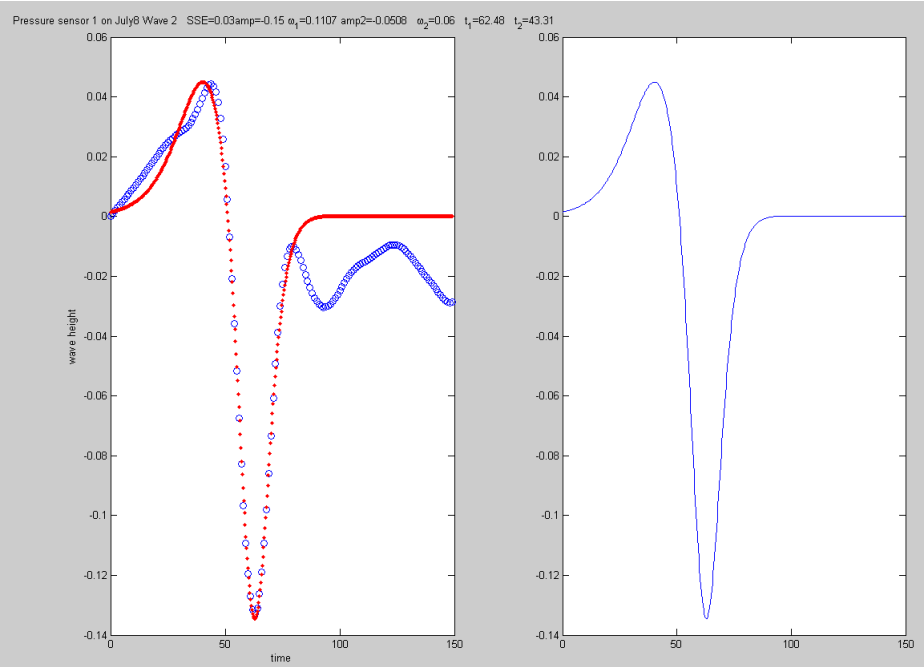

Ship ID	PS #	Start Time	End Time	Amp1	Ω1	Amp2	Ω2	t1	t2	SSE	Notes
8.365	1	100	250	-0.15	0.111	-0.051	0.06	62	43	0.03	

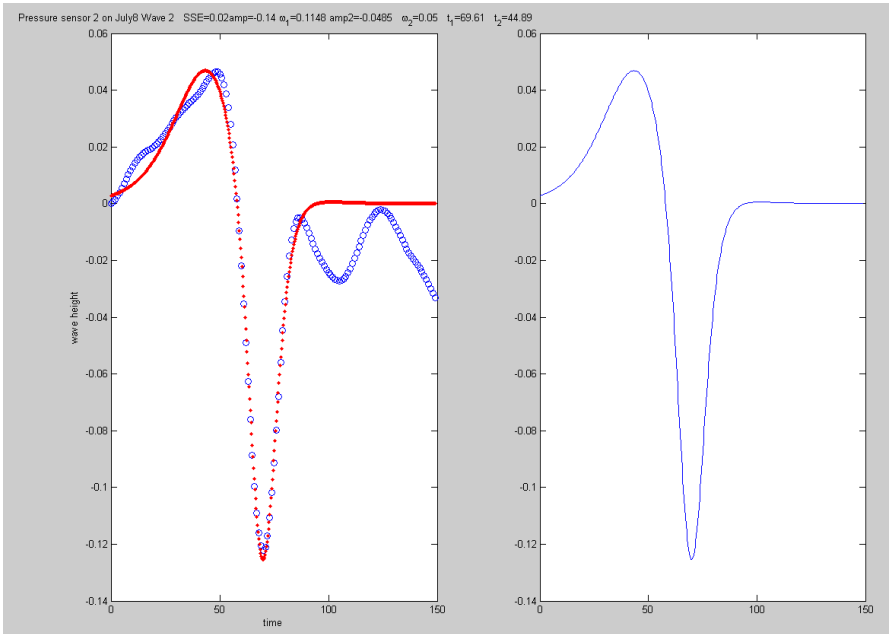

Ship ID	PS #	Start Time	End Time	Amp1	Ω1	Amp2	Ω2	t1	t2	SSE	Notes
8.365	2	100	250	-0.14	0.115	-0.05	0.05	69	44	0.02	

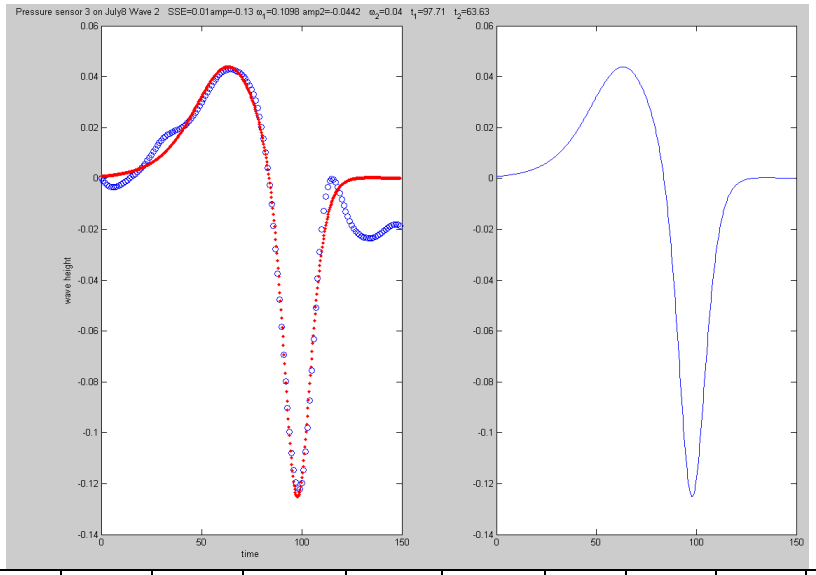

Ship ID	PS #	Start Time	End Time	Amp1	Ω1	Amp2	Ω2	t1	t2	SSE	Notes
8.365	3	100	250	-0.13	0.110	-0.04	0.04	98	64	0.01	

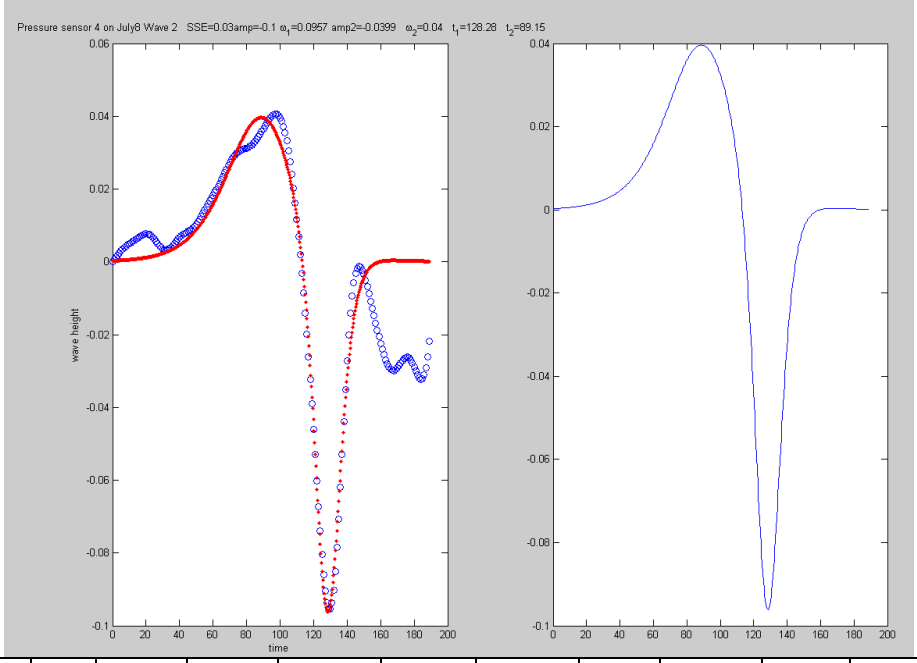

Ship ID	PS #	Start Time	End Time	Amp1	Ω1	Amp2	Ω2	t1	t2	SSE	Notes
8.365	4	100	250	-0.1	0.096	-0.04	0.04	128	89	0.03	

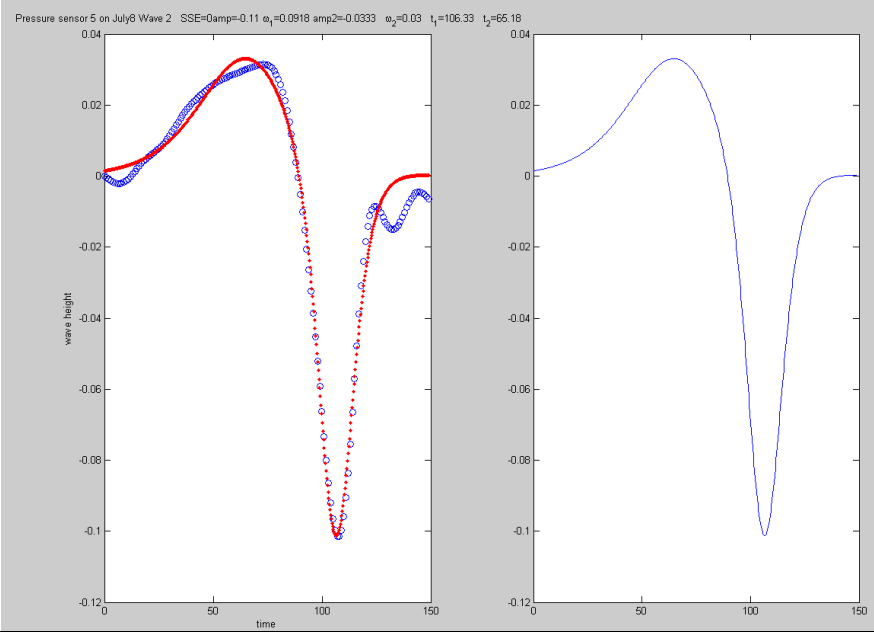

Ship ID	PS #	Start Time	End Time	Amp1	Ω1	Amp2	Ω2	t1	t2	SSE	Notes
8.365	5	150	300	-0.11	0.092	-0.03	0.03	106	65	0.11	

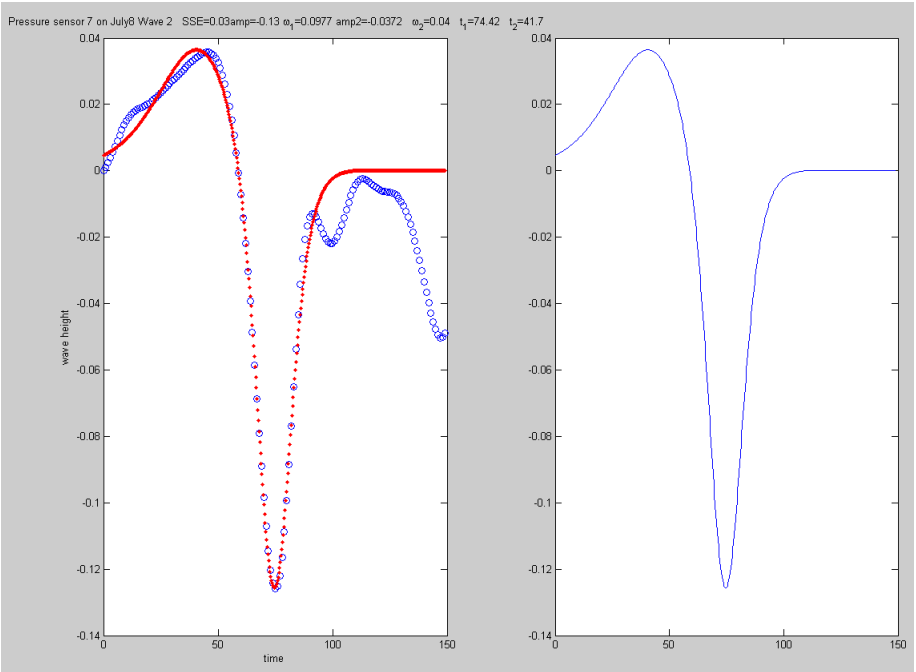

Ship ID	PS #	Start Time	End Time	Amp1	Ω1	Amp2	Ω2	t1	t2	SSE	Notes
8.365	7	150	300	-0.13	0.098	-0.04	0.04	74	41	0.03	

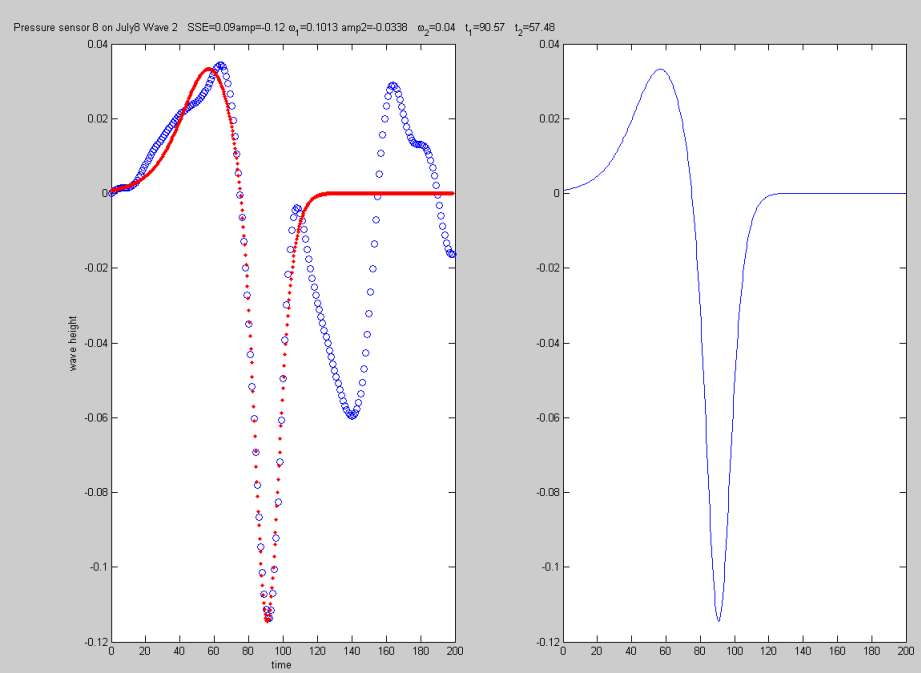

Ship ID	PS #	Start Time	End Time	Amp1	Ω1	Amp2	Ω2	t1	t2	SSE	Notes
8.365	8	100	300	-0.12	0.101	-0.034	0.04	90.57	57.48	0.09	

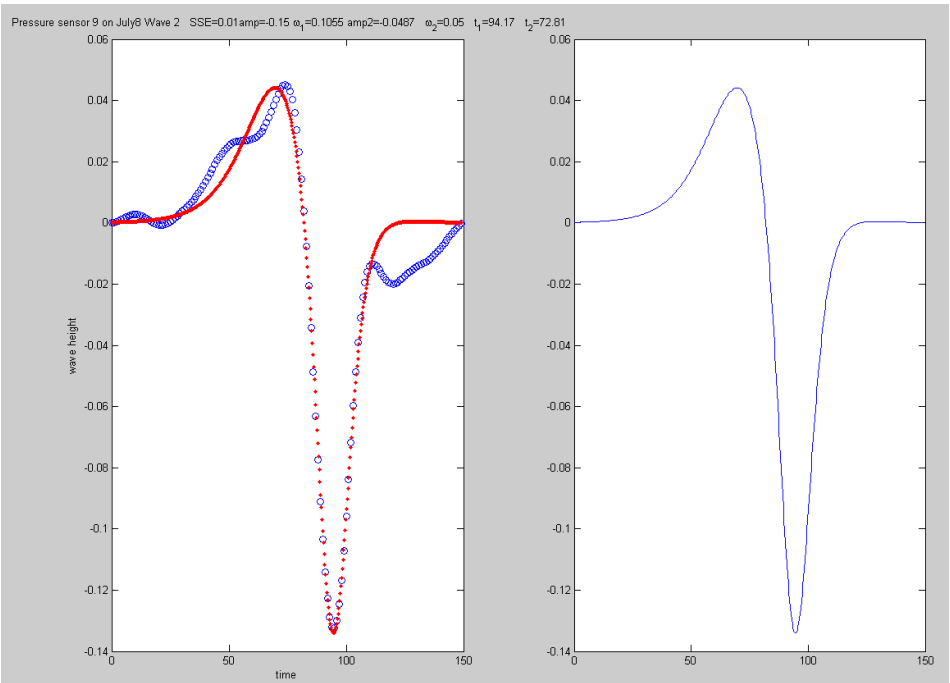

Ship ID	PS #	Start Time	End Time	Amp1	Ω1	Amp2	Ω2	t1	t2	SSE	Notes
8.365	9	100	250	-0.15	0.106	-0.05	0.05	94.17	72.81	0.01	

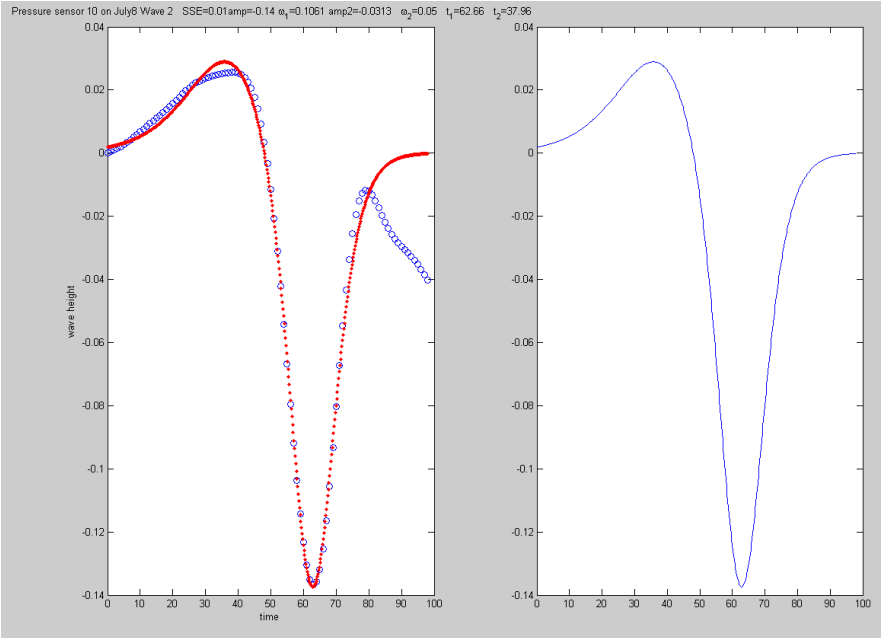

Ship ID	PS #	Start Time	End Time	Amp1	Ω1	Amp2	Ω2	t1	t2	SSE	Notes
8.365	10	100	200	-0.14	0.106	-0.031	0.05	62.66	37.96	0.01	Fit to leading peak

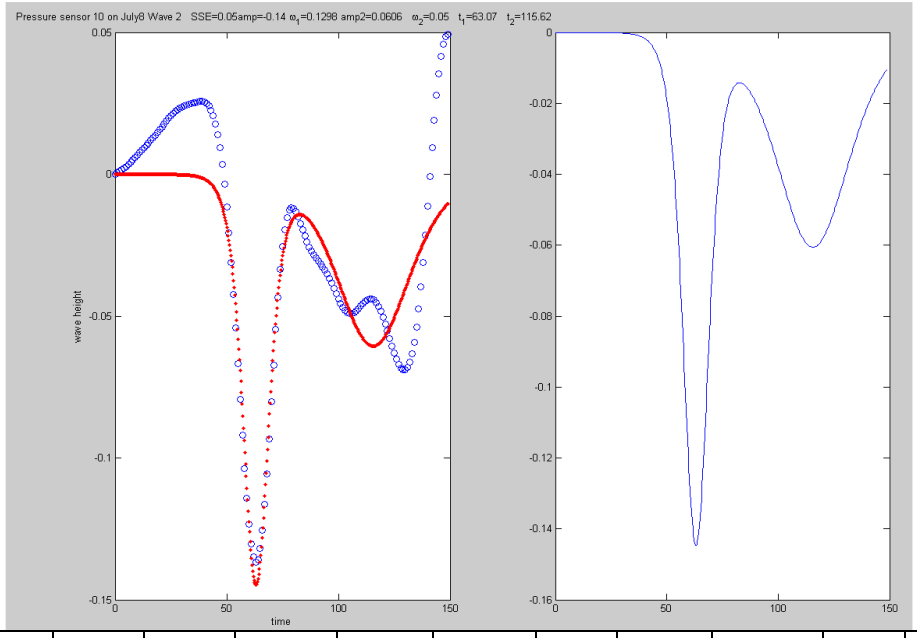

Ship ID	PS #	Start Time	End Time	Amp1	Ω1	Amp2	Ω2	t1	t2	SSE	Notes
8.365	10.1	100	250	-0.14	0.130	0.061	0.05	63.07	115.62	0.05	Fit to trailing trough

Coral Leaf (8.440)

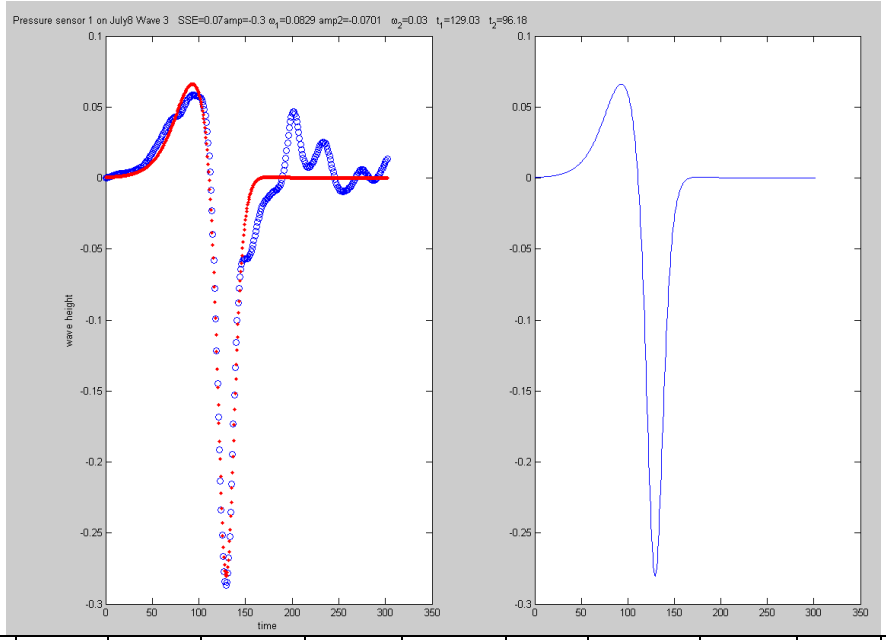

Ship ID	PS #	Start Time	End Time	Amp1	Ω1	Amp2	Ω2	t1	t2	SSE	Notes
8.440	1	x	x	-0.3	0.083	-0.070	0.03	129.03	96.18	0.07	Fit to leading peak

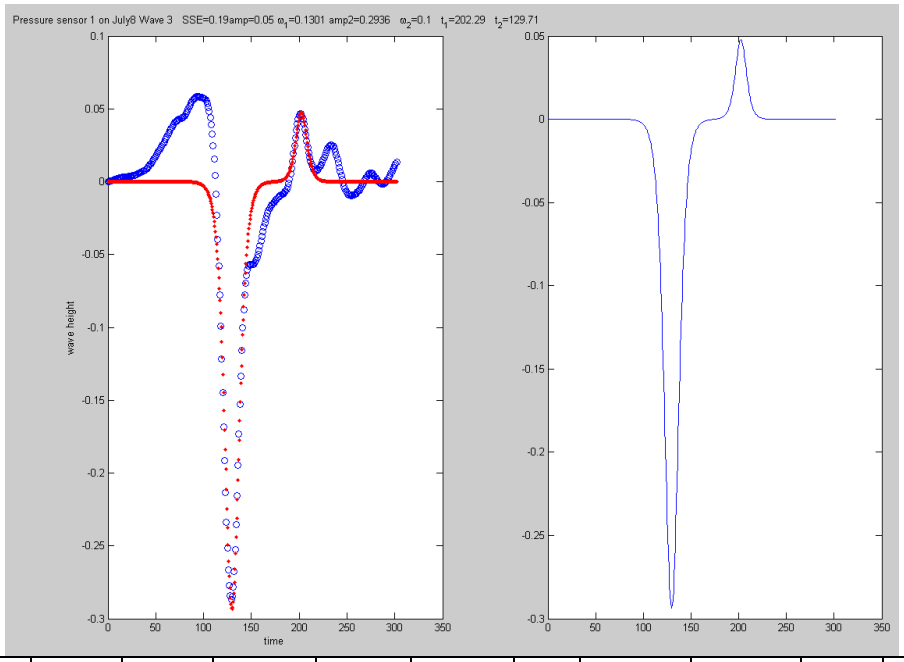

Ship ID	PS #	Start Time	End Time	Amp1	Ω1	Amp2	Ω2	t1	t2	SSE	Notes
8.440	1.1	x	x	0.05	0.130	0.294	0.1	202.29	129.71	0.19	Fit to trailing peak

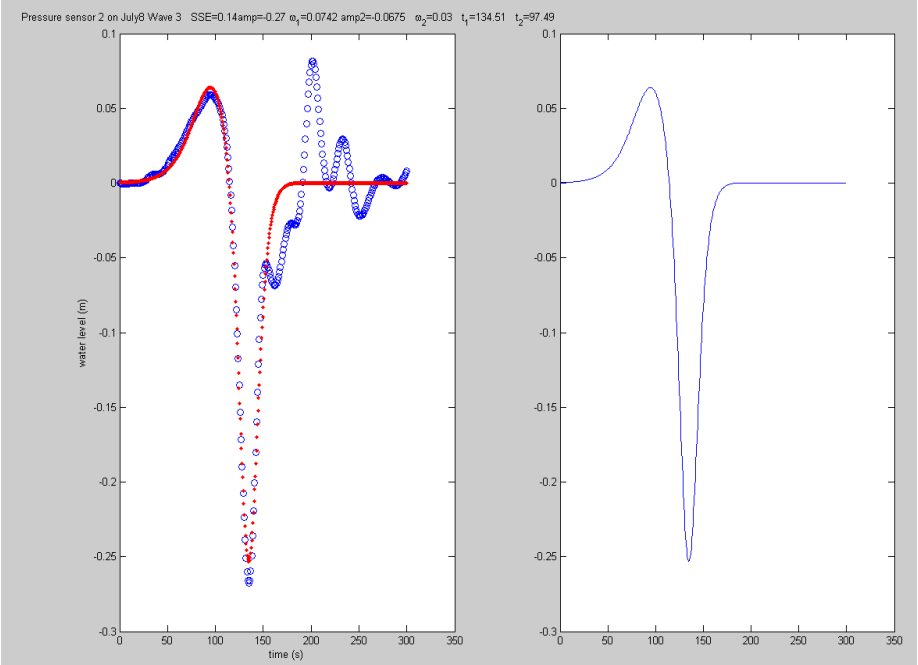

Ship ID	PS #	Start Time	End Time	Amp1	Ω1	Amp2	Ω2	t1	t2	SSE	Notes
8.440	2	x	x	-0.27	0.074	0.068	0.03	134.51	97.49	0.14	Fit to leading peak

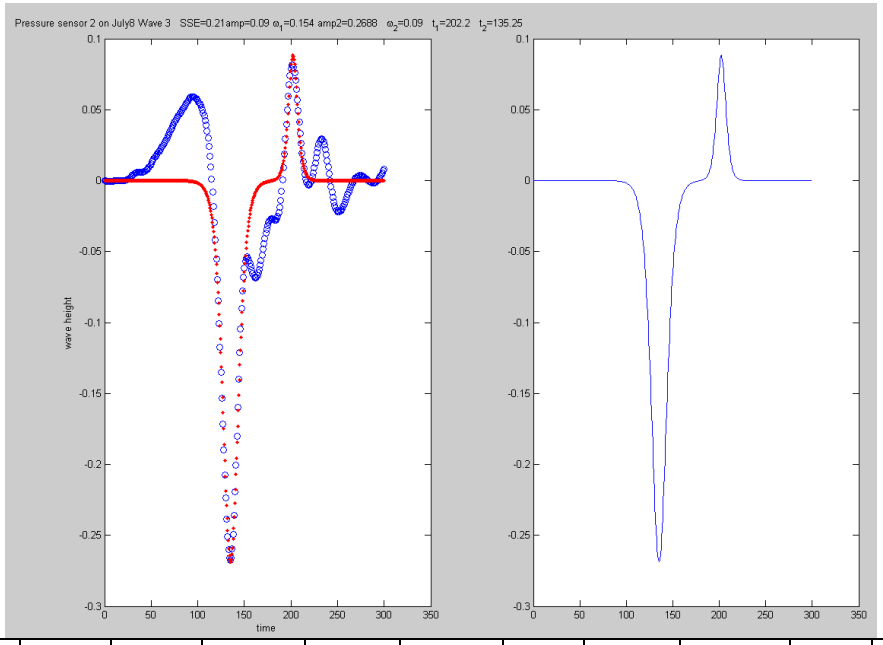

Ship ID	PS #	Start Time	End Time	Amp1	Ω1	Amp2	Ω2	t1	t2	SSE	Notes
8.440	2.1	x	x	0.09	0.154	0.269	0.09	202.2	135.25	0.21	Fit to trailing peak

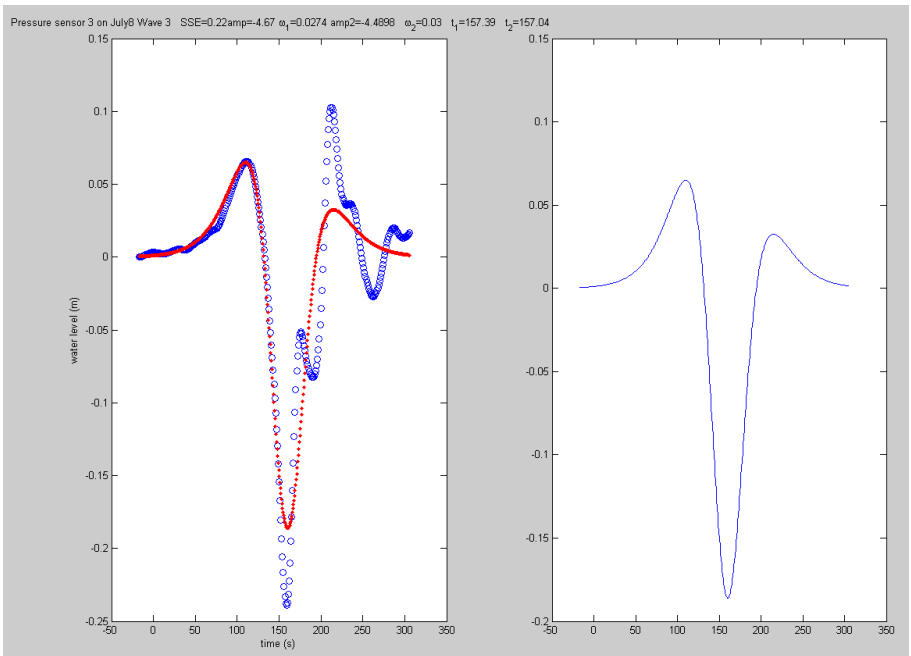

Ship ID	PS #	Start Time	End Time	Amp1	Ω1	Amp2	Ω2	t1	t2	SSE	Notes
8.440	3	x	x	-4.67	0.027	-4.490	0.03	157.39	157.04	0.22	Fit to leading peak

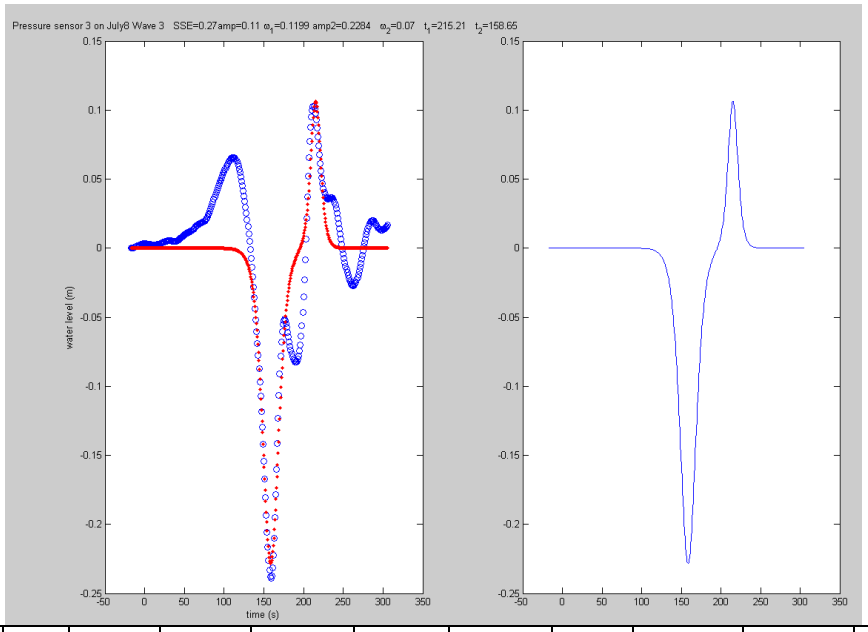

Ship ID	PS #	Start Time	End Time	Amp1	Ω1	Amp2	Ω2	t1	t2	SSE	Notes
8.440	3.1	x	x	0.11	0.120	0.228	0.07	215.21	158.65	0.27	Fit to trailing peak

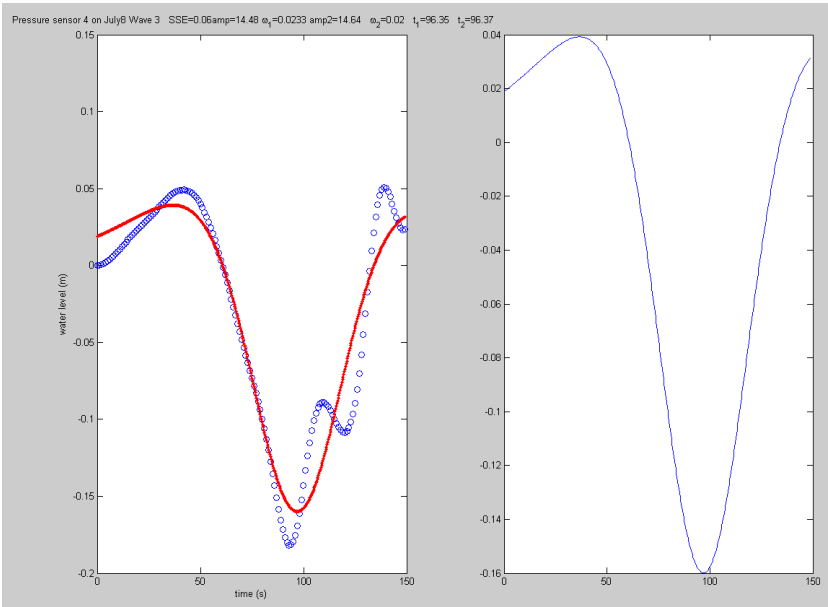

Ship ID	PS #	Start Time	End Time	Amp1	Ω1	Amp2	Ω2	t1	t2	SSE	Notes
8.440	4	90	240	14.48	0.023	14.640	0.02	96.35	96.37	0.06	Fit to leading peak

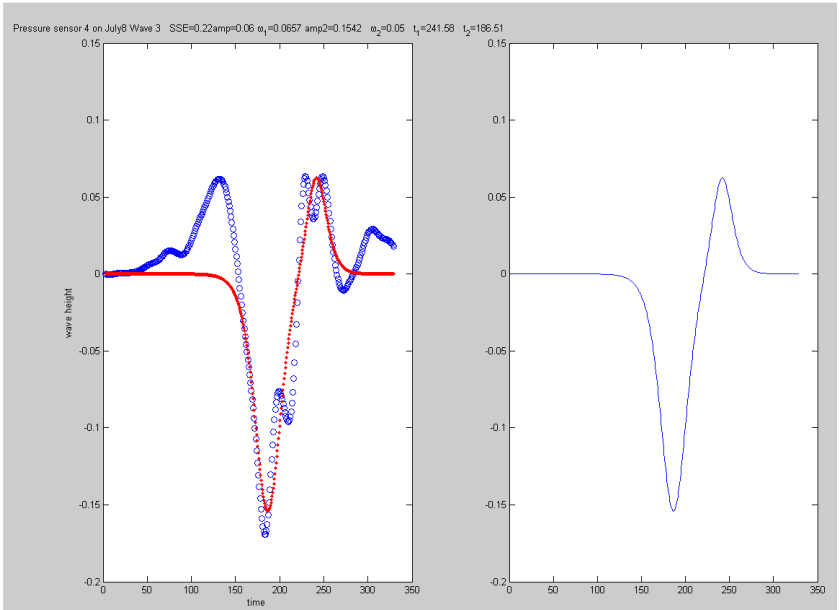

Ship ID	PS #	Start Time	End Time	Amp1	Ω1	Amp2	Ω2	t1	t2	SSE	Notes
8.440	4.1	x	x	0.06	0.066	0.154	0.05	241.58	186.51	0.22	Fit to trailing peak

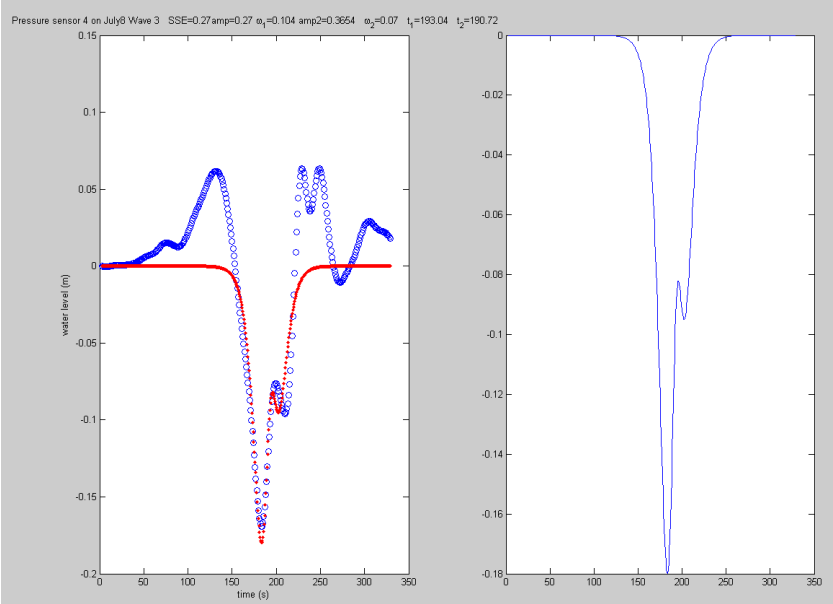

Ship ID	PS #	Start Time	End Time	Am p1	Ω1	Amp 2	Ω2	t1	t2	SSE	Notes
8.440	4.2	x	x	0.27	0.104	0.36	0.07	193	191	0.27	Fit to secondary trough

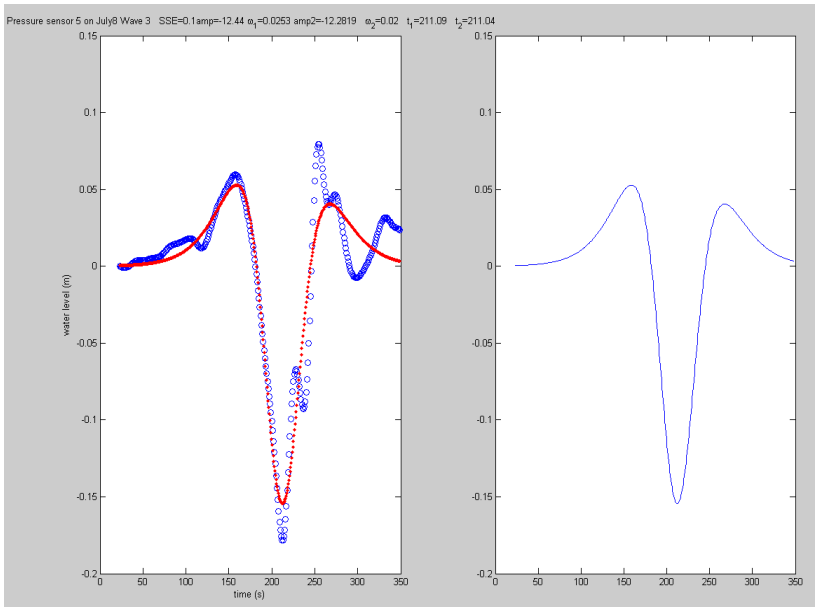

Ship ID	PS #	Start Time	End Time	Amp 1	Ω1	Amp2	Ω2	t1	t2	SSE	Notes
8.440	5	x	x	-12.44	0.025	-12.28	0.02	211	211	0.1	Fit to leading peak

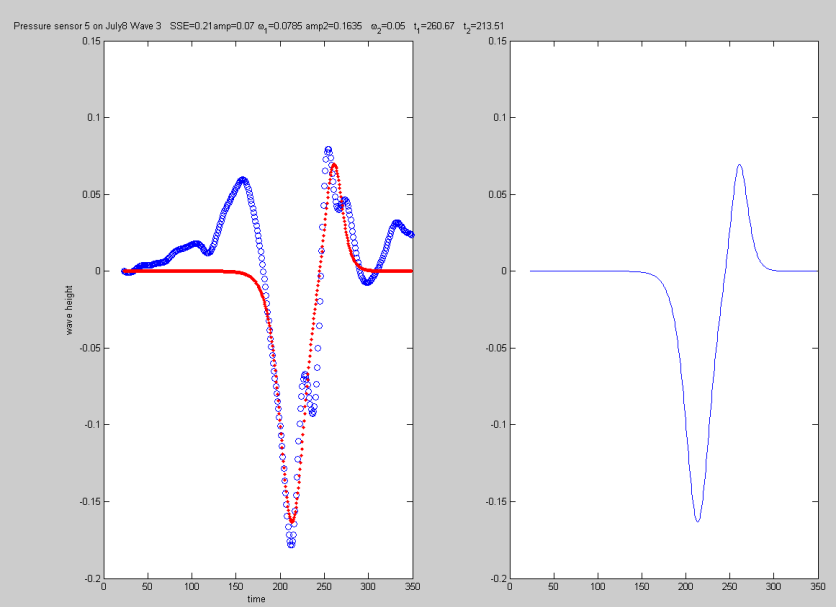

Ship ID	PS #	Start Time	End Time	Amp1	Ω1	Amp2	Ω2	t1	t2	SSE	Notes
8.440	5.1	x	x	0.07	0.079	0.164	0.05	260.67	213.51	0.21	Fit to trailing peak

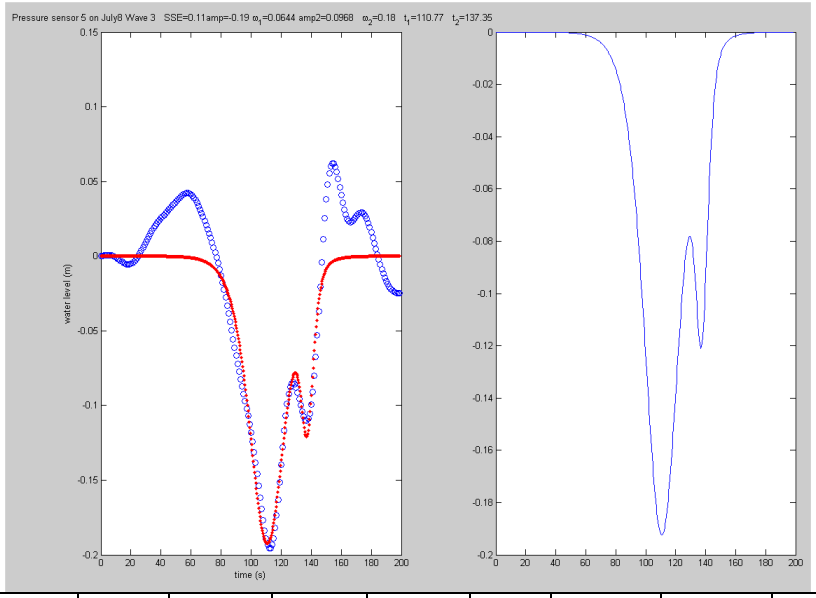

Ship ID	PS #	Start Time	End Time	Amp1	Ω1	Amp2	Ω2	t1	t2	SSE	Notes
8.440	5.2	100	300	-0.19	0.064	0.097	0.18	110.77	137.35	0.11	Fit to secondary trough

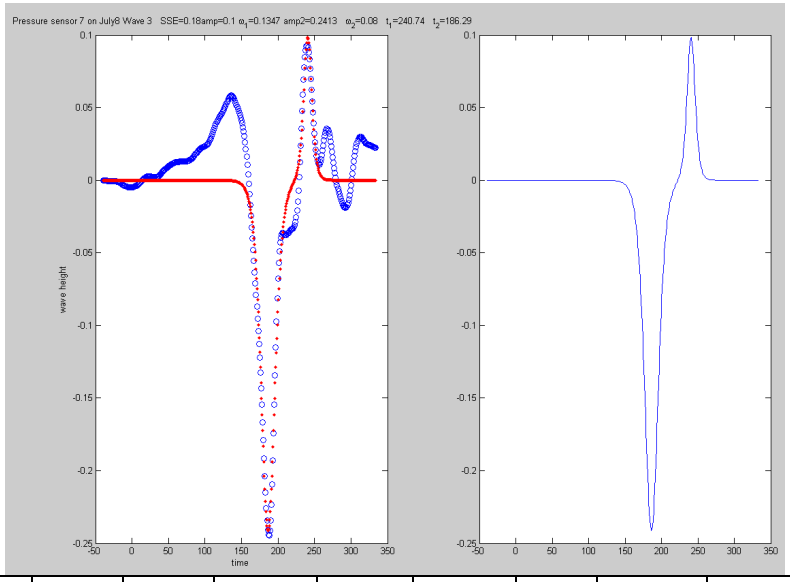

Ship ID	PS #	Start Time	End Time	Amp1	Ω1	Amp2	Ω2	t1	t2	SSE	Notes
8.440	7	x	x	0.1	0.135	0.241	0.08	240.74	186.29	0.18	Fit to trailing peak

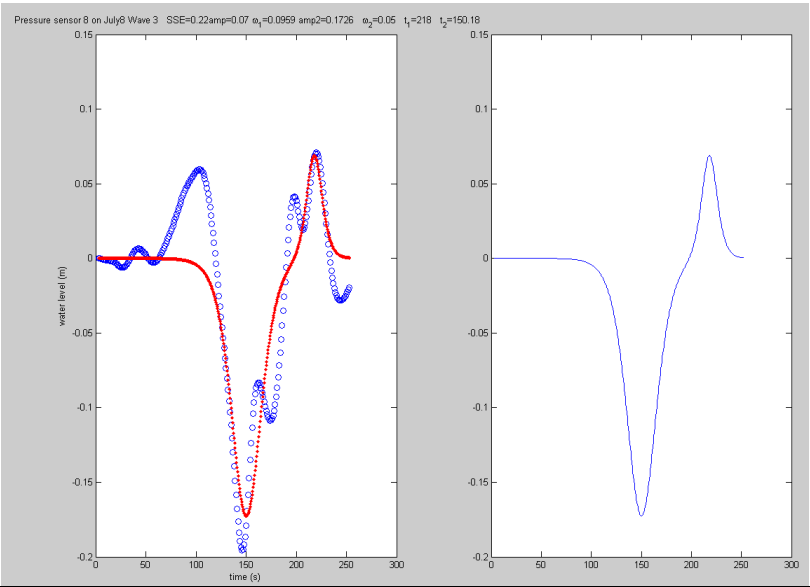

Ship ID	PS #	Start Time	End Time	Amp1	Ω1	Amp2	Ω2	t1	t2	SSE	Notes
8.440	8	x	x	0.07	0.096	0.173	0.05	218	150.18	0.22	Fit to trailing peak

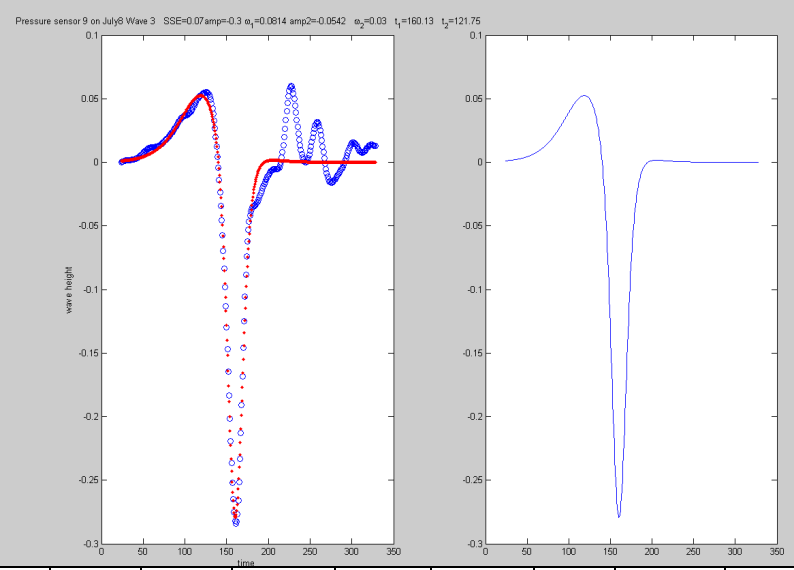

Ship ID	PS #	Start Time	End Time	Amp1	Ω1	Amp2	Ω2	t1	t2	SSE	Notes
8.440	9	x	x	0.3	0.081	0.054	0.03	160.13	121.75	0.07	Fit to leading peak

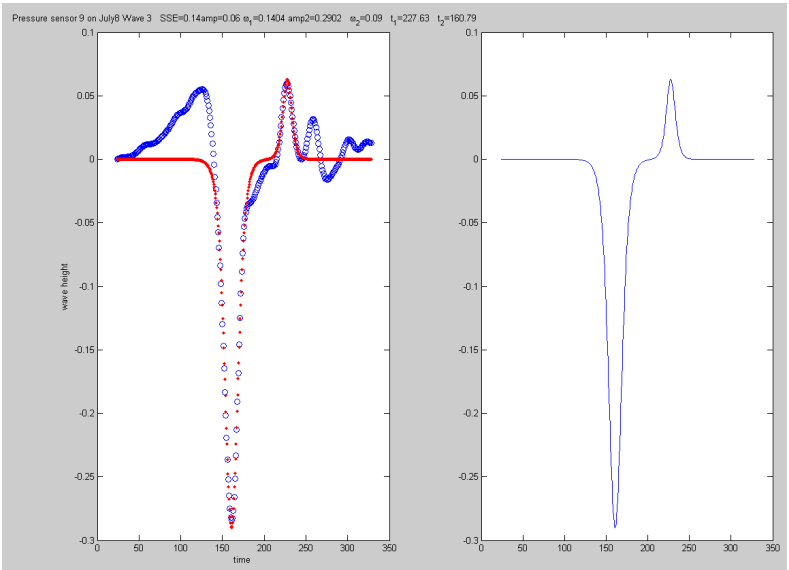

Ship ID	PS #	Start Time	End Time	Amp1	Ω1	Amp2	Ω2	t1	t2	SSE	Notes
8.440	9.1	x	x	0.06	0.140	0.290	0.09	227.63	160.79	0.14	Fit to trailing peak

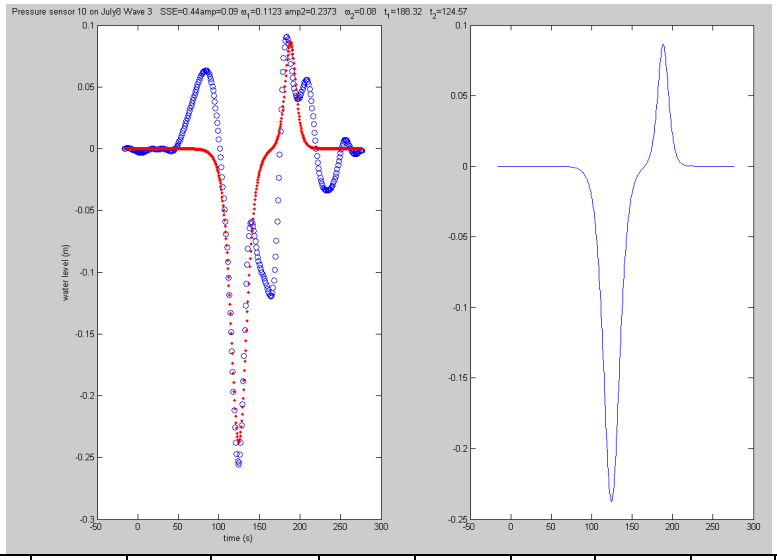

Ship ID	PS #	Start Time	End Time	Amp1	Ω1	Amp 2	Ω2	t1	t2	SSE	Notes
8.440	10	x	x	0.09	0.112	0.237	0.08	188	124	0.44	Fit to trailing peak